Neural Enhancement of Schapery-Prony Viscoelastic Model

Enabling Material Discovery in Synthetic Fibre Characterisation

J.Kevin 5929296

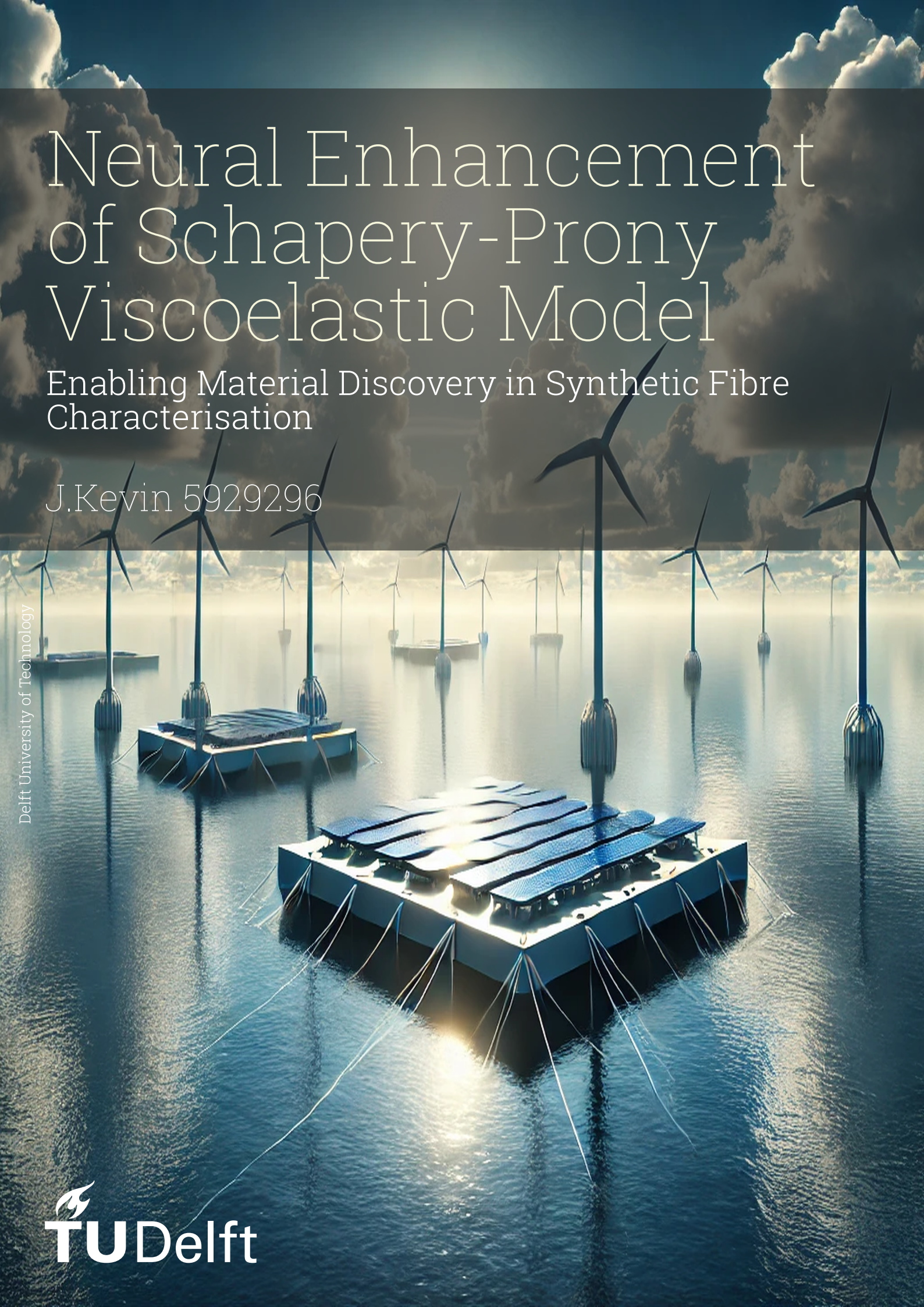

Delft University of Technology

TU Delft

Neural Enhancement of Schapery-Prony Viscoelastic Model

Enabling Material Discovery in Synthetic Fibre Characterisation

by

J.Kevin 5929296

Kevin Jonathan

Chair:	J.O. (Oriol) Colomes Gene, PhD
Daily Supervisor I:	S. (Shagun) Agarwal, PhD
Daily Supervisor II:	Dr.ir. F.P. (Frans) van der Meer
Project Duration:	November 2024 - July 2025
Faculty:	Faculty of Civil Engineering and Geosciences, Delft
Company/Research Partner:	CMOE Group, Tu Delft
Data Provider:	CMOE Group, Tu Delft

Style: TU Delft Report Style, with modifications by Daan Zwaneveld

TU Delft

Abstract

Offshore renewable energy deployment faces a fundamental materials challenge: synthetic fibre mooring lines offer an 8-fold weight reduction and tension reduction compared to steel chains [36, 42], yet their certification requires predicting 20-year operational behaviour from necessarily limited experimental observations. Current approaches employ polynomial functions to represent stress-dependent material behaviour within established viscoelastic frameworks. Still, these rigid mathematical forms constrain material characterisation by forcing complex behaviour into predetermined equations rather than discovering true material physics. This research develops a neural-physics integration framework that replaces polynomial constraints with adaptive neural networks whilst preserving established Schapery-Prony physics principles. The core innovation employs functional decomposition, where neural networks learn stress-dependent nonlinearity functions (g_0, g_1, g_2), while the proven Schapery-Prony framework handles temporal evolution, enabling the discovery of true material behaviour rather than mathematical fitting to predetermined forms.

A systematic five-phase methodology guides development from baseline optimisation through operational validation. Phase 1 employs 13-dimensional Latin Hypercube Sampling across neural architecture, training protocols, and physics parameters. Phase 2 sensitivity analysis identifies optimal methodological choices: Percentage Difference loss functions for scale-invariant learning, Multiple-Steps loading patterns for comprehensive material exercising, and enhanced relaxation spectra for improved temporal coverage. Phase 3 capability testing reveals model limitations through progressive validation scenarios. Phase 4 diagnostic analysis identifies physics model resolution as the primary constraint, leading to targeted improvement from 10 to 14 relaxation terms that address slow relaxation modes critical for long-term accuracy. Phase 5 validates robustness under realistic marine loading using industry-standard JONSWAP wave spectra [27]. The implementation employs a shared-head neural architecture with shared backbone layers (3 layers, 96 neurons) feeding specialised heads (2 layers, 128 neurons each) for individual nonlinearity function learning. Two-stage training coordinates neural network and physics parameter optimisation through differential learning rates whilst maintaining physical consistency. The twin experiment methodology leverages validated HDPE material parameters to generate unlimited synthetic training data spanning stress ranges and loading patterns that are impossible to achieve through physical experimentation alone.

Results demonstrate that the neural enhancement approach enables reliable material characterisation from limited experimental data. Temporal validation achieves 85-95% accuracy across 128-fold duration scaling, enabling decades-long predictions from short-term training data, following established principles for temporal extrapolation in physics-inspired neural networks [44]. Marine validation under realistic JONSWAP loading conditions achieves 5.7-13.2% error across diverse sea states spanning significant wave heights 1.5-7.0m and peak periods 8-15s, demonstrating robustness comparable to validated approaches for viscoelastic modelling under complex loading conditions [11]. The diagnostic insight that physics model completeness rather than neural network architectural sophistication determines model capability guides efficient improvement strategies applicable across computational materials science domains. The validated framework transforms synthetic fibre characterisation from an experimental constraint to a predictive capability, while establishing reproducible principles for neural physics integration across materials science applications that require improved understanding from limited observations. This enables accelerated deployment of offshore renewable energy systems whilst preserving the physical foundations necessary for reliable engineering applications.

Keywords: Neural-physics integration, Synthetic fibre characterisation, Nonlinear viscoelasticity, Schapery theory, Materials discovery, Offshore renewable energy, Computational materials science, Physics-guided machine learning

Preface

The intersection of computational materials science and offshore renewable energy presents unique challenges where traditional mathematical approaches may constrain our understanding of material behaviour. This thesis documents a research journey that began with investigating temporal extrapolation challenges in synthetic fibre characterisation and evolved into developing systematic approaches for neural physics integration that transcend polynomial mathematical limitations while preserving established physics principles. The investigation reveals that adequate material characterisation requires more than simply applying neural networks to materials problems. Success emerges from carefully integrating adaptive learning capabilities within proven physical frameworks rather than abandoning established theoretical foundations. This research demonstrates how neural networks can replace rigid polynomial constraints that force material behaviour into predetermined mathematical forms, enabling the discovery of true stress-dependent characteristics whilst maintaining the temporal evolution accuracy essential for engineering applications.

The five-phase methodology documents the systematic progression from initial optimisation through operational validation. Each phase addresses specific aspects of neural physics integration, including establishing reliable baseline configurations, identifying optimal methodological choices through controlled experimentation, testing model capabilities under demanding scenarios, implementing targeted improvements based on diagnostic analysis, and validating robustness under realistic operational conditions. This structured approach ensures that improvements address root causes rather than symptoms, whilst building toward practical deployment capabilities. A crucial insight emerges from diagnostic analysis during capability testing: physics model completeness, rather than neural network architectural sophistication, determines model performance. This finding challenges conventional approaches that focus on increasing neural network complexity and instead highlights the importance of adequate physics representation. The targeted solution—increasing relaxation spectrum resolution from 10 to 14 terms—addresses slow relaxation modes critical for long-term accuracy, enabling reliable temporal extrapolation whilst maintaining computational efficiency suitable for standard engineering workstations.

The twin experiment methodology provides unlimited synthetic training data using validated HDPE material parameters, enabling the systematic exploration of material behaviour across ranges that are impossible through physical experimentation alone. This approach resolves the tension between neural network data requirements and experimental constraints whilst maintaining a connection to validated material physics throughout the development process. Results validate the paradigm shift from assumption-driven to discovery-driven material characterisation. Models achieve 85-95% accuracy across 128-fold temporal scaling whilst maintaining 5.7-13.2% error under realistic marine loading conditions generated from industry-standard JONSWAP wave spectra [27]. This capability transforms materials characterisation from an experimental limitation to a predictive tool, enabling the reliable prediction of long-term material behaviour from limited experimental observations while preserving the physical consistency necessary for engineering deployment.

The research establishes reproducible principles for neural-physics integration applicable across computational materials science domains where traditional mathematical constraints may limit the discovery of actual material behaviour. This work provides the technical foundations for the accelerated deployment of offshore renewable energy systems, while contributing methodological advances relevant to diverse materials characterisation challenges that require an improved understanding from limited experimental observations. It builds upon emerging approaches that demonstrate extreme temporal extrapolation capabilities in physics-inspired neural networks [44].

Acknowledgments

Sincere gratitude to Dr. J.O. Colomes Gene (thesis chair), Dr. S. Agarwal and Dr.ir. F.P. van der Meer (daily supervisors) for guidance throughout this investigation. Derek van Bochove provided technical

support at Stevin Laboratory. G. Stamoulis, Dr. S. Sánchez Gómez, and Somansundar Sakthivel offered assistance during development phases. The Faculty of Civil Engineering and Geosciences at TU Delft and CMOE Group provided institutional support and computational resources.

This work builds upon experimental contributions by Lai and Nguyen in nonlinear viscoelastic characterisation, whose work provided the physics foundation essential for twin experiment validation and synthetic data generation.

J.Kevin 5929296
Delft, July 2025

Contents

List of Figures

List of Tables

Nomenclature

Abbreviations and Acronyms

Abbreviation	Definition
ABS	American Bureau of Shipping
AR	Amplitude Ratio (loss function)
CNN	Convolutional Neural Network
FFT	Fast Fourier Transform (loss function)
HDPE	High-Density Polyethylene (validation material)
HMPE	High Modulus Polyethylene
IQR	Interquartile Range
JONSWAP	Joint North Sea Wave Project (marine spectra)
LHS	Latin Hypercube Sampling
MAE	Mean Absolute Error (loss function)
MLP	Multi-Layer Perceptron
MSE	Mean Squared Error (loss function)
NPZ	NumPy Compressed Archive Format
PD	Percentage Difference (loss function)
ReLU	Rectified Linear Unit (activation function)
RNN	Recurrent Neural Network

Mathematical Symbols

Symbol	Definition	Unit
A_i	Amplitude of i-th wave component	[m]
C_D	Drag coefficient	[-]
C_M	Mass coefficient	[-]
D	Structural diameter	[m]
D_0	Instantaneous compliance	[Pa^{-1}]
D_i	i-th Prony series compliance coefficient	[Pa^{-1}]
E	Elastic modulus	[Pa]
F	Force	[N]
f	Frequency	[Hz]
$g_0(\sigma)$	Instantaneous compliance nonlinearity function	[-]
$g_1(\sigma)$	Transient compliance nonlinearity function	[-]
$g_2(\sigma)$	Loading rate nonlinearity function	[-]
H_s	Significant wave height	[m]
$h^{(l)}$	Hidden layer activation for layer l	[-]
$J(t)$	Compliance function	[Pa^{-1}]
N	Number of Prony series terms	[-]
n	Number of data points	[-]
PD	Percentage Difference error	[%]
$q_i(t)$	i-th internal state variable	[Pa]
R^2	Coefficient of determination	[-]
$S(\omega)$	Wave power spectral density	[m^{2}s/rad]
T	Time period	[s]
T_p	Peak wave period	[s]

Symbol	Definition	Unit
t	Time	[s]
u	Fluid velocity	[m/s]
$W^{(l)}$	Weight matrix for layer l	[-]
$\mathbf{X}$	Input parameter matrix	[-]
Y	Model output	[-]
α	Learning rate or contraction factor	[various]
β	Adam optimizer momentum parameter	[-]
γ	JONSWAP peak enhancement factor	[-]
Δ	Increment or difference operator	[various]
Δt	Time increment	[s]
$\Delta\psi$	Reduced time increment	[s]
ε	Strain	[-]
ε_{act}	Actual strain	[-]
ε_{pred}	Predicted strain	[-]
η	Viscosity	[Pa·s]
θ	Neural network parameters	[various]
λ_i	i-th relaxation rate parameter	[s^{-1}]
μ	Mean value	[various]
ω	Angular frequency	[rad/s]
ω_p	Peak angular frequency	[rad/s]
ϕ	Activation function	[-]
ψ	Reduced time	[s]
ρ	Density	[kg/m^3]
σ	Stress	[Pa]
σ_{std}	Standardized stress input	[-]
τ_i	i-th relaxation time constant	[s]

Subscripts and Superscripts

Notation	Definition
$(\cdot)_0$	Initial or reference value
$(\cdot)_{act}$	Actual value
$(\cdot)_{baseline}$	Baseline configuration value
$(\cdot)_{enhanced}$	Enhanced/improved configuration value
$(\cdot)_{max}$	Maximum value
$(\cdot)_{min}$	Minimum value
$(\cdot)_{neural}$	Neural network parameter
$(\cdot)_{opt}$	Optimal value
$(\cdot)_{physics}$	Physics-based parameter
$(\cdot)_{pred}$	Predicted value
$(\cdot)_{shared}$	Shared backbone parameter
$(\cdot)_{std}$	Standardized value
$(\cdot)_{training}$	Training parameter
$(\cdot)^{(t)}$	Value at time step t
$(\cdot)^{(n)}$	Value at n-th iteration
$(\cdot)^{(l)}$	Value at neural network layer l
$(\cdot)^*$	Optimal or target value

Mathematical Operators and Functions

Operator	Definition
∇	Gradient operator
∂	Partial derivative operator
$\int$	Integration operator
$\sum$	Summation operator
$\prod$	Product operator
$\exp(\cdot)$	Exponential function
$\log(\cdot)$	Natural logarithmic function
$\max(\cdot)$	Maximum function
$\min(\cdot)$	Minimum function
$\mathsf{Softplus}(\cdot)$	Softplus activation function
$\mathsf{ReLU}(\cdot)$	Rectified Linear Unit activation function
$\mathbb{E}[\cdot]$	Expectation operator
$\mathsf{Var}(\cdot)$	Variance operator
$\|\cdot\|$	Norm operator
$\lvert\cdot\rvert$	Absolute value or magnitude
$\langle\cdot,\cdot\rangle$	Inner product operator
$\odot$	Element-wise (Hadamard) product
$\circ$	Function composition operator
$\sim$	Distributed as or approximately equal
$\propto$	Proportional to
$\ll$	Much less than
$\gg$	Much greater than

Specialized Notation

Notation	Definition
$\mathcal{L}$	Loss function (general)
$\mathcal{L}_{PD}$	Percentage Difference loss function
$\mathcal{L}_{MSE}$	Mean Squared Error loss function
$\mathcal{L}_{MAE}$	Mean Absolute Error loss function
$\mathcal{L}_{AR}$	Amplitude Ratio loss function
$\mathcal{L}_{FFT}$	Fast Fourier Transform loss function
$\mathcal{R}$	Regularization term
$\phi(\cdot)$	Activation function (general)
$W^{(l)}$	Weight matrix for layer l
$b^{(l)}$	Bias vector for layer l
$h^{(l)}$	Hidden state for layer l
h_{shared}	Shared backbone features
$\boldsymbol{\theta}$	Parameter vector
$CI_{1-\alpha}$	Confidence interval at level $1-\alpha$
IQR	Interquartile range
$FFT(\cdot)$	Fast Fourier Transform operator
$\mathsf{MLP}(\cdot)$	Multi-Layer Perceptron function

”What we know is a drop, what we don’t know is an ocean.”

— Isaac Newton

1

Introduction

The deployment of offshore renewable systems is becoming increasingly widespread [26], with experimental validation demonstrating that hybrid mooring systems can achieve reasonable agreement between experimental and numerical results under realistic sea conditions, including beam sea, heading sea, and quarter sea states simulated using JONSWAP spectrum [58]. The dynamic performance of these systems demonstrates that mooring damping effects have a significant influence on low-frequency motion responses and mooring tensions under irregular wave conditions [59]. This performance dependency means that the reliability of mooring systems plays a crucial role in the design of deepwater installations [58, 14]. Synthetic fibre ropes offer advantages over traditional steel chains, with experimental investigations confirming their suitability for mooring applications [34]. They are approximately 8 times lighter in seawater, which helps reduce platform loading. However, using these synthetic ropes requires accurate predictions of material behaviour over a 20-year operational lifespan based on limited experimental data [36, 41]. These synthetic systems can lead to reductions in tension for floating wind turbines and wave energy converters [42, 56]. In deepwater applications, synthetic fibre systems can also lower costs by avoiding the weight increase associated with steel chain systems [31]. Synthetic materials are well-suited for marine applications, with nylon rope technology exhibiting dynamic stiffness characteristics that demonstrate nonlinear behaviours for both mean tension and amplitude [53]. Experimental evaluation confirms that extended Kalman filter methods can reliably estimate parameters for systematic rope dynamic stiffness [60]. Figure 1.1 compares these characteristics across performance metrics, including weight differences, mooring radius requirements, and loading characteristics.

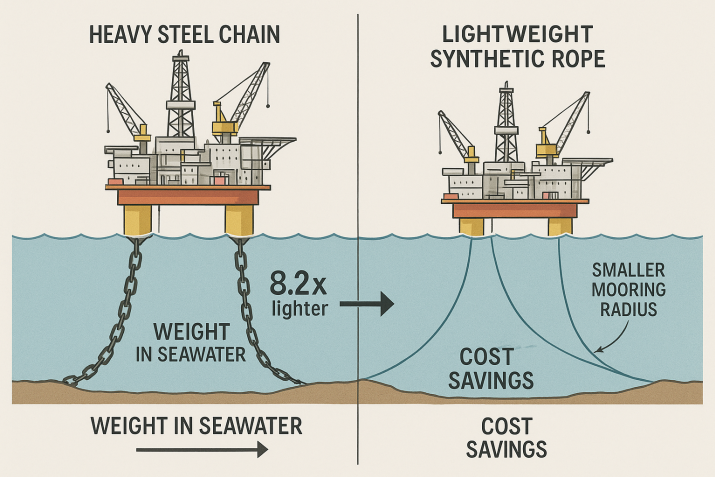

Figure 1.1: Comparison of steel chain and synthetic fibre rope mooring systems.

This approach has limitations in how we characterise materials. The challenge arises from discrepancies between experimental timeframes and the required service life predictions. Limitations in how we mathematically represent material behaviour under varying stress conditions add to this problem.

1.1. Nonlinear Material Behaviour Challenges

Synthetic fibres exhibit time-dependent viscoelastic behaviour under marine loading conditions, reflecting the combined viscous and elastic responses of materials that are intermediate between liquids and solids in character [15], where material response depends on both loading history and stress-dependent nonlinear mechanisms. Experimental work shows that synthetic fibres exhibit nonlinear responses under cyclic loading conditions [35, 23], with long-term durability prediction remaining challenging for engineering deployment [4, 56]. Material modelling becomes difficult under these conditions when combined with the stochastic loading patterns of ocean environments. Figure 1.2 illustrates this behaviour through controlled laboratory testing, showing how constant stress inputs generate strain responses that evolve.

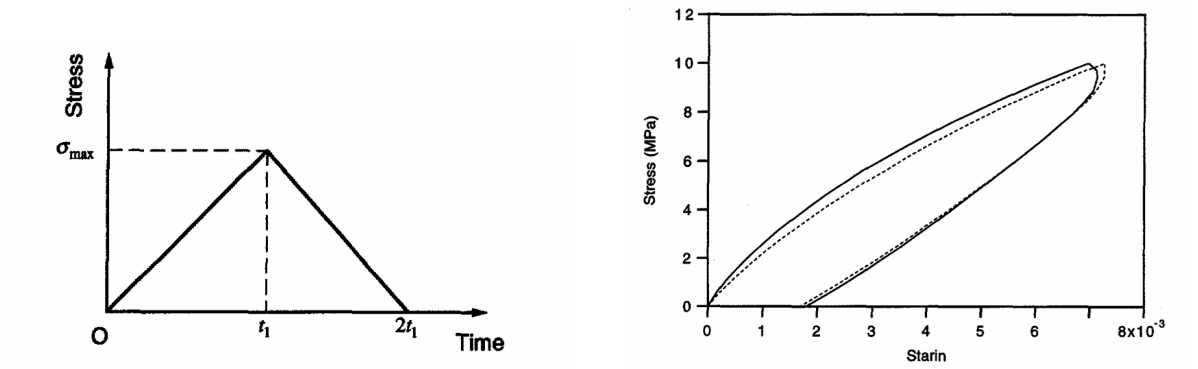

(a) Constant stress loading history representative of controlled laboratory testing.

(b) Viscoelastic strain response showing time-dependent material behaviour.

Figure 1.2: Viscoelastic material response under controlled loading conditions.

Current modelling approaches struggle to capture nonlinear material behaviour. Linear viscoelastic models exhibit limitations in accurately predicting material responses under varying stress conditions, whereas nonlinear approaches based on Schapery's framework demonstrate improved accuracy in specific scenarios [38, 16]. Lai and Nguyen [32, 38] have developed a nonlinear viscoelastic model for synthetic fibres through polynomial representations of stress-dependent functions, achieving agreement with experimental observations under controlled conditions. Studies of synthetic fibre mechanical behaviour indicate that material characterisation remains a challenge across loading scenarios [13]. These polynomial-based approaches face mathematical limitations that constrain their ability to represent the complexity of material behaviour. The challenge lies in representing nonlinear functions within the Schapery framework, where traditional polynomial approaches create a tension between mathematical tractability and physical accuracy.

1.2. Mathematical Approach Limitations

Nonlinear viscoelastic modelling requires representing the stress-dependent functions (g_0, g_1, g_2) that govern material nonlinearity within Schapery's framework [49], building upon foundational work establishing the mechanics of non-linear materials with memory [18] and integral series representations for non-linear viscoelastic response to arbitrary strain histories where experimental data can be incorporated directly [43]. Current approaches, such as those by Lai and Nguyen [32, 38], employ polynomial functions to model these nonlinear parameters. This approach offers mathematical malleability and has worked well under controlled conditions; however, it has limitations that constrain material characterisation. Polynomial representations employ predetermined mathematical forms that may not fully account for the stress-dependent behaviour exhibited by real materials, as demonstrated by molecular changes in polymer systems during stretching, which reveal complex deformation mechanisms not captured by

simple analytical approaches [21]. Computational implementation can encounter numerical challenges and convergence difficulties when applied to loading scenarios [20].

This creates the ”polynomial constraint challenge.” Material behaviour is often required to align with smooth and predictable curves defined by polynomial mathematics. While this approach offers a structured framework, it may not fully capture the complexities and nuances of actual material behaviour. Polynomial approaches are rigid, so even high-order polynomials represent single curves that average out local behaviours, potentially missing material characteristics that could inform material understanding. These limitations can manifest as nonphysical structural behaviour when predetermined mathematical forms are applied beyond their intended scope, as demonstrated in large-strain applications where polynomial-based constitutive models produce instabilities rather than realistic material responses [48]. This mathematical constraint arises from the polynomial nature, where any polynomial of degree n has exactly n derivatives, creating limitations in representing local behaviours that require different mathematical descriptions in different stress regions.

Polynomial approaches have a sensitivity problem. Low-order polynomials offer mathematical stability but prove too simplistic to accurately capture material responses, resulting in smooth representations that may not accurately reflect reality. High-order polynomials can theoretically follow patterns but become mathematically unstable. Experimental uncertainties can be amplified when using polynomial coefficients, thereby affecting the accuracy of predictions. This creates a choice between simplified physics and error sensitivity. Neural network approaches show promise, with recurrent neural networks demonstrating that their intrinsic computational aspects are very similar to those of classical stress update algorithms in modelling history-dependent materials, with an emphasis on viscoelasticity. RNN data-driven modelling can serve as an alternative to conventional viscoelasticity models [19, 1, 10]. However, they interpolate accurately but perform poorly beyond the training conditions, because they lack integration with physical principles. Better approaches are needed that can capture material behaviour while maintaining the physical consistency required for engineering applications.

1.3. Research Approach and Innovation

The approach addresses the mathematical constraint challenge by integrating neural networks that are trained to solve supervised learning tasks while respecting given laws of physics described by general nonlinear partial differential equations [44], combining neural networks within the framework of viscoelastic physics. Rather than replacing physical principles, the approach modifies the traditional framework by using neural networks to learn the nonlinear functions (g_0, g_1, g_2) that govern stress-dependent behaviour, without imposing predetermined mathematical forms. The method employs a shared-head neural network architecture, where neural networks learn only the stress-dependent Schapery functions, while the Schapery-Prony framework handles all temporal evolution. This functional decomposition preserves the physical foundation for temporal behaviour while allowing the identification of material laws that extend beyond polynomial constraints, building upon established principles where neural networks can be combined with structural mechanics to replace constitutive equations through artificial intelligence approaches [52] and data-driven computational mechanics that carry out calculations directly from experimental material data [30].

Synthetic fibre nonlinear behaviour may follow patterns that polynomial functions cannot represent, regardless of order or complexity. By replacing polynomial constraints with neural networks, this research enables materials to exhibit their behaviour patterns rather than being framed within predetermined mathematical frameworks, revealing aspects of material physics that were previously hidden by mathematical assumptions. Development includes five phases. The first phase involves hyperparameter optimisation using Latin Hypercube Sampling across a 13-dimensional parameter space. The second phase conducts a sensitivity analysis, identifying design choices for loss functions, loading patterns, and relaxation spectra. The third phase performs capability testing to validate the model’s performance across scenarios. The fourth phase implements targeted improvements. The fifth phase provides operational validation under realistic marine loading conditions using industry-standard JONSWAP spectra.

The approach uses High-Density Polyethylene (HDPE) as the validation case, leveraging experimental data from previous work [38] whilst developing principles for use across synthetic fibre materials.

The twin experiment methodology generates training datasets whilst maintaining a connection to validated experimental behaviour, enabling exploration of parameter spaces not available through physical experimentation.

1.4. Research Objectives

The thesis examines a research question through six investigations that explore neural-physics integration:

Primary Research Question: *How can neural networks be integrated within Schapery's viscoelastic formulation to represent stress-dependent nonlinear functions while maintaining physical consistency and enabling prediction from limited experimental observations?*

Primary Objective: To develop a neural-physics integration approach that learns nonlinear material parameters (g_0, g_1, g_2) for synthetic fibres under multiple loading conditions while preserving physical consistency and providing material characterisation beyond current polynomial-based approaches through validation, including temporal testing and realistic marine loading scenarios.

Six supporting questions examine this challenge:

SQ1: To what extent can a 'twin experiment' methodology, using synthetically generated data, train a neural-physics integration approach to learn known viscoelastic physics and serve as a substitute for limited experimental data while enabling exploration of the model?

SQ2: How robust is the trained neural-physics approach when validated against realistic, stochastic marine loading conditions generated from industry-standard JONSWAP spectra, particularly regarding maintenance of temporal capabilities under operational complexity?

SQ3: What are the physical interpretations of learned parameters and computational requirements for standard engineering implementation?

SQ4: What are the limitations of a neural-physics approach in scenarios, and what improvements are necessary to reach capabilities that address these limitations?

SQ5: What protocols are required for integration into offshore engineering workflows while preserving the model's capabilities?

SQ6: How can the model's reliability be quantified for engineering applications?

These questions guide the work presented in subsequent chapters, with theoretical foundations in Chapter 2, methodology detailed in Chapter 3, results presented in Chapter 4, and implications discussed in Chapter 5.

1.5. Thesis Structure

Chapter 2 covers theoretical foundations from classical viscoelastic theory to neural network integration approaches, identifying why traditional polynomial representations constrain material characterisation and how neural networks offer capabilities when integrated with physics frameworks. Chapter 3 describes the five-phase research framework: baseline optimisation, sensitivity analysis, capability testing, targeted improvement, and operational validation. The chapter describes the development of neural-physics integration architecture, training strategies, and validation protocols for neural-physics integration. Chapter 4 presents the investigation that validates neural network integration through optimisation outcomes, sensitivity analysis, model capabilities and performance, and marine loading validation across various sea states. Chapter 5 summarises research contributions while addressing each supporting question, discussing implications, current limitations, and future research directions. Appendices contain sensitivity analysis results.

2

Literature Review

2.1. Viscoelastic Materials and Marine Applications

Current nonlinear viscoelastic modelling limitations provide the foundation for developing methodologies that use physics while enabling the discovery of material behaviour. The review encompasses theoretical foundations ranging from classical viscoelastic theory to neural network integration approaches, establishing the case for integrating neural networks with physics frameworks to transcend the mathematical constraints that may limit our understanding of material physics. The challenge involves addressing the tension between mathematical tractability and physical accuracy. Polynomial approaches offer computational convenience but impose constraints that may prevent the discovery of material behaviour. Neural networks provide learning capabilities but require integration with physics to maintain the temporal evolution accuracy necessary for engineering applications, while enabling the representation of stress-dependent material characteristics.

2.1.1. Physical Nature of Viscoelastic Behaviour

Viscoelastic materials exhibit both elastic and viscous behaviour simultaneously, creating time-dependent responses needed for synthetic fibre mooring line performance, with experimental validation demonstrating that dynamic stiffness characteristics show non-linearity with respect to both mean tension and amplitude under realistic loading conditions [15, 53]. This behaviour requires constitutive relationships governing material behaviour across temporal scales relevant for offshore applications. The mathematical representation of these relationships has often prioritised computational tractability; it's essential to recognise the potential for enhancing physical accuracy. Ideal elastic response follows Hooke's Law, where stress (σ) relates directly to strain (ε) through elastic modulus (E):

$$\sigma = E\varepsilon \tag{2.1}$$

The mathematical representation of these relationships has often prioritised computational tractability; it's essential

This shows instantaneous and recoverable characteristics. Conversely, ideal viscous response follows Newton's Law of Viscosity, where stress is proportional to strain rate ($\dot{\varepsilon}$) through the viscosity coefficient (η):

$$\sigma = \eta\dot{\varepsilon} \tag{2.2}$$

Real materials combine these responses through mechanical analogues that provide conceptual frameworks for understanding material behaviour [46]. Figure 2.1 shows basic mechanical models where the Maxwell model captures stress relaxation behaviour, whilst the Kelvin-Voigt model represents creep response. These form the conceptual foundation for Prony series representation, where multiple Maxwell elements create multiscale temporal behaviour in synthetic fibres. However, the question

arises whether these simplified analogues capture the complexity of real material behaviour or whether they represent mathematical convenience rather than physical reality.

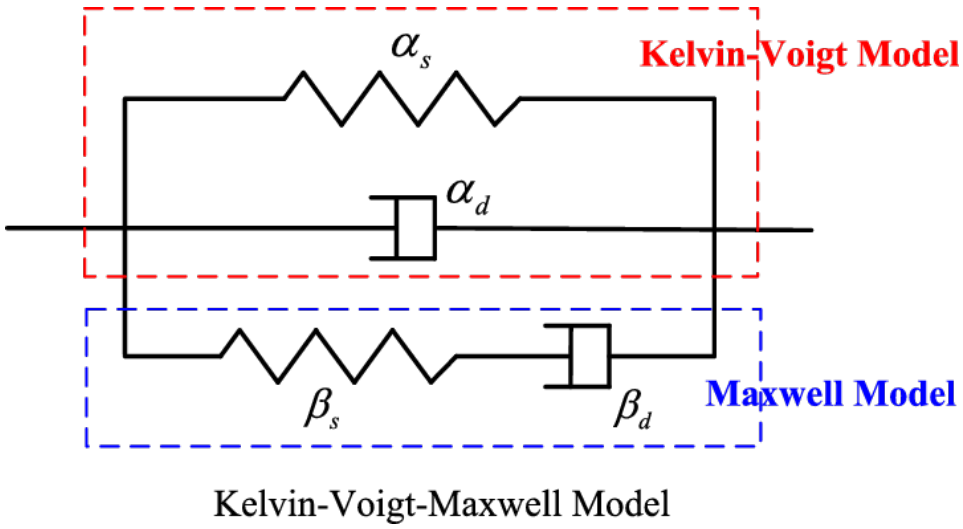

Figure 2.1: Mechanical analogue models for viscoelastic behaviour.

The progression from simple mechanical analogues to mathematical formulations raises questions about whether our mathematical representations reflect material physics or impose constraints on our understanding of material behaviour. This distinction becomes important when considering integration approaches that enable materials to show behaviour patterns beyond traditional mathematical assumptions.

2.2. Classical Viscoelastic Theory

2.2.1. Hereditary Integral Formulation

Classical viscoelastic theory provides mathematical frameworks through hereditary integrals that capture material memory effects for time-dependent material behaviour [18, 43]. It illustrates how mathematical assumptions can influence our understanding of material physics. The hereditary integral originates from the superposition principle, which states that the material response to loading equals the sum of responses to individual loading increments. Development begins with Duhamel's theorem for linear viscoelastic materials:

$$\varepsilon(t) = \int_{-\infty}^{t} J(t-\tau)\frac{d\sigma(\tau)}{d\tau}d\tau \tag{2.3}$$

where $J(t-\tau)$ represents the creep compliance function. The argument $(t-\tau)$ indicates that the material response depends only on the elapsed time since the loading application, not on absolute time. For use, the hereditary integral splits into instantaneous and time-dependent components:

$$\varepsilon(t) = D_0\sigma(t) + \int_{0}^{t} \Delta D(t-\tau)\frac{d\sigma(\tau)}{d\tau}d\tau \tag{2.4}$$

where D_0 captures instantaneous compliance and $\Delta D(t-\tau)$ represents transient compliance. Each stress increment affects the current strain according to the material's characteristic response function, providing the foundation for approaches that separate the temporal evolution of physics from stress-dependent mathematical representations, as discussed in Chapter 3.

2.2.2. Prony Series Implementation

The Prony series provides implementation through discrete approximation of continuous relaxation spectra, yet this discretisation reveals the tension between computational necessity and physical reality. Materials have continuous relaxation spectra where molecular motions occur across all timescales simultaneously [55]. Implementation requires finite representations that may limit our understanding of material behaviour:

$$D(t) = D_0 + \sum_{i=1}^{n} D_i \left[1 - \exp\left(-\frac{t}{\tau_i}\right)\right] \tag{2.5}$$

Each term represents a Maxwell element with characteristic relaxation time τ_i and strength D_i. The exponential decay captures basic physics where relaxation processes decay exponentially with time constants determined by molecular mechanisms [15]. However, the discrete approximation raises questions about whether the assumed exponential forms represent material relaxation characteristics or impose mathematical constraints on our understanding.

Approximation quality depends on how well discrete terms capture the characteristics of the continuous spectrum. For material characterisation applications:

$$\|D_{continuous}(t) - D_{Prony}(t)\| < \epsilon_{acceptable} \quad \forall t \in [0, T_{application}] \tag{2.6}$$

Relaxation spectrum resolution affects material representation, as investigated in Chapter 4. The quality of this approximation determines whether our mathematical models enable the discovery of material behaviour or constrain understanding through resolution.

Figure 2.2 shows how total material response emerges from the superposition of individual exponential modes. This forms the mathematical foundation, where the Prony series provides a framework for temporal evolution. At the same time, neural networks can improve the representation of stress-dependent behaviour without being constrained by predetermined mathematical forms.

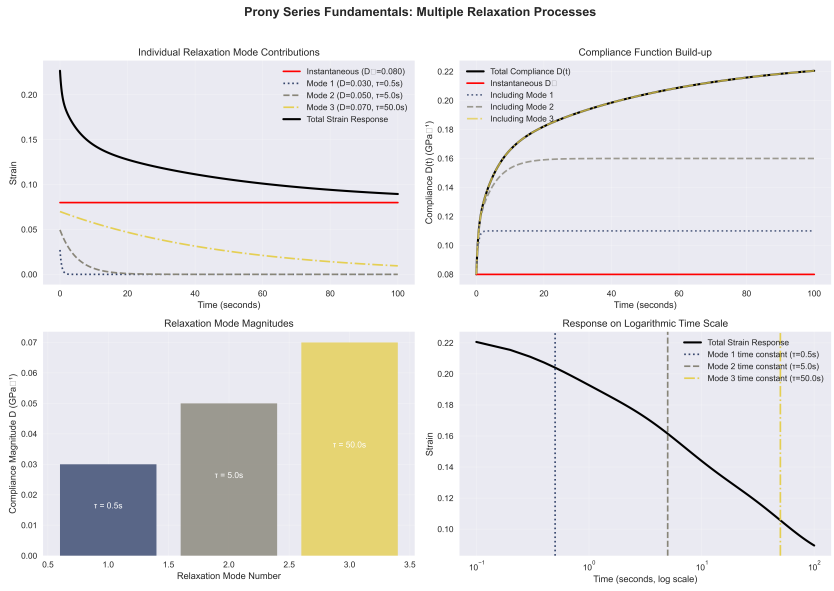

Figure 2.2: Prony series representation of individual exponential modes and total response.

2.2.3. Incremental Formulation

The incremental formulation converts hereditary integrals into computationally tractable recursive algorithms. Direct implementation would require storing stress histories, which creates computational complexity that grows quadratically with the number of time steps. The incremental formulation reaches

linear computational scaling whilst preserving the physics of material memory. For the time interval from t^n to t^{n+1}, the strain increment becomes:

$$\Delta\varepsilon^{n+1} = D_0\Delta\sigma^{n+1} + \sum_{i=1}^{N} D_i \left[\Delta\sigma^{n+1} - \Delta q_i^{n+1}\right] \tag{2.7}$$

Internal state variables q_i capture material memory through recursive updating:

$$q_i^{n+1} = q_i^n \exp\left(-\frac{\Delta t}{\tau_i}\right) + \sigma^n \left[1 - \exp\left(-\frac{\Delta t}{\tau_i}\right)\right] \tag{2.8}$$

Each internal state variable represents the convolution integral's contribution from the i-th relaxation mode. The incremental strain formulation becomes:

$$\varepsilon^{n+1} = g_0^{n+1} D_0 \sigma^{n+1} + g_1^{n+1} \sum_{i=1}^{N} D_i (g_2^{n+1}\sigma^{n+1} - q_i^{n+1}) \tag{2.9}$$

where nonlinearity functions g_0, g_1, and g_2 modify linear viscoelastic response. This formulation reveals the separation between temporal evolution (handled by physics) and stress-dependent modifications (traditionally constrained by polynomial representations), providing the framework for approaches that enable learning of these functions, as implemented in Chapter 3.

2.3. Schapery's Nonlinear Viscoelastic Theory

2.3.1. Mathematical Foundation

Schapery's framework utilises the mathematical structure of linear viscoelastic theory, introducing stress-dependent modifications through nonlinear functions [49]. This allows stress-dependent material behaviour while maintaining the temporal evolution framework. However, the representation of these nonlinear functions has been limited by mathematical assumptions rather than guided by material physics. The Schapery constitutive equation gives the relationship:

$$\varepsilon(t) = g_0(\sigma) D_0 \sigma(t) + g_1(\sigma) \int_0^t \Delta D(\psi - \psi') \frac{d[g_2(\sigma)\sigma(\tau)]}{d\tau} d\tau \tag{2.10}$$

Where nonlinearity functions represent distinct physical mechanisms. The function $g_0(\sigma)$ modifies instantaneous elastic response, $g_1(\sigma)$ scales transient compliance effects, and $g_2(\sigma)$ accounts for loading rate effects [37]. The key point is that while the temporal evolution framework is established through physics principles, the mathematical forms of these stress-dependent functions have been limited by computational convenience rather than physical necessity. The framework processes stress input patterns $\sigma(t)$ to generate strain output responses $\varepsilon(t)$. Prediction quality depends on both the temporal evolution accuracy and how well the nonlinearity functions capture stress-dependent material behaviour, raising questions about whether traditional polynomial representations reflect material physics.

2.3.2. Detailed Incremental Implementation

Implementation for synthetic fibre applications requires detailed incremental strain formulation that separates temporal physics from stress-dependent mathematical representations. Development begins with the uniaxial integral form:

$$\varepsilon^t = g_0^t D_0 \sigma^t + g_1^t \int_0^t \Delta D^{(\psi^t - \psi^\tau)} \frac{d(g_2^\tau \sigma^\tau)}{d\tau} d\tau \tag{2.11}$$

Where ψ represents reduced-time accounting for stress-dependent effects:

$$\psi^t = \int_0^t \frac{d\xi}{a_\sigma^\xi a_T^\xi} \tag{2.12}$$

For this research, the time-scaling factor a_σ, a_T is disregarded for simplicity while maintaining focus on the three nonlinearity functions that represent the challenge in material characterisation. The uniaxial transient compliance uses Prony series representation from Equation 2.5:

$$\Delta D^{\psi^t} = \sum_{n=1}^{N} D_n(1 - \exp[-\lambda_n \psi^t]) \tag{2.13}$$

Substituting into the Schapery equation yields:

$$\varepsilon^t = g_0^t D_0 \sigma^t + g_1^t g_2^t \sum_{n=1}^{N} D_n - g_1^t \sum_{n=1}^{N} D_n q_n^t \tag{2.14}$$

Where hereditary integral terms are:

$$q_n^t = \int_0^t \exp[-\lambda_n(\psi^t - \psi^\tau)] \frac{d(g_2^\tau \sigma^\tau)}{d\tau} d\tau \tag{2.15}$$

Recursive integration divides into previous time step contributions and current increment contributions:

$$q_n^t = \int_0^{t-\Delta t} \exp[-\lambda_n(\psi^t - \psi^\tau)] \frac{d(g_2^\tau \sigma^\tau)}{d\tau} d\tau + \int_{t-\Delta t}^{t} \exp[-\lambda_n(\psi^t - \psi^\tau)] \frac{d(g_2^\tau \sigma^\tau)}{d\tau} d\tau \tag{2.16}$$

With reduced time increment $\Delta\psi^t = \psi^t - \psi^{t-\Delta t}$, the first integral becomes:

$$\int_0^{t-\Delta t} \exp[-\lambda_n(\psi^t - \psi^\tau)] \frac{d(g_2^\tau \sigma^\tau)}{d\tau} d\tau = \exp[-\lambda_n \Delta\psi^t] q_n^{t-\Delta t} \tag{2.17}$$

Assuming $(g_2^\tau \sigma^\tau)$ varies linearly over the current time step, the second integral reduces to:

$$\int_{t-\Delta t}^{t} \exp[-\lambda_n(\psi^t - \psi^\tau)] \frac{d(g_2^\tau \sigma^\tau)}{d\tau} d\tau = \frac{1 - \exp[-\lambda_n \Delta\psi^t]}{\lambda_n \Delta\psi^t} (g_2^t \sigma^t - g_2^{t-\Delta t} \sigma^{t-\Delta t}) \tag{2.18}$$

The hereditary integral expression at the current time becomes:

$$q_n^t = \exp[-\lambda_n \Delta\psi^t] q_n^{t-\Delta t} + (g_2^t \sigma^t - g_2^{t-\Delta t} \sigma^{t-\Delta t}) \frac{1 - \exp[-\lambda_n \Delta\psi^t]}{\lambda_n \Delta\psi^t} \tag{2.19}$$

Substituting recursive relationships into the strain equation yields:

$$\begin{aligned} \varepsilon^t = & \left[g_0^t D_0 + g_1^t g_2^t \sum_{n=1}^{N} D_n - g_1^t g_2^t \sum_{n=1}^{N} D_n \frac{1 - \exp[-\lambda_n \Delta\psi^t]}{\lambda_n \Delta\psi^t} \right] \sigma^t \\ & - g_1^t \sum_{n=1}^{N} D_n \left[\exp[-\lambda_n \Delta\psi^t] q_n^{t-\Delta t} - g_2^{t-\Delta t} (1 - \exp[-\lambda_n \Delta\psi^t]) \frac{\sigma^{t-\Delta t}}{\lambda_n \Delta\psi^t} \right] \end{aligned} \tag{2.20}$$

Current incremental strain is:

$$\Delta\varepsilon^t = \varepsilon^t - \varepsilon^{t-\Delta t} = (\tilde{D}^t\sigma^t - \tilde{D}^{t-\Delta t}\sigma^{t-\Delta t}) - (f^t - f^{t-\Delta t}) \tag{2.21}$$

This reaches computational complexity reduction from $O(T^2)$ to $O(T \cdot N)$ while maintaining equivalence to hereditary integral formulation.

2.3.3. Physical Parameter Roles

Understanding parameter roles enables appreciation of how approaches aid traditional modelling while preserving physical meaning. The framework reveals a natural separation between physics parameters and stress-dependent functions that may benefit from representation approaches. **Instantaneous compliance (D_0)** represents the instantaneous elastic response before time-dependent viscoelastic effects become significant. Physically analogous to the spring component in Figure 2.1, this quantifies immediate, reversible deformation that remains well-characterised through experimental methods. **Relaxation timescales (τ_i)** define characteristic times governing viscous response mechanisms across multiple scales. Small values correspond to fast molecular processes, whilst large values represent slow bulk polymer rearrangement. These create a temporal hierarchy necessary for multi-scale material representation, as shown in Figure 2.2, which means physics that benefits from preservation rather than modification.

Prony coefficients (D_i) represent the magnitudes of each relaxation timescale, controlling the exponential mode strength. These serve as components in approaches where determination becomes important for characterisation, yet they remain within physics frameworks. Lastly, **Nonlinearity functions (g_0, g_1, g_2)** capture stress-dependent scaling effects introducing material nonlinearity. These represent the challenge in viscoelastic modelling, as representation determines the prediction ability under stress conditions.

2.3.4. Traditional Polynomial Limitations

Traditional methodologies employ polynomial functions for Schapery nonlinear parameters, creating limitations that constrain material characterisation whilst potentially masking material behaviour :

$$g_0(\sigma) = a_0 + a_1\sigma + a_2\sigma^2 + \dots \tag{2.22}$$

$$g_1(\sigma) = b_0 + b_1\sigma + b_2\sigma^2 + \dots \tag{2.23}$$

$$g_2(\sigma) = c_0 + c_1\sigma + c_2\sigma^2 + \dots \tag{2.24}$$

This suffers from the constraint problem where polynomials impose functional forms that cannot capture sharp transitions, plateaus, or discontinuous slope changes characteristic of real material behaviour. Even high-order polynomials represent single curves that average out local behaviours, potentially missing material characteristics that could inform material understanding. Polynomials typically fitted to experimental datasets tend to overfit, capturing experimental particulars rather than underlying material laws. This single-condition bias limits generalisation across loading conditions while potentially concealing material behaviour patterns that transcend experimental limitations. The mathematical constraint arises from the polynomial nature, where any polynomial of degree n has exactly n derivatives, creating limitations in representing local behaviours that require different mathematical descriptions in different stress regions. This motivates approaches that discover material behaviour rather than forcing predetermined mathematical forms, potentially revealing material physics that polynomial constraints have obscured.

2.4. Established Parameter Framework for HDPE Synthetic Fibres

2.4.1. Validated Material Parameters

Implementation of Schapery-Prony framework for High-Density Polyethylene (HDPE) synthetic fibres uses experimental characterisation that provides parameters for synthetic training data while keeping connection to physical material behaviour. The work of Lai and Nguyen [32, 38] represents a significant contribution to synthetic fibre modelling, demonstrating how polynomial approaches can achieve agreement with experimental data and highlighting the mathematical constraints inherent in predetermined

functional forms. Table 2.1 presents the parameter framework that allows for the generation of synthetic datasets while maintaining physical consistency with material characterisation. This framework represents current polynomial-based approaches, providing a foundation while showing opportunities for representation beyond mathematical constraints.

Table 2.1: Viscoelastic parameters for HDPE synthetic fibres from experimental characterisation.

Parameter	Expression/Value
a_σ	$(6.290\text{E-}06)\sigma^6 - (3.110\text{E-}04)\sigma^5 + (5.487\text{E-}03)\sigma^4 - 0.0375\sigma^3 + 0.02362\sigma^2 + 0.509\sigma + 1.010$
g_0	1.0
g_1	$4.723\text{E-}24\sigma^3 + 6.547\text{E-}16\sigma^2 + 3.897\text{E-}10\sigma + 1.003$
g_2	$5.956\text{E-}22\sigma^3 - 1.287\text{E-}14\sigma^2 + 1.273\text{E-}07\sigma + 1.002$

n	λ_n (s^{-1})	D_n (10^{-4} MPa^{-1})
1	1	2.23
2	10^{-1}	2.27
3	10^{-2}	1.95
4	10^{-3}	3.50
5	10^{-4}	5.50
6	10^{-5}	5.50
$D_0 = 2.205e-04$ (MPa^{-1})		

These parameters represent a polynomial approach to nonlinear function representation, where functions g_1 and g_2 are polynomial equations whilst g_0 remains constant. The parameter a_σ represents time-scaling effects disregarded in this research for simplicity.

2.4.2. Framework Validation

The framework aligns with experimental observations across multiple loading conditions, as illustrated in Figure 2.3. Validation encompasses stress-strain relationships and temporal response characteristics under various loading rates, thereby confirming the framework's validity within the tested conditions.

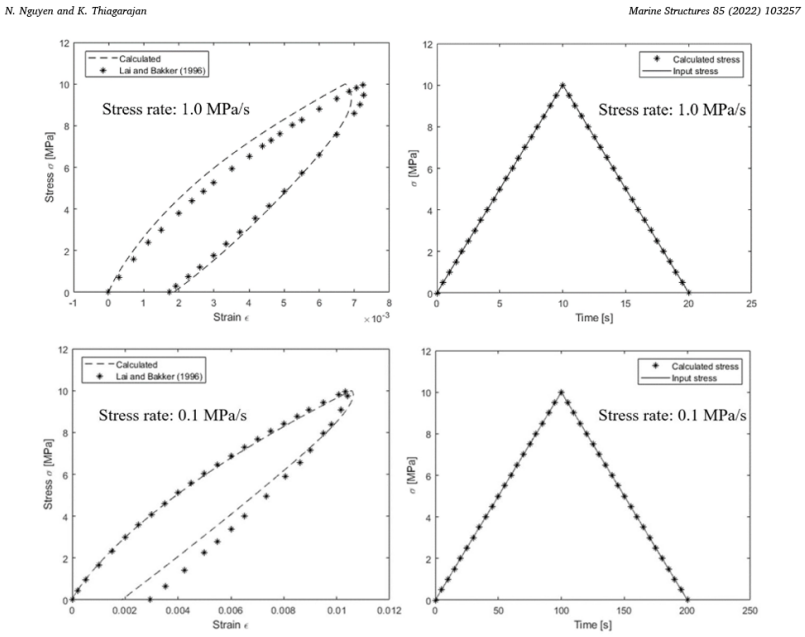

Figure 2.3: Validation of Schapery-Prony framework against experimental data for HDPE synthetic fibres.

The framework serves as a foundation for generating synthetic training data through the twin experiment methodology in Chapter 3, whilst providing a baseline for exploring whether approaches can discover material behaviour patterns beyond current polynomial representations.

2.5. Loading Patterns and Material Exercising Principles

2.5.1. Information Theory Foundation

Material characterisation depends on how experimental protocols exercise material mechanisms across operational ranges. Yet, traditional approaches often focus on mathematical convenience rather than the potential for material discovery. Information theory explains why specific loading patterns provide better material characterisation by enabling the discovery of material behaviour patterns rather than confirming mathematical assumptions, as shown in Chapter 4. The information content of loading patterns relates to their ability to activate different material mechanisms simultaneously, while providing distinguishable responses, thereby allowing for the identification of parameters. Patterns with rich frequency content exercise multiple relaxation modes, whilst stress levels activate nonlinear material responses, creating opportunities for discovering material behaviour patterns beyond traditional mathematical constraints, rather than checking predetermined functional forms.

Stress inputs to the Schapery-Prony framework take the form of time-varying loading patterns designed to exercise different aspects of viscoelastic behaviour. These represent inputs where stress histories $\sigma(t)$ are processed through incremental strain formulation to generate corresponding strain responses $\varepsilon(t)$, enabling discovery of material behaviour patterns through material exercising rather than targeted confirmation of polynomial assumptions.

2.5.2. Loading Pattern Categories

Six loading pattern categories exercise different aspects of viscoelastic behaviour, each with characteristics that reveal their material properties rather than their ability to conform to predetermined mathematical forms.

Cyclic loading employs sinusoidal stress variations as shown in Figure 2.4, incorporating multiple amplitudes at the same frequency value.

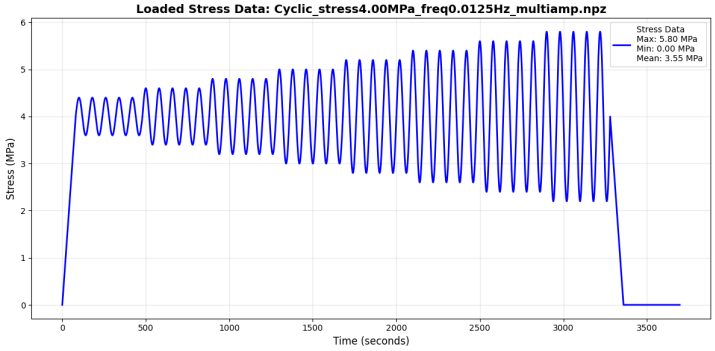

Figure 2.4: Cyclic loading pattern with sinusoidal stress variation.

Multi-step cyclic loading combines step transitions with cyclic movement on every stress level as shown in Figure 2.5, generated through stepping mechanisms incorporating cyclic phases with varying amplitude and frequency.

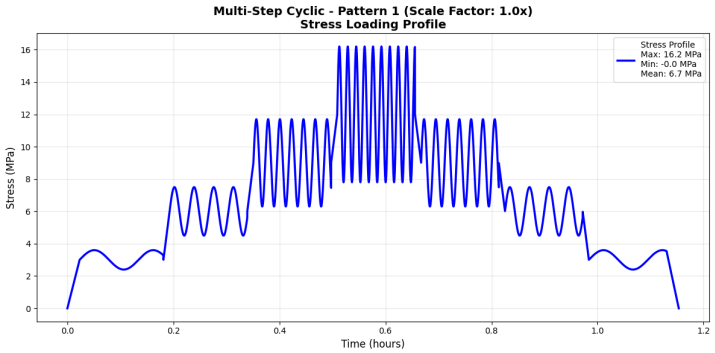

Figure 2.5: Multi-step cyclic loading combining step transitions with cyclic components.

Multi-frequency loading provides frequency-domain exercising through the combination of harmonic content, as shown in Figure 2.6, by combining multiple frequency components to exercise different relaxation mechanisms.

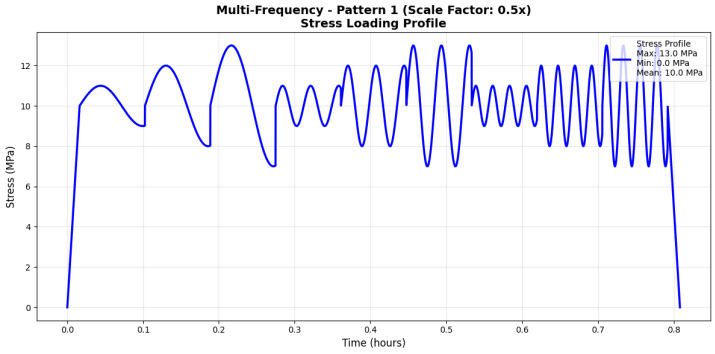

Figure 2.6: Multi-frequency loading with harmonic content.

Multi-step loading reaches material exercising through parameter activation across stress levels and temporal scales, as shown in Figure 2.7. Sharp stress transitions create rich frequency content probing fast relaxation modes, whilst long hold periods provide zero-frequency components for observing slow creep behaviour.

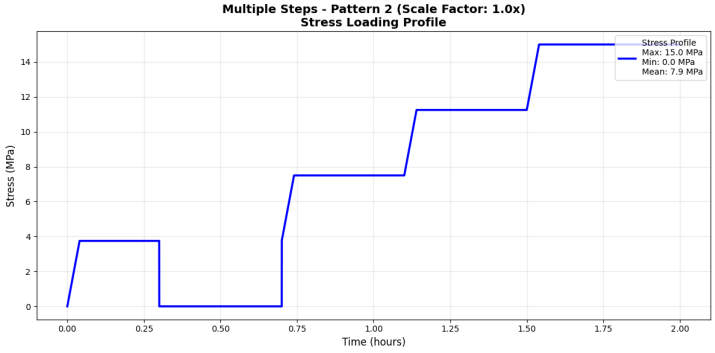

Figure 2.7: Multi-step loading with stress level progression.

Step-and-hold loading enables targeted long-term relaxation testing through sustained stress levels followed by relaxation periods, as shown in Figure 2.8, targeting slow relaxation modes for characterisation.

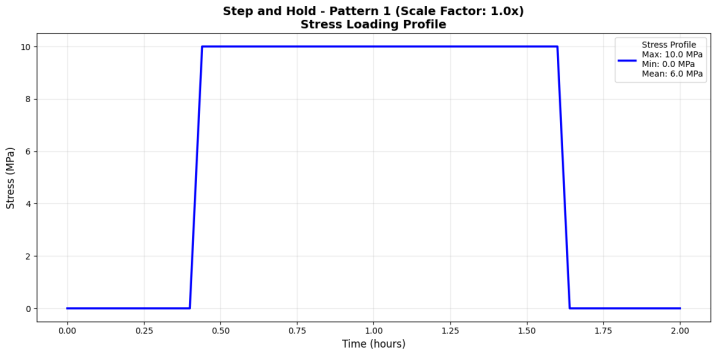

Figure 2.8: Step and hold loading for long-term relaxation characterisation.

Triangle loading implements controlled loading and unloading cycles, enabling the characterisation of hysteresis and recovery behaviour, as shown in Figure 2.9. This approach provides controlled stress rate variations while maintaining simple mathematical descriptions.

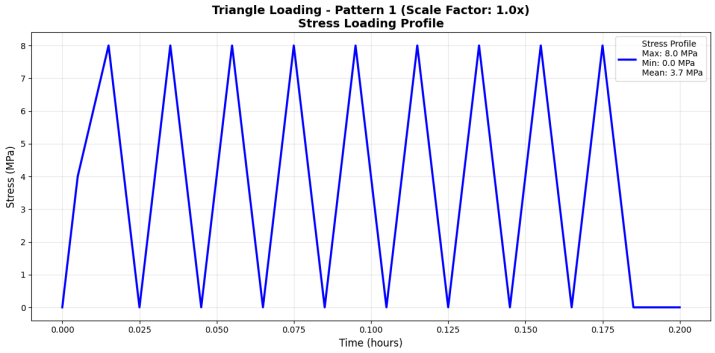

Figure 2.9: Triangle loading with controlled loading and unloading cycles.

These loading patterns serve as stress inputs processed through the Schapery-Prony framework to generate corresponding strain outputs, forming the foundation for datasets capturing viscoelastic behaviour across different loading scenarios. The diversity of patterns enables the discovery of material behaviour patterns that may be obscured when using limited experimental protocols focused on checking mathematical assumptions, as validated in Chapter 4.

2.6. Neural Networks and Machine Learning Foundations

2.6.1. Neural Networks vs Polynomial Approaches

Neural networks represent a shift in material modelling, moving from constraint-based polynomial fitting to discovery-based learning that shows actual material behaviour without predetermined mathematical assumptions. This theoretical foundation rests on mathematical proof that standard multilayer feedforward networks with as few as one hidden layer are capable of approximating any measurable function from one finite dimensional space to another to any desired degree of accuracy, provided sufficiently many hidden units are available, establishing that multilayer feedforward networks are a class of universal approximators [12, 22]. In this research context, neural networks offer a different approach to modelling Schapery nonlinearity functions g_0, g_1, and g_2, enabling the discovery of material behaviour through data-driven learning while maintaining physical consistency.

This addresses the constraint problem in polynomial approaches by allowing data to show underlying functional relationships rather than forcing them into predetermined mathematical forms. The Universal Approximation Theorem demonstrates that finite linear combinations of compositions of a fixed, univariate function and a set of affine functionals can uniformly approximate any continuous function of n real variables, enabling neural networks to learn functional relationships that govern material behaviour, sur-

passing the limitations imposed by polynomial assumptions in traditional approaches [12]. Traditional material modelling asks: ”How can we fit material behaviour into our preferred mathematical forms?” Approaches ask: ”What mathematical forms best represent material behaviour?” This distinction helps uncover material physics that mathematical constraints in historical computational approaches may have obscured.

2.6.2. Multi-Layer Perceptron Architecture

Multi-Layer Perceptrons represent the neural network architecture employed for learning Schapery nonlinear functions. The mathematical structure implements function composition through successive transformations:

$$f(x) = f^{(L)} \circ f^{(L-1)} \circ \ldots \circ f^{(2)} \circ f^{(1)}(x) \tag{2.25}$$

Each layer transformation follows the basic neural network operation:

$$h^{(l)} = \phi^{(l)} \left(W^{(l)} h^{(l-1)} + b^{(l)} \right) \tag{2.26}$$

Where $W^{(l)}$ and $b^{(l)}$ represent weight matrices and bias vectors, respectively, whilst $\phi^{(l)}$ denotes the nonlinear activation function enabling pattern recognition that goes beyond polynomial limitations. The network architecture processes normalised stress inputs through multiple hidden layers to generate corresponding nonlinear function outputs. This represents a departure from polynomial approaches, where networks learn stress-dependent relationships through training rather than assuming predetermined functional forms that may not accurately reflect the underlying material physics. Figure 2.10 shows the MLP architecture where stress inputs are processed through successive hidden layers, each applying linear transformations followed by nonlinear activation functions.

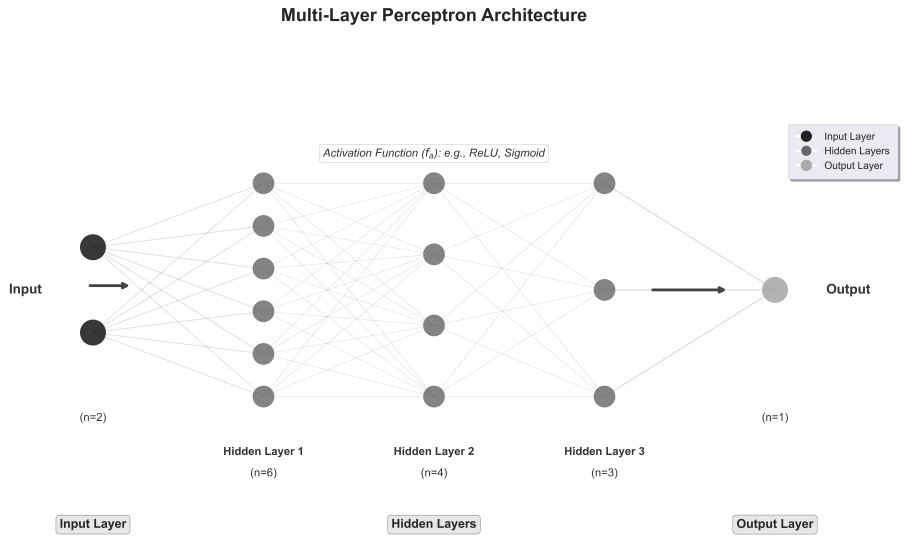

Figure 2.10: Multi-Layer Perceptron architecture for stress-dependent function learning.

The feedforward architecture proves appropriate for learning static nonlinear functions g_0, g_1, and g_2 that depend only on the current stress state, rather than temporal sequences, distinguishing it from recurrent architectures designed for temporal sequence modelling while focusing learning on stress-dependent behaviour patterns.

2.6.3. Universal Approximation Capabilities

The theoretical foundation for neural network function approximation rests on the Universal Approximation Theorem, which demonstrates that feedforward networks can approximate continuous functions

to arbitrary accuracy without imposing constraints on functional forms. For any continuous function f defined on compact subset K and any $\epsilon > 0$, there exists a neural network N such that:

$$\sup_{x \in K} |f(x) - N(x)| < \epsilon \tag{2.27}$$

This theoretical guarantee enables neural networks to discover material behaviour rather than being constrained by predetermined functional forms. Neural networks learn appropriate representations through piecewise-linear approximations that capture local behaviours impossible with global polynomial constraints. The significance emerges from the guarantee that sufficiently wide neural networks can approximate any continuous function to a desired accuracy. This is particularly important for materials modelling, where functional forms of nonlinear relationships may be unknown, requiring flexible approximation methods rather than polynomial assumptions, as shown in Chapter 4. The Universal Approximation Theorem alters our approach to material characterisation: instead of asking "which polynomial order best fits our data," we can ask "what functional relationships do our materials exhibit?" This shift from fitting to discovery enables the identification of material behaviour patterns that polynomial constraints may have prevented us from recognising.

2.6.4. Activation Functions

Activation functions introduce nonlinearity, enabling neural networks to learn patterns beyond linear relationships. The Rectified Linear Unit (ReLU) provides computational efficiency while addressing vanishing gradient problems:

$$\text{ReLU}(x) = \max(0, x) \tag{2.28}$$

ReLU offers computational simplicity, preserves gradients for positive inputs, and promotes sparsity. This makes ReLU suitable for hidden layers in networks learning Schapery nonlinearity functions, enabling pattern recognition whilst maintaining the computational efficiency needed for implementation. Other activation functions include hyperbolic tangent:

$$\tanh(x) = \frac{e^x - e^{-x}}{e^x + e^{-x}} \tag{2.29}$$

Sigmoid functions provide smooth, bounded outputs:

$$\text{sigmoid}(x) = \frac{1}{1 + e^{-x}} \tag{2.30}$$

Leaky ReLU addresses the "dying ReLU" problem by allowing small negative gradients:

$$\text{LeakyReLU}(x) = \begin{cases} x & \text{if } x > 0 \\ \alpha x & \text{if } x \leq 0 \end{cases} \tag{2.31}$$

For applications requiring positive outputs, Softplus ensures physical constraints whilst maintaining differentiability:

$$\text{Softplus}(x) = \ln(1 + e^x) \tag{2.32}$$

Softplus guarantees positive outputs needed for Schapery nonlinearity functions g_0, g_1, and g_2, which must remain positive for physical consistency, as implemented in Chapter 3. This activation function enables the discovery of material behaviour patterns while maintaining the physically meaningfulness needed for engineering applications.

2.6.5. Optimisation Algorithms

Neural network training requires optimisation algorithms navigating parameter spaces whilst handling diverse parameter types and scales typical of hybrid physics-neural approaches.

Stochastic Gradient Descent (SGD) provides a basic approach through iterative parameter updates:

$$\theta_t = \theta_{t-1} - \alpha g_t \tag{2.33}$$

SGD with momentum incorporates historical gradient information to accelerate convergence:

$$\theta_t = \theta_{t-1} - \alpha \left(\beta m_{t-1} + (1-\beta) g_t\right) \tag{2.34}$$

The Adam algorithm combines adaptive learning rates with momentum for convergence, where the method is straightforward to implement, is computationally efficient, has little memory requirements, and is invariant to diagonal rescaling of the gradients [29]:

$$m_t = \beta_1 m_{t-1} + (1-\beta_1) g_t \tag{2.35}$$

$$v_t = \beta_2 v_{t-1} + (1-\beta_2) g_t^2 \tag{2.36}$$

$$\theta_t = \theta_{t-1} - \alpha \frac{\hat{m}_t}{\sqrt{\hat{v}_t} + \epsilon} \tag{2.37}$$

Adam's adaptive nature proves valuable for hybrid physics-neural approaches, where different parameter types exhibit varying scales and update frequencies, enabling the discovery of material behaviour patterns while maintaining the computational stability needed for material characterisation, as implemented in Chapter 3.

RMSprop addresses gradient scaling challenges through adaptive learning rates:

$$\theta_t = \theta_{t-1} - \frac{\alpha}{\sqrt{v_t + \epsilon}} g_t \tag{2.38}$$

AdaGrad provides adaptive learning rates that decrease over time:

$$\theta_t = \theta_{t-1} - \frac{\alpha}{\sqrt{G_t + \epsilon}} g_t \tag{2.39}$$

The choice depends on problem characteristics, with Adam often providing performance across applications, for discovering material behaviour patterns that may challenge traditional polynomial representations.

2.7. Loss Functions for Materials Modelling

2.7.1. Traditional Loss Functions and Limitations

Loss functions affect what neural networks learn by defining optimisation objectives that guide parameter updates during discovery processes [54]. Understanding the theoretical foundations and experimental performance characteristics of different loss functions proves essential for materials modelling applications, as comprehensive analysis shows that loss function selection significantly influences the performance of models across different tasks, with theoretical discussion and experimental research revealing how various formulations affect both classification and regression applications [54]. For materials modelling applications, loss function selection is crucial since different formulations can lead to distinct learned behaviours, potentially enabling or limiting the discovery of material characteristics.

Mean Squared Error (MSE) represents the most common loss function:

$$\mathcal{L}_{MSE} = \frac{1}{n}\sum_{i=1}^{n}(y_i - \hat{y}_i)^2 \tag{2.40}$$

MSE offers computational simplicity and differentiability, but it has a dimensional bias when the training data spans multiple orders of magnitude. Significant absolute errors dominate optimisation while proportional accuracy receives insufficient attention, potentially limiting the discovery of material behaviour patterns that manifest across different stress ranges.

Mean Absolute Error (MAE) has reduced sensitivity to outliers:

$$\mathcal{L}_{MAE} = \frac{1}{n}\sum_{i=1}^{n}|y_i - \hat{y}_i| \tag{2.41}$$

MAE provides more optimisation but keeps similar dimensional bias characteristics where large absolute values dominate optimisation, potentially limiting the discovery of material patterns that occur across operational ranges.

2.7.2. Scale-Invariant Loss Functions

Materials exhibiting wide dynamic ranges create optimisation challenges that require scale-invariant approaches, ensuring balanced learning across operational envelopes while enabling the discovery of material behaviour patterns without bias toward stress regions.

Percentage Difference (PD) loss addresses heteroscedasticity through relative error formulation:

$$\mathcal{L}_{PD} = \sqrt{\frac{\sum_{i=1}^{N}(\varepsilon_{pred,i} - \varepsilon_{actual,i})^2}{\sum_{i=1}^{N}(\varepsilon_{actual,i})^2 + \epsilon}} \tag{2.42}$$

Where ϵ prevents division by zero, this ensures that optimisation attention remains proportional across all response magnitudes, achieving scale-invariant properties necessary for material characterisation without bias toward specific operational regions, as validated in Chapter 4.

Amplitude Ratio (AR) loss focuses on relative magnitude relationships:

$$\mathcal{L}_{AR} = \frac{1}{n}\sum_{i=1}^{n}\left|\frac{y_i - \hat{y}_i}{y_i}\right| \tag{2.43}$$

Scale-invariant loss functions are necessary for material discovery because they enable neural networks to learn material behaviour patterns across operational envelopes, rather than focusing on mathematically convenient regions that may not represent the full spectrum of material physics.

2.7.3. Frequency Domain Loss Functions

Fast Fourier Transform (FFT) based loss functions operate in the frequency domain to emphasise spectral content matching:

$$\mathcal{L}_{FFT} = \frac{1}{n}\sum_{i=1}^{n}|\mathcal{F}\{y\}_i - \mathcal{F}\{\hat{y}\}_i| \tag{2.44}$$

where $\mathcal{F}\{\}$ denotes the Fourier transform. This is particularly relevant for viscoelastic materials, where frequency domain characteristics influence material behaviour, enabling the discovery of frequency-dependent material patterns that may be obscured by time-domain fitting approaches, as shown in Chapter 4. Frequency domain loss functions enable the discovery of spectral characteristics that traditional time-domain approaches may miss, potentially revealing frequency-dependent material behaviour patterns beyond assumptions in polynomial representations.

2.8. Statistical Analysis and Uncertainty Quantification

2.8.1. Confidence Intervals

Statistical analysis helps quantify model reliability and creates confidence bounds needed for engineering applications of material behaviour patterns. The bootstrap methodology has proven effective for determining confidence intervals in engineering applications where traditional statistical assumptions may not hold [6]. Bootstrapping provides confidence intervals for parameters related to the distribution of simulation output statistics, particularly when output distributions are non-normal. Confidence intervals indicate ranges within which parameter values are likely to reside, given specific probability levels, enabling the assessment of discovery reliability. For the parameter estimate $\hat{\theta}$ derived from sample data, the confidence interval at confidence level $(1-\alpha)$ satisfies:

$$P(L \leq \theta \leq U) = 1 - \alpha \tag{2.45}$$

Bootstrap methodology creates confidence intervals through resampling approaches, creating multiple dataset versions from limited experimental data:

$$CI_{1-\alpha} = \left[\hat{\theta}_{(\alpha/2)}, \hat{\theta}_{(1-\alpha/2)}\right] \tag{2.46}$$

Bootstrap methods are well-suited for materials modelling, where experimental data limitations restrict traditional statistical approaches and where parameter distributions may not conform to standard assumptions, enabling the quantification of discovery reliability without imposing mathematical constraints on material behaviour patterns.

2.8.2. Box Plot Analysis

Box plots provide visualisation of data distribution characteristics through quartile-based representations, highlighting central tendency, spread, and the presence of outliers in material behaviour patterns. The box plot serves as a simple visual method to interpret data, using the median, the approximate quartiles, and the lowest and highest data points to convey the level, spread, and symmetry of a distribution of data values [57]. Box plot construction begins with a five-number summary: minimum, first quartile (Q_1), median (Q_2), third quartile (Q_3), and maximum values:

$$Q_1 = \text{Percentile}_{25}(X) \tag{2.47}$$
$$Q_2 = \text{Percentile}_{50}(X) \tag{2.48}$$
$$Q_3 = \text{Percentile}_{75}(X) \tag{2.49}$$

Interquartile range (IQR) provides measures of data spread:

$$IQR = Q_3 - Q_1 \tag{2.50}$$

Outlier identification follows the criteria:

$$\text{Lower Fence} = Q_1 - 1.5 \times IQR \tag{2.51}$$
$$\text{Upper Fence} = Q_3 + 1.5 \times IQR \tag{2.52}$$

This provides identification of unusual measurements that may indicate material behaviour or experimental errors, requiring further investigation, while enabling the assessment of material patterns with statistical rigour.

2.9. Latin Hypercube Sampling and Design of Experiments

2.9.1. Space-Filling Experimental Design

Latin Hypercube Sampling enables the exploration of high-dimensional parameter spaces while maintaining the computational efficiency required for model development beyond traditional polynomial constraints. LHS provides several methods for creating and augmenting Latin Hypercube Samples, ensuring balanced exploration across all parameter dimensions simultaneously [25]. For a hyperparameter space with d dimensions, LHS generates n sample points such that each dimension is divided into n equally probable intervals, with exactly one sample point in each interval. LHS point generation follows:

$$x_{i,j} = \frac{\pi_j(i) - u_{i,j}}{n} \tag{2.53}$$

Where $u_{i,j}$ represents uniform random variables providing variability within each interval whilst maintaining stratification properties. Final sample points are scaled to the desired parameter ranges:

$$\mathbf{x}_i = \mathbf{L} + (\mathbf{U} - \mathbf{L}) \odot \mathbf{s}_i \tag{2.54}$$

LHS ensures that every hyperparameter dimension receives exactly n samples, distributed across its entire range, allowing for exploration regardless of dimensionality while enabling the discovery of configurations for material behaviour learning.

2.9.2. Space Refinement

LHS enables iterative refinement approaches that combine sampling with performance feedback to focus searches on promising parameter regions, thereby allowing for more effective material discovery. Space contraction follows mathematical frameworks:

$$\mathbf{L}^{(k+1)} = \mathbf{P}_{best}^{(k)} - \alpha \cdot (\mathbf{P}_{best}^{(k)} - \mathbf{L}^{(k)}) \tag{2.55}$$

$$\mathbf{U}^{(k+1)} = \mathbf{P}_{best}^{(k)} + \alpha \cdot (\mathbf{U}^{(k)} - \mathbf{P}_{best}^{(k)}) \tag{2.56}$$

where $\mathbf{P}_{best}^{(k)}$ represents best-performing configuration and α represents contraction factor balancing exploration with refinement. The convergence criterion can be expressed through performance consistency:

$$\text{Convergence} = \frac{\sigma_{performance}}{\mu_{performance}} < \epsilon_{convergence} \tag{2.57}$$

Figure 2.11 shows space refinement where the initial broad hyperparameter space undergoes contraction around promising regions that enable material discovery.

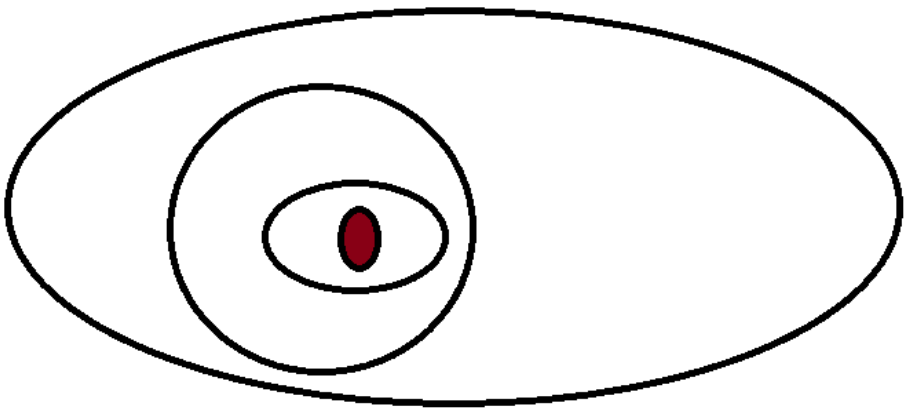

Figure 2.11: Hyperparameter space refinement through space contraction.

This allows optimisation across high-dimensional parameter spaces while maintaining computational efficiency needed for discovering configurations that would enable material behaviour learning beyond traditional polynomial constraints, as implemented in Chapter 3.

2.10. Current Material Characterisation Approaches

2.10.1. Time-Temperature Superposition

Traditional material characterisation approaches use time-temperature superposition principles, where material behaviour at different temperatures constructs master curves spanning extended ranges [39, 5]. This allows for the characterisation of material behaviour by using temperature-dependent acceleration of material processes. However, mathematical assumptions about the separability of effects constrain these approaches. However, time-temperature superposition requires experimental programmes across multiple temperatures and assumes that temperature effects can be separated from other material dependencies. For loading conditions and stress-dependent materials, these assumptions may not hold, potentially limiting the discovery of material behaviour patterns beyond traditional mathematical separability assumptions.

2.10.2. Parametric Methods

Parametric methods use mathematical relationships to characterise creep and stress relaxation data across extended ranges [24, 8]. These approaches fit experimental data to functional forms, including power laws, logarithmic functions, or exponential relationships, then use fitted parameters for characterisation across broader ranges. While parametric methods can provide characterisation for some materials, they have limitations similar to polynomial representations: functional forms that may not capture material behaviour and poor performance when the assumed functional form proves incorrect. The constraint lies in predetermined mathematical assumptions rather than material discovery.

2.10.3. Machine Learning Approaches

Machine learning has introduced various approaches to materials modelling and characterisation [45, 7]. Pure neural network approaches work well for interpolation within training ranges but often work poorly beyond training because they lack physical grounding and tend to overfit to training particulars. Neural network approaches that incorporate physics principles aim to address limitations by directly integrating physical laws into training [44, 3]. However, most work focuses on solving partial differential equations rather than learning constitutive relationships for materials, thereby missing opportunities to discover material behaviour patterns. Hybrid approaches that combine neural networks with physics frameworks represent a new area of research [30, 52], but methodologies for developing hybrid models are currently limited. The challenge lies in integrating data-driven learning with physical constraints while maintaining both accuracy and physical consistency needed for discovering material behaviour, as addressed through this research.

2.11. Research Opportunities

Current nonlinear viscoelastic modelling approaches have limitations that create opportunities for innovation through the discovery of material behaviour, rather than relying on mathematical constraints. The challenge involves balancing the tension between mathematical tractability and physical accuracy while maintaining what is necessary for engineering applications that may require a deeper understanding of materials beyond current mathematical limitations. The integration challenge comes from existing methods struggling to combine data-driven learning with physical constraints, often losing either discovery or physical consistency. Traditional approaches force material behaviour into predetermined mathematical forms, potentially hiding material patterns that could inform engineering understanding. Scale-invariant optimisation has difficulties where traditional loss functions create dimensional bias, reducing the ability to learn across wide dynamic ranges typical of viscoelastic materials. This bias may prevent the discovery of material behaviour patterns that manifest differently across operational ranges, limiting our understanding of material physics.

Data use is another area where methodologies for using experimental loading patterns in neural network training are underdeveloped. Current approaches often focus on checking predetermined mathematical assumptions rather than discovering material behaviour patterns beyond those assumptions.

Statistical reliability frameworks face challenges, particularly in the absence of strategies for creating confidence bounds on model predictions, which limits the deployment of models in engineering applications. Traditional statistical methods assume mathematical forms that may not accurately reflect material behaviour, potentially reducing the reliability of assessments. These challenges present opportunities for improvement through the integration of neural networks with physics frameworks, while maintaining the requirements necessary for engineering applications. The path forward involves integrating neural networks within proven physical frameworks, rather than abandoning principles, enabling the discovery of material behaviour patterns while preserving the theoretical rigour needed for engineering deployment.

2.12. Summary

The review covers the theoretical foundation for integrating neural networks with viscoelastic frameworks through the discovery of material behaviour. The review shows that while traditional polynomial approaches are mathematically tractable, their functional forms limit the discovery of material behaviour. The Universal Approximation Theorem provides theoretical justification for replacing these constrained representations with neural network approximations, enabling materials to exhibit their behaviour patterns. The path forward involves integrating neural networks within the Schapery-Prony framework, rather than abandoning physical principles. By using neural networks to learn only stress-dependent nonlinearity functions while preserving the temporal evolution framework based on physics, these approaches address limitations while maintaining the physical foundation required for engineering applications. The methodology detailed in Chapter 3 provides approaches for this integration. In contrast, the validation presented in Chapter 4 demonstrates the neural network integration for material characterisation, addressing the challenges identified in this review. This shift from constraint-based fitting to discovery-based learning enables material characterisation while preserving the theoretical rigour needed for engineering deployment.

3

Theoretical Framework and Computational Methodology

Following the theoretical foundations presented in Chapter 2, this chapter outlines the methodology developed to achieve material characterisation through the integration of neural networks with physics frameworks. The challenge involves translating theoretical concepts into a working computational system that can systematically discover material behaviour patterns through improved nonlinear function learning rather than being limited by polynomial assumptions. This methodology addresses three implementation challenges that arise when moving from theory to practice. First, traditional polynomial approaches for representing material nonlinearity are too rigid to capture the stress-dependent behaviour observed in real materials, as shown in Chapter 2. Second, neural networks, while flexible, can learn physically meaningless relationships unless guided by physical principles that ensure the temporal evolution accuracy required for engineering applications, while also enabling the representation of stress-dependent material characteristics [44]. Third, validating neural integration requires a systematic investigation to identify which methodological choices enable material understanding versus those that only improve short-term performance metrics without revealing material behaviour.

These challenges require a systematic five-phase development process for neural integration, where each phase builds upon results from the previous stage whilst maintaining adherence to physical principles throughout the material characterisation process. The approach enables exploration of how neural networks can replace polynomial constraints while preserving the physics that governs temporal material behaviour.

3.1. Framework Verification

The computational implementation shows that the incremental strain formulation detailed in Chapter 2 correctly processes stress inputs through Schapery-Prony parameters [49] to generate corresponding strain responses. This validation provides confidence that our computational foundation functions properly before proceeding to neural network integration, ensuring that discovered material behaviour patterns reflect physics rather than computational artefacts.

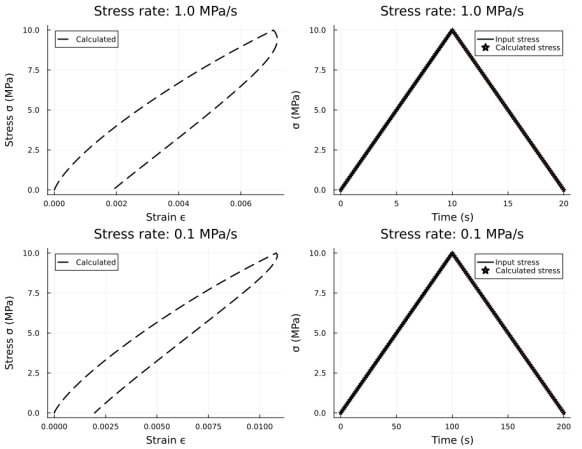

(a) Strain response without a_σ parameter.

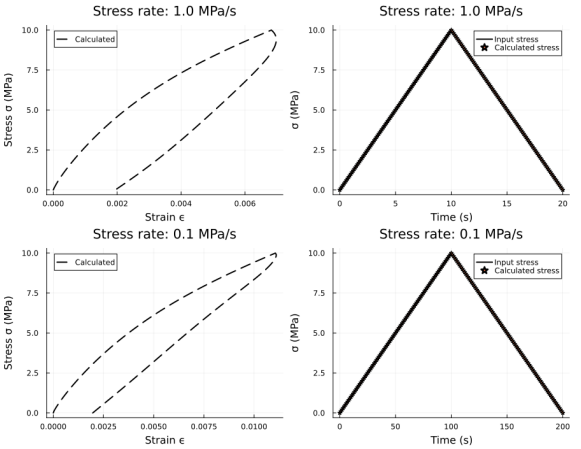

(b) Strain response with a_σ parameter included.

Figure 3.1: Framework validation with and without a_σ parameter.

Figure 3.1 shows that excluding the a_σ parameter produces minimal differences in strain response predictions. This validates the simplification approach while maintaining a physics representation for subsequent neural network integration methodologies that focus on discovering representations for stress-dependent functions rather than time-scaling effects. The strain responses show agreement between both implementations, with differences remaining within engineering tolerances.

Algorithm 1 Polynomial Framework Validation Protocol

1: **Input:** Stress history $\sigma(t)$, HDPE parameters from Table 2.1
2: **Output:** Strain response $\varepsilon(t)$
3:
4: • Initialise internal state variables $q_i = 0$ for $i = 1, ..., N$
5: • For each time step: compute nonlinearity functions using Equations 2.22-2.24
6: • Update internal state variables using Equation 2.19
7: • Compute strain using Equation 2.21

Algorithm 1 processes stress inputs through the incremental strain formulation using a systematic step-by-step procedure [20, 38, 17]. This computational validation demonstrates the credibility of the framework. It confirms that our implementation accurately reproduces material behaviour before proceeding with neural network integration methodologies that aim to discover representations of material nonlinearity without compromising the proven temporal evolution framework. Recent validation studies [47] confirm that such incremental approaches achieve high accuracy when properly implemented.

3.2. Development Overview

Development follows a five-phase progression designed to address neural network integration challenges while maintaining mathematical rigour and physical consistency throughout the material characterisation process. This addresses the polynomial constraint problems shown in Chapter 2 through the integration of neural networks with physics frameworks, which enable the learning of material behaviour rather than mathematical fitting [9].

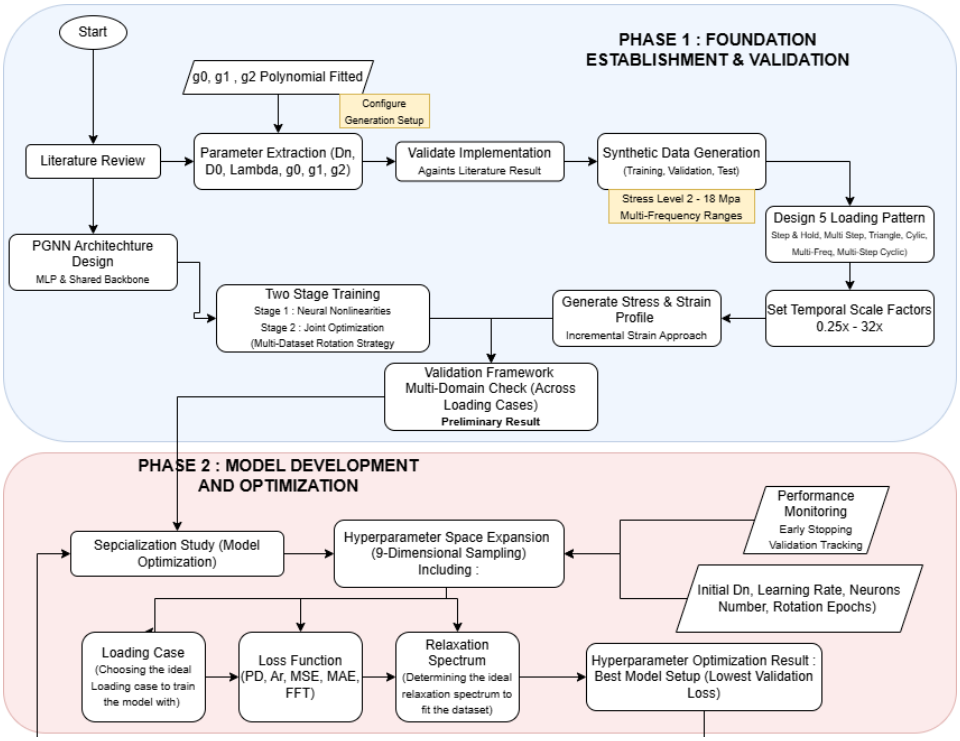

Figure 3.2: Research methodology progression.

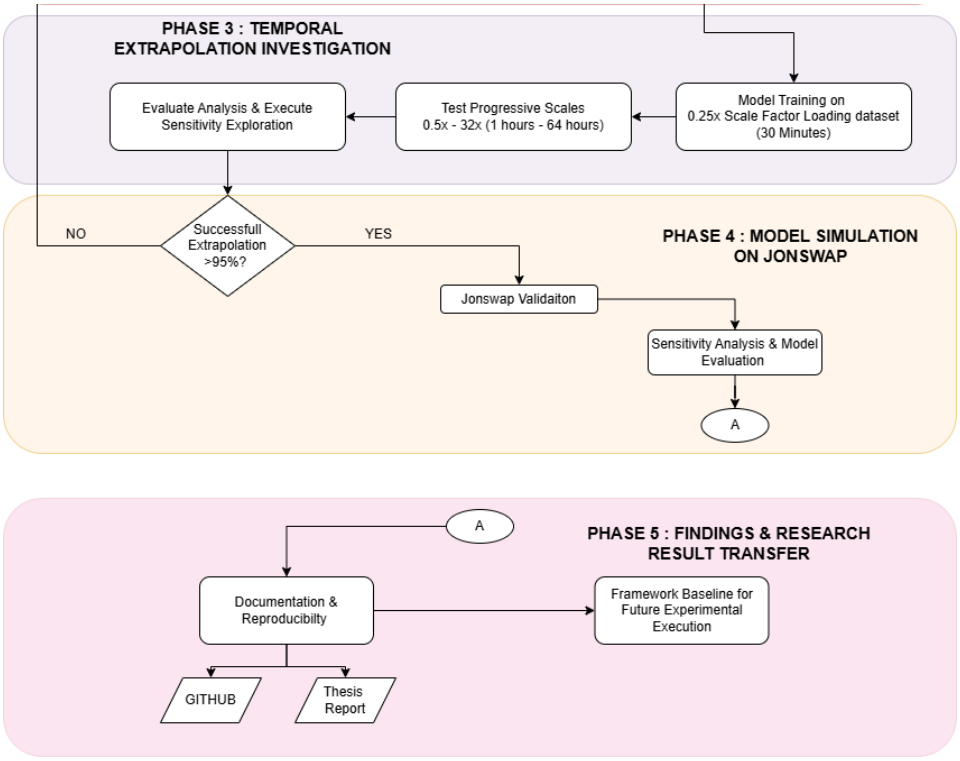

Figure 3.3: Implementation workflow with technical components and decision points.

Figures 3.2 and 3.3 illustrate the phase-by-phase development, where each phase builds upon previous results while addressing technical challenges in neural integration. The flowcharts guide understanding of the approach, showing how each phase contributes to development while maintaining decision

points and feedback loops that ensure neural networks discover material behaviour rather than learning spurious patterns. The five-phase approach came from recognising that developing neural integration needs more than simply combining neural networks with physics equations. Each phase addresses an aspect of the challenge: how do we build confidence that our model discovers material behaviour patterns rather than memorising training data or fitting to mathematical artefacts?

Phase 1 creates a solid foundation by exploring the vast space of possible configurations, ensuring our starting point represents optimality for material understanding rather than arbitrary choices that might bias neural learning. Phase 2 identifies the methodological decisions that most significantly impact material learning, providing evidence-based guidance rather than relying on intuition about neural integration approaches. Phase 3 tests the system's knowledge, revealing any limitations that standard evaluation cannot detect, whilst determining whether neural networks learned material physics. Phase 4 targets the root causes of identified limitations through diagnostic analysis, avoiding the standard approach of applying solutions to problems whilst focusing on physics improvements that enable better material understanding. Phase 5 validates that laboratory-developed learning maintains effectiveness when confronted with the complexity of real-world operational conditions.

Table 3.1: Five-phase methodology overview

Phase	Objective	Activities	Expected Outcome
Phase 1: Baseline Optimisation	Create baseline configuration for material understanding through exploration	13-dimensional Latin Hypercube Sampling across architecture, training, physics	Baseline configuration with validated learning
Phase 2: Sensitivity Analysis	Identify combinations across dimensions affecting learning capability	Exploration of loss functions, loading patterns, relaxation spectra	Evidence-based recommendations for material understanding approaches
Phase 3: Capability Testing	Test neural integration learning and identify limitations	Testing across scenarios	Identification of learning limitations and diagnostic insights
Phase 4: Model Refinement	Address identified limitations through refinement	Targeted improvements	Model reaching better learning
Phase 5: Marine Validation	Validate robustness under realistic operational conditions	JONSWAP marine loading across sea states	Confirmed deployment readiness under realistic conditions

Table 3.1 provides an overview of the research progression, illustrating how each phase contributes to building toward the goal of neural integration, which enables material understanding from limited experimental observations while maintaining the physical consistency required for engineering applications.

3.3. Data Generation and Twin Experiment Implementation

Neural network training requires large amounts of data to learn patterns and understand the material. However, physical testing of viscoelastic materials has its constraints. Multi-year experiments are needed to capture long-term behaviour, but these are economically and logistically challenging. In contrast, shorter tests may not exercise the full range of material mechanisms required for characterisation, which enables neural networks to discover material behaviour patterns. The twin experiment methodology [38] addresses this constraint by using material characterisation work as a "digital twin" that generates synthetic training data with known behaviour. This approach enables the exploration of loading conditions and parameter ranges that would be prohibitively expensive to study through physical experimentation, while maintaining a connection to validated material physics throughout the data generation process, which provides neural networks with material behaviour examples for learning. Following the computational validation in Section 3.1, the data generation framework extends our

verified implementation to create training scenarios. This transition moves from validating our computational foundation to utilising it for the systematic exploration of material behaviour through synthetic data generation.

3.3.1. Data Preprocessing and Standardisation Strategy

The preprocessing protocol ensures consistent data quality whilst maintaining physical meaning through standardisation approaches that address neural network training requirements for material understanding.

Standardisation Methodology

All training data is concatenated and standardised to the range $[-1, 1]$ based on global minimum and maximum values across the entire dataset.

Mathematical formulation:

$$x_{scaled} = 2 \cdot \frac{x - x_{min}}{x_{max} - x_{min}} - 1 \tag{3.1}$$

Scientific Rationale for $[-1, 1]$ Range

The $[-1, 1]$ range provides advantages over $[0, 1]$ normalisation for marine loading applications. Marine loading often involves oscillatory motions around a mean value from waves and vibrations. The $[-1, 1]$ range naturally accommodates positive and negative deviations from a centre point, where negative values correctly represent force or movement opposite to positive direction. For boundary handling, values outside the training range $[x_{min}, x_{max}]$ are correctly identified as cases that require special attention. This maintains clear delineation between interpolation and regimes whilst preserving the physical interpretation of loading directions.

Computational Efficiency Considerations

Standardisation proves necessary for neural network stability. Stress values in MPa (10^6 Pa) are too large for stable neural network training, creating a risk of exploding gradients where significant inputs cause enormous activations, leading to unstable gradient updates. Without standardisation, the optimiser cannot converge due to erratic gradient behaviour. Standardised values utilise the complete precision of floating-point representation, leading to more predictable computational costs during training.

3.3.2. Twin Experiment Methodology Implementation

The twin experiment approach generates synthetic training data whilst maintaining a connection to validated material physics using the HDPE parameters from Table 2.1 [32]:

Algorithm 2 Twin Experiment Data Generation Implementation

1: **Input:** Loading pattern specifications, stress ranges, HDPE parameters
2: **Output:** Synthetic dataset with known ground truth
3:
4: • Define loading pattern library covering material exercising for learning
5: • Specify stress ranges spanning operational and evaluation envelopes
6: • For each pattern-stress combination: create history, process through validated framework
7: • Generate corresponding strain response with known ground truth
8: • Store input-output pairs with metadata annotations
9: • Compile training dataset with coverage for neural learning

The twin experiment methodology in Algorithm 2 uses the validated polynomial framework from Section 3.1 to create datasets that would be impossible to generate through physical experimentation alone due to cost, time, and constraints. This provides neural networks with examples of material behaviour patterns that enable learning of stress-dependent relationships without being limited by experimental constraints.

3.3.3. Loading Pattern Generation Framework

The loading pattern library exercises different aspects of viscoelastic behaviour through stress history characteristics, with theoretical foundations detailed in Chapter 2, enabling neural networks to learn material behaviour patterns across operational ranges, taken as an example, Multi-Step Loading pattern:

Algorithm 3 Multi-Step Loading Pattern Generation

Input: Stress levels, hold durations, transition specifications
Output: Multi-step stress history with material exercising

• Initialise stress history with zero loading condition
• Define stress level progression for material exercising
• For each target stress: apply sharp transition, maintain constant stress
• Monitor for relaxation time coverage
• Apply controlled unloading sequence and validate pattern quality for learning

Algorithm 4 Data Preprocessing Protocol

Input: Raw synthetic datasets from twin experiment generation
Output: Preprocessed training data ready for neural network learning

• Compute global statistics across the dataset ensemble
• Calculate stress and strain ranges globally across all datasets
• For each dataset: apply standardisation to $[-1, 1]$ range using Equation 3.1
• Validate standardisation preserves physical relationships for learning
• Verify neural network input compatibility and training readiness

The standardisation approach in Algorithm 4 addresses neural network training requirements while preserving physical meaning through a mathematical transformation that maintains characteristics necessary for learning material behaviour patterns, rather than learning artefacts from data scaling.

3.4. Material Model Construction

The material model implementation translates the Schapery-Prony theory from Chapter 2 into a computational framework that allows for neural network integration while maintaining physics consistency and positivity constraints necessary for material understanding [52]. The approach separates physics parameters from stress-dependent functions that benefit from neural integration for learning material behaviour. This section builds upon the data generation framework presented in Section 3.3, transitioning from creating synthetic training data to constructing the model architecture that will learn from this data. The material model connects our physics understanding and the neural network components that will learn stress-dependent material behaviour.

3.4.1. Strategic Parameter Classification Implementation

The framework employs parameter separation, addressing identifiability problems discussed in Chapter 2 through a hybrid parameterisation approach that prevents ill-posed optimisation challenges whilst enabling targeted material understanding:

$$\text{Fixed Parameters:} \quad \{D_0, \lambda_i\} \text{ (from literature)} \tag{3.2}$$

$$\text{Trainable Physics:} \quad \{D_i\} \text{ (logarithmic domain optimisation)} \tag{3.3}$$

$$\text{Neural Parameters:} \quad \{\text{weights, biases}\} \text{ (learning-focused optimisation)} \tag{3.4}$$

Table 3.2: Strategic parameter classification for hybrid physics-neural network optimisation

Parameter Type	Parameters	Treatment	Implementation
Fixed Parameters	D_0, λ_i	Literature values from Table 2.1	Physical anchoring and scaffolding
Trainable Physics	D_i coefficients	Log-domain optimisation	Positivity constraints
Neural Parameters	Weights, biases	Standard gradient descent for learning	Flexible function approximation

Table 3.2 shows the classification strategy that provides physical scaffolding through fixed parameters whilst enabling adaptive learning through trainable components. This addresses the challenge that training all parameters simultaneously creates non-unique solutions where multiple parameter combinations produce similar strain responses, potentially preventing neural networks from learning material behaviour patterns.

3.4.2. Parameter Initialisation Implementation

The material parameters employ values from Chapter 2, Table 2.1, providing physical foundation for neural integration that enables material understanding: Instantaneous compliance (D_0) is fixed at 2.205×10^{-4} MPa^{-1} from experimental characterisation. Relaxation timescales (λ_i) use fixed distribution from 1×10^{0} to 1×10^{-5} seconds providing temporal hierarchy. Prony coefficients (D_i) are trainable parameters that control the strengths of the relaxation modes for learning. Initial D_i coefficients are selected through testing within physically reasonable ranges whilst ensuring positivity through logarithmic domain implementation detailed in Section 3.6. This provides neural networks with physically meaningful starting points for learning material representations.

3.4.3. Logarithmic Domain Training Implementation

The physics parameter training employs a logarithmic transformation, ensuring positivity constraints whilst enabling optimisation algorithms for material understanding:

Algorithm 5 Logarithmic Domain Physics Parameter Implementation

Input: Physics parameters requiring positivity constraints
Output: Positive parameters through log-domain training for learning

• Transform parameters to log domain: $p_i = \log(D_i)$ for all i
• For each training iteration: transform to physical domain $D_i = \exp(p_i)$
• Apply gradient chain rule: $\frac{\partial \mathcal{L}}{\partial p_i} = \frac{\partial \mathcal{L}}{\partial D_i} \cdot D_i$
• Update log-domain parameters: $p_i \leftarrow p_i - \alpha \nabla_{p_i} \mathcal{L}$
• Final transformation: $D_i = \exp(p_i)$ (guaranteed positive for physical consistency)

The logarithmic approach in Algorithm 5 resolves constraint optimisation challenges through mathematical transformation rather than algorithmic complexity, ensuring all D_i values remain positive whilst enabling standard optimisation algorithms for material understanding. This maintains physical meaningfulness whilst allowing neural networks to learn parameter distributions.

3.5. Neural Model Construction

The neural network implementation faces a design challenge: how do we use the flexibility of neural networks to learn material behaviour while ensuring the learned relationships remain physically meaningful? Traditional approaches either constrain neural networks so much that they lose their adaptive advantages, or allow such freedom that they learn spurious correlations that fail under new conditions without reflecting material physics. The approach addresses this tension through functional decomposition, where neural networks learn only the stress-dependent nonlinearity functions whilst the physics framework handles all temporal evolution [52]. This separation allows neural networks to focus on their strengths—learning functional relationships—while physics provides the temporal structure that

ensures learned behaviour remains consistent with material memory principles needed for learning material behaviour. Neural model construction builds upon the material model framework from Section 3.4, where we defined the hybrid parameter strategy. Now we implement the neural network components that will learn the stress-dependent functions within this physically grounded framework.

3.5.1. Shared Backbone Architecture Implementation

The architecture employs shared feature extraction feeding specialised heads for individual function learning, implementing the functional decomposition principle that separates neural network learning from physics-based temporal evolution:

$$\text{Shared Features:} \quad h_{shared} = \text{MLP}_{shared}[\sigma_{std}] \tag{3.5}$$

$$\text{Specialised Outputs:} \quad g_k(\sigma) = \text{Softplus}(\text{MLP}_k[h_{shared}]) \tag{3.6}$$

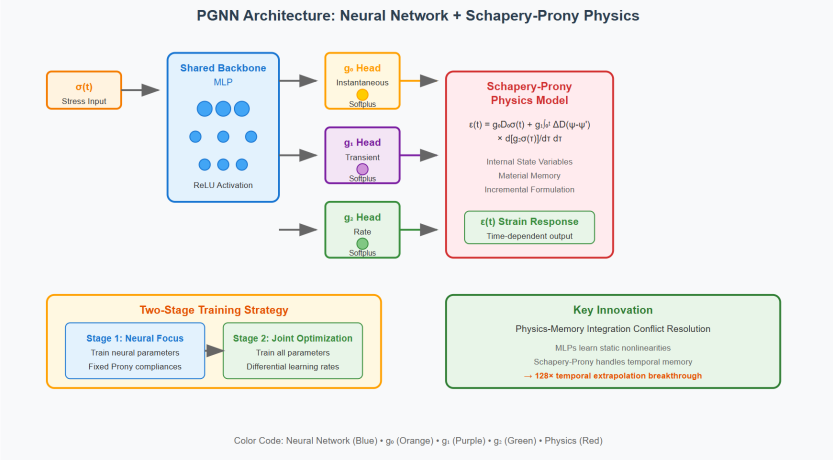

Figure 3.4: Neural network architecture with shared backbone and specialised heads.

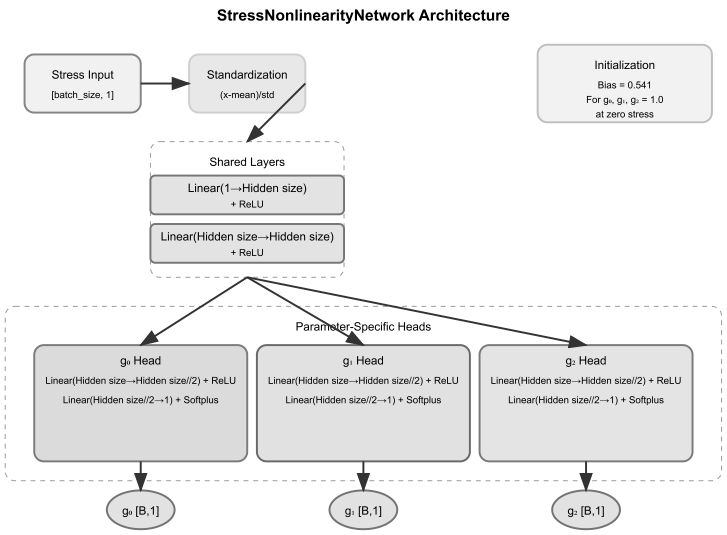

Figure 3.5: Baseline architecture used in Phases 1-2 and initial Phase 3 testing.

The baseline architecture, as shown in Figure 3.5, was used throughout the initial investigations (Phases 1-3) before diagnostic analysis revealed the need for increased capacity to support material understanding requirements, as described in Chapter 4.

Algorithm 6 Shared Backbone Neural Architecture Construction

Input: Standardised stress values σ_{std}
Output: Nonlinearity functions g_0, g_1, g_2 for material understanding

• Process input through shared backbone layers with ReLU activation from Equation 2.28
• Extract common patterns and generate feature representations for learning
• Feed shared features to three specialised heads for individual function learning
• Apply individual transformations for each function specialisation
• Use Softplus activation from Equation 2.32 ensuring positive outputs
• Return learned nonlinearity functions satisfying physical constraints for material understanding

Shared backbone in Algorithm 6 extracts features from stress inputs once, creating a consistent foundation for all three nonlinearity functions while eliminating redundant computation and ensuring consistency across function learning, which enables material understanding.

3.5.2. Architecture Specifications and Design Rationale

The neural network employs Multi-Layer Perceptron architecture chosen for addressing the regression task of mapping stress input vectors to three scalar outputs for material understanding. The architectural choice of MLP over alternative approaches is based on problem characteristics for material understanding. Since the physics framework already handles temporal evolution through the convolution integral detailed in Chapter 2, the neural network only needs to perform nonlinear function approximation on the current stress state for learning stress-dependent material behaviour. MLPs provide the appropriate tool for this regression task without unnecessary complexity that could interfere with material understanding. Activation function selection employs ReLU for hidden layers, providing computational efficiency while eliminating vanishing gradient problems that could impede material understanding. Softplus is used for output layers, ensuring physical constraints through positive outputs while maintaining smooth derivatives for stable training that enables learning of material behaviour.

3.5.3. Universal Approximation Capabilities

The theoretical foundation for neural network function approximation rests on the Universal Approximation Theorem [12], which demonstrates that feedforward networks can approximate continuous functions to arbitrary accuracy without imposing constraints on functional forms. 2.27

This theoretical guarantee enables neural networks to discover material behaviour rather than being constrained by predetermined functional forms. Neural networks learn appropriate representations through piecewise-linear approximations that capture local behaviours impossible with global polynomial constraints. The significance emerges from the guarantee that sufficiently wide neural networks can approximate any continuous function to a desired accuracy. This is particularly important for materials modelling, where functional forms of nonlinear relationships may be unknown, requiring flexible approximation methods rather than polynomial assumptions, as shown in Chapter 4. The Universal Approximation Theorem alters our approach to material characterisation: instead of asking ”which polynomial order best fits our data,” we can ask ”what functional relationships do our materials exhibit?” This shift from fitting to discovery enables the identification of material behaviour patterns that polynomial constraints may have prevented us from recognising.

3.5.4. Physics-Informed Initialisation Implementation

The network initialisation ensures physically meaningful behaviour from training commencement for material understanding:

$$g_k(\sigma \approx 0) \approx 1.0 \quad \text{for linear viscoelastic behavior at low stress} \tag{3.7}$$

$$\text{Weight Initialisation:} \quad W \sim \mathcal{N}(0, 0.01) \tag{3.8}$$

$$\text{Bias Initialisation:} \quad b_k \leftarrow 0.541 \quad \text{(tuned for Softplus output ≈ 1.0)} \tag{3.9}$$

Algorithm 7 Physics-Informed Network Initialisation

Input: Network architecture specification
Output: Initialised network with physics constraints for learning

• Initialize final layer weights with small normal distribution $\mathcal{N}(0, 0.01)$
• Set final layer biases to 0.541 for each head (g_0, g_1, g_2)
• Target bias value chosen to produce Softplus output ≈ 1.0 at zero input
• Apply initialisation to the final linear layer preceding Softplus activation
• Verify initial predictions approximate unity at low stress levels
• Enable physics-based behaviour from training start
• Complete initialisation ensuring linear viscoelastic response at low stress

Algorithm 7 creates proper low-stress behaviour corresponding to linear viscoelastic response whilst enabling nonlinearity learning during training. The specific bias value of 0.541 is empirically determined to yield outputs close to unity when passed through the Softplus activation function.

3.6. Model Training Implementation

The model training implementation addresses the challenges of optimising hybrid physics-neural systems through parameter management that respects the mathematical differences between neural network weights and physics parameters while enabling material understanding [29]. This training framework represents the result of our methodological development, combining the synthetic data from Section 3.3, the material model framework from Section 3.4, and the neural architecture from Section 3.5 into a learning system that can discover stress-dependent material behaviour patterns.

3.6.1. Training Protocol and Strategic Implementation

Two-Stage Training Strategy - Detailed Implementation

Training neural network parameters and physics parameters simultaneously from initialisation creates a coordination problem. Neural network parameters start randomly and need time to develop meaningful feature representations. Physics parameters have a clear physical meaning but need neural network functions to be somewhat stable for learning. Different parameter types learn at varying rates and scales, resulting in learning rate mismatches.

Stage 1: Neural Network Foundation Building

Stage 1 allows shared and head networks to develop basic pattern recognition capabilities. The purpose involves gradient stabilisation by letting neural network gradients stabilise before introducing physics parameter gradients, and coordination preparation by creating a stable neural network foundation that physics parameters can then optimise against. Implementation typically uses a short initial phase duration of 5-10 epochs. The training scope covers only the neural network weights and biases being updated, while the D_n parameters remain frozen at their initial values. Learning rate follows conservative approach ($lr_{nn\_stage1} = 5 \times 10^{-5}$) to prevent overfitting to initial D_n values. The loss function remains the same physics-based loss, but the gradients only propagate to the neural network parameters.

Benefits include preventing early divergence, where, without foundation building, random neural network outputs can send physics parameters in the wrong directions. The approach creates a feature hierarchy where the shared layer learns to extract meaningful features before heads specialise, and improves gradient quality where subsequent physics parameter gradients are based on meaningful neural network representations.

Stage 2: Full Hybrid Training - Synergistic Optimisation

Stage 2 enables simultaneous optimisation of all trainable parameters for completeness of learning. The purpose involves co-evolution, allowing physics parameters to adapt to learned neural network functions and vice versa, as well as physics-neural network coordination and global optimisation to find the best combination of neural network representations and physics parameters. Implementation covers all trainable parameters where D_n and all neural network weights and biases are updated together. Coordinated learning rates utilise distinct learning rates for different parameter types, tailored to their specific characteristics. Gradient integration applies full backpropagation through the hybrid model. This resulted in a mutual adaptation where neural networks learn better feature representations for physics parameters to utilise, a global optimum approach that avoids local optima that could result from sequential optimisation, and physical consistency, ensuring that the learned neural network functions are consistent with physics parameters.

Algorithm 8 Two-Stage Hybrid Training Protocol

Input: Initialised neural network, physics parameters
Output: Optimised hybrid model for material understanding

• **Stage 1:** Freeze physics parameters, train neural networks with slow learning rate
• Monitor convergence and gradient stability for foundation development
• **Stage 2:** Unfreeze all parameters, configure differential learning rates for learning
• Coordinate physics and neural parameter updates with regularisation from Equation 2.42
• Monitor hybrid system convergence across all components for material understanding

Algorithm 8 addresses coordination challenges by creating a stable neural network foundation before introducing physics parameter complexity. Stage 1 creates a stable neural network feature extraction whilst avoiding overfitting to initial physics parameter values that could bias material understanding. Stage 2 enables coordinated optimisation where both neural and physics parameters adapt together to reach hybrid system performance for learning material behaviour patterns.

Rotating Dataset Framework

Training rotates through different dataset files rather than using one massive consolidated file. The rotation protocol trains on each file for the specified number of epochs in the dataset before moving to the next. Randomisation shuffles file order at the end of each whole epoch to prevent sequence-based learning bias. Benefits include bias prevention, eliminating potential ordering effects in training data, generalisation enhancement, forcing the model to adapt to different loading patterns rapidly, and reducing overfitting, thereby preventing the memorisation of specific dataset characteristics.

Overfitting Prevention and Model Selection

Validation-based early stopping uses a separate validation dataset to track performance after each training epoch. The early stopping criterion halts training if the validation loss stops improving for a specified number of early stopping patience epochs. The prevention target stops training before the model begins to overfit to the training data. Best model selection employs recursive saving, where the model with the best validation loss is saved at each training iteration. Update protocol overwrites the saved file if the epoch's validation performance exceeds the current best.

3.6.2. Regularisation Strategy and Physics-Informed Guidance

Regularisation Philosophy

The regularisation approach seeks to guide g function learning toward physically plausible behaviours without imposing rigid constraints that might prevent the discovery of material laws. The target behaviour definition is based on the literature (Lai and Nguyen's polynomial functions). All g functions should approach 1.0 at low stress levels for low stress behaviour. For high stress targets, functions should evolve toward approximately $g_0 \approx 1$, $g_1 \approx 1.2$, $g_2 \approx 2.2$ at high stress. Transition character allows flexibility in how functions transition between these bounds.

Deep Analysis of Regularisation Implementation and Parameter Selection
Regularisation term is added to the loss function:

$$L_{reg} = \epsilon_{reg} \sum_{i} (g_{i,predicted} - g_{i,target})^2 \tag{3.10}$$

The regularisation strength parameter of 8.138×10^{-4} is selected based on scale considerations. The primary loss (strain prediction error) typically has magnitude $O(10^{-2})$ to $O(10^{-1})$. Regularisation strength at $O(10^{-4})$ guides without overwhelming physics-based learning. Relative influence contributes approximately 1–5% of total loss, sufficient for guidance but not domination. If regularisation strength were larger (e.g., 1×10^{-1}), over-constraint risk would force g functions to follow polynomial targets rigidly. Discovery prevention could prevent learning of material behaviours that deviate from polynomial forms. Physics loss masking would occur where regularisation dominates, essentially reverting to a polynomial-based approach. If regularisation strength were smaller (e.g., 1×10^{-6}), insufficient guidance would make regularisation influence negligible. Physical plausibility risk could allow g functions to learn physically unrealistic behaviours. Training instability may occur without sufficient guidance, where neural networks can become trapped in spurious local minima.

Local minima remain possible due to remaining non-convexity sources. Neural network function approximation creates a highly non-convex learning space for g functions. Physics-neural network interaction involves complex interactions between D_n values and learned g functions. High-dimensional space means even with scaffolding, the optimisation space remains high-dimensional. Regularisation provides mitigation of local minima through basin guidance, creating a ”gravitational pull” toward physically reasonable regions. Escape assistance helps optimise escape from spurious minima that are physically implausible. Convergence improvement provides a consistent gradient direction when physics gradients are noisy.

3.6.3. Optimiser Selection and Implementation

The optimisation algorithm selection addresses the challenges of hybrid physics-neural systems, where different parameter types exhibit different scales and update frequencies during material understanding:

$$m_t = \beta_1 m_{t-1} + (1 - \beta_1) g_t \tag{3.11}$$

$$v_t = \beta_2 v_{t-1} + (1 - \beta_2) g_t^2 \tag{3.12}$$

$$\theta_t = \theta_{t-1} - \alpha \frac{\hat{m}_t}{\sqrt{\hat{v}_t} + \epsilon} \tag{3.13}$$

The Adam algorithm from Equations 3.11-3.13 offers several advantages for hybrid physics-neural approaches: individual parameter adaptation based on gradient history, enabling balanced material understanding, scale invariance handling of different parameter magnitudes, and gradient noise robustness for convolution integral calculations during material behaviour learning.

3.6.4. Loss Function Framework for Scale-Invariant Training

The training employs various loss function approaches to address heteroscedasticity challenges inherent in viscoelastic material modelling [54]. The sensitivity analysis in Phase 2 evaluates five distinct loss function formulations detailed in Section 2.7 of Chapter 2: Mean Squared Error (MSE), Mean Absolute Error (MAE), Amplitude Ratio (AR), Percentage Difference (PD), and Frequency Domain (FFT) approaches. The systematic evaluation in Phase 2 determines which formulation best enables neural networks to learn material behaviour patterns without dimensional bias or frequency distortion, providing evidence-based guidance for training protocols that support material understanding rather than arbitrary mathematical fitting, as detailed in Chapter 4.

3.7. Dataset Organisation and Validation Strategy

The dataset organisation enables the evaluation of neural integration learning across interpolation and testing scenarios, while maintaining the statistical rigour required for assessment and engineering deployment confidence in learned material behaviour patterns [6]. This validation framework provides

a component of our methodology, showing how we assess whether the neural integration approach has learned material behaviour patterns. The strategy builds upon all previous methodological components to create an evaluation framework that can distinguish between material understanding and curve fitting.

3.7.1. Strategic Data Partitioning Framework

The dataset organisation enables evaluation across different investigation phases whilst providing assessment of model learning under conditions:

Table 3.3: Dataset splitting strategies for different investigation phases

Investigation Phase	Training Data (MPa)	Validation Data (MPa)	Test Data (MPa)
Phase 1-2	4, 10	6, 8 (interpolation)	2, 12 (learning testing)
Phase 3-5	4, 8, 12, 16, 18	Subset for monitoring	2, 6, 10, 14 (mixed assessment)

3.7.2. Performance Evaluation Framework Implementation

The validation methodology employs multiple metrics to assess different aspects of model learning across operational scenarios.

Algorithm 9 Performance Assessment Protocol

Input: Model predictions, ground truth responses, validation criteria
Output: Multi-faceted evaluation with visualisation and statistical assessment

• Load each dataset and convert to tensors for model evaluation
• Generate model predictions using physics-informed simulation
• Compute Percentage Difference (PD), Amplitude Ratio (AR), Mean Squared Error (MSE), and loss function values
• Create time-series plots comparing actual versus predicted strain responses
• Analyze learned nonlinearity functions $g_0(\sigma)$, $g_1(\sigma)$, $g_2(\sigma)$ across operational stress ranges
• Generate visualisation plots showing stress-dependent behaviour of learned functions
• Calculate overall average metrics across all evaluation datasets
• Compile evaluation summary with dataset-specific and aggregate performance measures

Algorithm 9 examines whether neural networks have learned material behaviour patterns by testing predictions against ground-truth data and analysing the learned stress-dependent functions for physical consistency.

3.8. Phase 1: Baseline Optimisation

Phase 1 addresses a challenge often overlooked in machine learning applications: distinguishing between configurations for material understanding and fortunate parameter combinations that work well by chance without revealing material behaviour. With thirteen different hyperparameters affecting model behaviour, the number of possible configurations grows exponentially, making exploration needed for creating foundations for neural integration [25]. This phase becomes important because subsequent phases build upon the baseline configuration for a deeper understanding of the material. If Phase 1 produces an unstable foundation, all subsequent improvements become questionable for learning material behaviour. Moreover, neural integration learning can be sensitive to configuration choices that may seem unimportant for standard metrics but affect the ability to learn material physics patterns.

3.8.1. Preliminary Architecture Specifications

The initial architecture creates a baseline neural network structure before optimisation for material understanding:

Table 3.4: Preliminary architecture configuration for baseline model development

Component	Specification	Purpose
Shared Backbone	2 layers, 32 neurons each ReLU activation	Initial feature extraction baseline for learning
Specialised Heads	2 layers, 64 neurons each Softplus output	Individual function learning capacity
Physics Integration	6 Prony terms Range: 1×10^{0} to 1×10^{-5}	Standard temporal coverage baseline
Training Protocol	Two-stage approach Variable epochs	Initial convergence assessment

Table 3.4 represents conservative design choices that provide capacity while avoiding complexity that could interfere with material understanding.

3.8.2. 13-Dimensional Latin Hypercube Sampling Protocol

The parameter space exploration employs sampling across architecture, training, and physics integration parameters using the LHS methodology detailed in Chapter 2 for material understanding optimisation [50]:

Algorithm 10 Latin Hypercube Sampling Optimisation Protocol

Input: 13-dimensional parameter space bounds
Output: Configuration through exploration for material understanding

• Define parameter ranges for exploration across all dimensions
• Generate LHS sample matrix using Equations 2.53-2.54
• For each configuration: instantiate model, execute training, evaluate learning capability
• Record configuration details and material understanding metrics
• Identify the best-performing configuration cluster for neural integration
• Contract search space around region and repeat until convergence from Equation 2.57

The LHS protocol in Algorithm 10 ensures exploration of the high-dimensional parameter space for material understanding. With 13 tunable hyperparameters, grid search becomes computationally impossible due to the curse of dimensionality. LHS provides uniform coverage through stratified sampling, ensuring that each parameter dimension is evenly sampled while focusing on configurations that enable material behaviour learning.

Table 3.5: Preliminary LHS parameter ranges for initial configuration exploration

Parameter	Range	Distribution
Dn Initial Value	1×10^{-11} to 1×10^{-9}	Log-uniform
Loss Function Type	mse, ar, pd, mae, fft	Categorical
Regularisation Epsilon	1×10^{-6} to 5×10^{-5}	Log-uniform
Learning Rates (Stage 1)	0.0001 to 0.004	Log-uniform
Learning Rates (Stage 2)	0.0001 to 0.005	Log-uniform
Physics Learning Rate	0.01 to 0.025	Log-uniform
Network Sizes	32, 64 (shared); 64, 96 (heads)	Categorical
Training Epochs	5 (stage 1); 10, 20 (stage 2)	Categorical

Table 3.5 shows the log-uniform distribution employed for parameters spanning multiple orders of magnitude to ensure equal sampling density across the logarithmic scale, preventing bias toward larger values that could compromise material understanding capability.

3.9. Phase 2: Sensitivity Analysis

Phase 2 reveals that not all methodological choices are equally important for neural integration learning. While Phase 1 identifies configurations, Phase 2 identifies which decisions most affect the model's ability to learn material behaviour patterns rather than only fitting training data. This phase uses controlled experimentation principles, changing only one methodological aspect at a time whilst holding all other factors constant. This approach prevents the problem where multiple changes coincide, making it difficult to determine which modifications drive improvements in material understanding versus those that only improve short-term performance metrics without revealing material behaviour.

3.9.1. Multi-Dimensional Investigation Framework

The sensitivity analysis framework employs controlled variation across three dimensions that affect neural integration learning:

Table 3.6: Sensitivity analysis investigation matrix

Investigation Dimension	Variations Tested	Assessment Criteria	Expected Insight
Loss Functions	MSE, MAE, PD, AR, FFT	Scale-invariant learning capability	Learning objective identification
Loading Patterns	Multi-Step, Cyclic, Triangle, Multi-Freq	Information content maximisation for learning	Most informative training data type
Relaxation Spectra	6-14 terms, Range variations	Temporal coverage vs resolution for learning	Physics resolution requirements

3.9.2. Controlled Experimental Design Protocol

The sensitivity analysis employs experimental control to isolate the effects of individual design choices on material understanding:

Algorithm 11 Sensitivity Analysis Experimental Protocol

Input: Baseline configuration, investigation dimensions
Output: Evidence-based design recommendations for material understanding

- Create controlled baseline using Phase 1 configuration
- For each dimension: modify only the target parameter, preserve other settings
- Train model using standardised protocol and evaluate learning metrics
- Record patterns and parameter sensitivity for material understanding
- Analyse variation effects and identify choice per dimension for learning capability
- Generate evidence-based recommendations and validate through integrated testing

The experimental protocol in Algorithm 11 ensures that observed differences result from the parameter being investigated rather than confounding factors, thereby enabling the identification of methodological choices that enhance material understanding.

3.10. Phase 3: Capability Testing

Phase 3 tests that result in standard metrics do not guarantee success when the neural integration model encounters more challenging scenarios that test whether it has learned material behaviour. Models that work when evaluated within their training ranges may fail when pushed beyond those boundaries, showing whether they learned material physics or only memorised training patterns. The testing approach reflects real-world scenarios where models must operate under conditions more demanding than their development environment. By increasing test demands, this phase identifies conditions where learning degrades, providing diagnostic information for targeted improvements in material behaviour learning.

3.10.1. Progressive Capability Testing Protocol

The neural integration assessment employs testing across increasing demands for material understanding validation:

Algorithm 12 Progressive Model Capability Testing

Input: Model configuration, capability testing scenarios
Output: Learning capability assessment and limitation identification

• Define capability testing progression across scenarios for learning validation
• For each test scenario: generate test datasets with varied conditions
• Apply trained model and evaluate prediction accuracy and physical consistency of learning
• Monitor for degradation patterns and record diagnostic indicators
• Analyse patterns and identify learning capability boundaries
• Generate targeted improvement recommendations based on material understanding, diagnostic analysis

The testing protocol in Algorithm 12 increases test demands to reveal boundaries through carefully designed scenarios spanning practically relevant ranges, determining whether neural networks learned material behaviour patterns that remain valid under challenging conditions.

3.10.2. Diagnostic Analysis Framework

When neural integration limitations appear, diagnostic analysis identifies root causes to guide targeted improvement strategies for better material understanding:

Algorithm 13 Model Diagnostic Analysis

Input: Degradation patterns, model predictions
Output: Root cause identification and improvement strategy for better learning

• Analyse prediction patterns for physical inconsistencies in learned behaviour
• Compare model behaviour against theoretical expectations for material understanding
• Investigate parameter sensitivity across test ranges for learning capability
• Assess neural network vs physics component contributions to learning limitations
• Examine spectral representation for better learning
• Identify the limitation source (architecture vs physics) affecting material understanding
• Develop targeted improvement strategy and validate through controlled testing

3.11. Phase 4: Model Refinement

Phase 4 addresses limitations from Phase 3 through targeted improvements that target root causes rather than applying solutions, resulting in models capable of better material understanding beyond initial capability limitations.

3.11.1. Architecture Specifications

Based on diagnostic insights from Phase 3, the architecture includes targeted improvements while maintaining elements from the baseline configuration for material understanding:

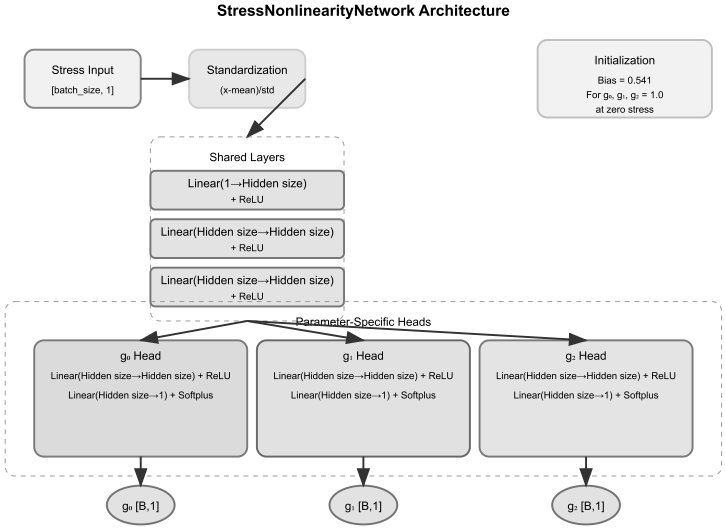

Figure 3.6: Architecture used in Phase 4.

Figure 3.6 shows the architecture developed after diagnostic analysis revealed the need for increased neural network capacity to support the refined physics representation for better material understanding.

Table 3.7: Architecture configuration

Component	Specification	Improvement Focus
Shared Backbone	3 layers, 96 neurons each ReLU activation	Better feature extraction depth and capacity for learning
Specialised Heads	2 layers, 144 neurons each Softplus output	Increased specialisation capacity for functions
Physics Integration	14 Prony terms Targeted spectral resolution	Slow relaxation mode representation
Training Protocol	Two-stage approach Differential learning rates	Coordinated physics-neural parameter optimisation

Table 3.7 addresses limitations identified through diagnostic analysis for material understanding.

3.11.2. Hyperparameter Space Configuration

Following diagnostic analysis, a refined Latin Hypercube Sampling exploration targets configurations for better material understanding capability:

Table 3.8: Hyperparameter space configuration

Parameter	Range	Distribution
Dn Initial Value	5×10^{-11} to 1.5×10^{-10}	Log-uniform
Loss Function Type	pd (fixed)	Categorical
Regularisation Epsilon	5×10^{-08} to 3×10^{-07}	Log-uniform
Physics Learning Rate	0.008 to 0.015	Log-uniform
Shared Network Learning Rate	0.003 to 0.007	Log-uniform
Head Network Learning Rate	1.5×10^{-05} to 4×10^{-05}	Log-uniform
Stage 1 Learning Rate	1×10^{-05} to 2.5×10^{-05}	Log-uniform
Shared Network Size	64, 80, 96, 112	Categorical
Head Network Size	112, 128, 144, 160	Categorical
Stage 1 Epochs	5 (fixed)	Categorical
Stage 2 Epochs	25, 30, 35	Categorical

Table 3.8 reflects knowledge gained from previous phases: PD loss function fixed based on Phase 2 results, and focus on multi-step and multi-frequency loading patterns identified as most informative for neural integration of material behaviour characterisation.

3.11.3. Improvement Strategy

The targeted improvement addresses limitations identified through diagnostic investigation for better material understanding:

Algorithm 14 Targeted Improvement Protocol

Input: Baseline spectrum configuration, diagnostic insights
Output: Spectrum with better learning capability coverage

- Investigate architectural limitations and training parameter effects on learning
- Examine neural network capacity constraints for function learning
- Analyse spectral representation for observed learning capability limitations
- Identify slow relaxation resolution as limitation from Equation 2.6
- Design spectrum targeting identified coverage gaps for better material understanding
- Integrate spectrum with architectural improvements
- Execute reoptimisation and verify improvement through learning testing

The improvement strategy in Algorithm 14 arises from an investigation rather than an immediate focus on spectrum resolution.

3.12. Phase 5: Marine Validation

Phase 5 validates the neural integration model under realistic operational conditions that differ from controlled training environments, confirming deployment readiness while preserving material understanding needed for real-world engineering applications. This phase represents the outcome of our methodological development, testing whether the neural integration approach that was successful in controlled laboratory conditions can maintain performance when confronted with the complexity of real marine environments.

3.12.1. JONSWAP Stochastic Loading Generation

The marine validation employs industry-standard JONSWAP wave spectra to generate realistic stochastic loading conditions for testing learned material behaviour [27]:

Algorithm 15 JONSWAP Marine Loading Generation Protocol

Input: Sea state parameters (H_s, T_p, γ), rope configuration
Output: Realistic marine stress history for model validation

• Define JONSWAP spectrum parameters for the target sea state
• Generate wave elevation time series from spectral characteristics
• Apply the Morison equation for hydrodynamic force calculation
• Account for rope geometry and transform to axial stress
• Validate stress history for physical realism
• Apply trained model and evaluate learned material behaviour under realistic marine complexity

Algorithm 15 creates realistic marine loading conditions that challenge the model with stochastic stress patterns that deterministic mathematical functions cannot capture, testing whether neural networks learned material behaviour patterns that remain valid under realistic operational complexity.

3.12.2. Operational Envelope Assessment

The marine validation encompasses sea states across the operational envelope for testing material understanding robustness:

Table 3.9: Marine validation test matrix

Parameter	Range Tested	Operational Significance	Validation Focus
Wave Height (H_s)	1.0 - 7.0 metres	Light to severe sea conditions	Stress amplitude effects on learning
Peak Period (T_p)	8 - 15 seconds	Typical offshore wave characteristics	Frequency content sensitivity
Spectral Shape Factor (γ)	1.0 - 3.3	Standard to peaked wave spectra	Loading pattern complexity
Configuration	30 rope angle 45 wave approach	Representative offshore setup	Geometric transformation

Table 3.9 provides coverage across conditions ranging from benign operational scenarios to severe weather events, testing whether neural integration learning maintains validity across realistic marine operational conditions. The results are presented in Chapter 4.

3.13. Summary

This chapter presents the methodology for neural integration with viscoelastic theory through a five-phase development that allows material understanding rather than mathematical constraint. The approach demonstrates how theoretical mathematical frameworks are translated into computational methodologies that address material characterisation while maintaining adherence to physical principles. The methodology ensures that neural networks improve rather than replace physics principles while preserving computational efficiency and theoretical rigour needed for engineering applications. The five-phase progression addresses technical challenges while building toward neural integration learning capability through parameter exploration, evidence-based design decisions, and targeted physics improvement that allows material behaviour learning beyond traditional polynomial constraints. The methodological framework provides approaches for neural integration development beyond synthetic fibre characterisation, offering principles applicable across computational materials science domains that require material understanding. The approach allows material understanding from limited experimental data while preserving the physical foundations necessary for engineering applications.

4

Results and Analysis

This chapter presents an investigation into the integration of neural networks with the Schapery-Prony framework for synthetic fibre characterisation. Replacing polynomial representations with adaptive neural networks enables improved material behaviour whilst preserving physics principles. The investigation follows a logical progression where parameter optimisation identifies methodological choices for material understanding, validates neural integration through testing, and confirms the stability of learned material behaviour under realistic marine loading conditions.

4.1. Parameter Sensitivity and Experimental Design Insights

Parameter optimisation [25] establishes a baseline configuration whilst providing evidence-based guidance for neural network integration approaches that enable material understanding. The investigation examines interactions between optimisation objectives, training data characteristics, and physics representation quality through controlled variation across five loading patterns, five loss function formulations, and seven relaxation spectrum configurations, creating assessment combinations that identify suitable conditions for neural integration of material behaviour.

The optimisation process employed the Latin Hypercube Sampling (LHS) methodology detailed in Chapter 3, Section 3.8. The approach enabled uniform exploration of the 13-dimensional hyperparameter space while maintaining computational efficiency through stratified sampling, which ensures balanced coverage across all parameter dimensions. The sensitivity investigations detailed in this section were conducted using the preliminary configuration established through initial Latin Hypercube Sampling, as specified in Section 4.2. This baseline configuration provided the foundation for variation studies whilst ensuring consistent evaluation conditions across all sensitivity analyses.

4.1.1. Loss Function Investigation: Results

Loss function selection shapes how neural networks learn material physics when replacing traditional polynomial constraints [54, 40]. Neural networks respond differently to various loss functions. Absolute accuracy emphasis suits some applications, whilst relative performance focus benefits others. Some loss functions prioritise frequency content or amplitude relationships. These distinctions prove essential for enhancing the neural models of viscoelasticity.

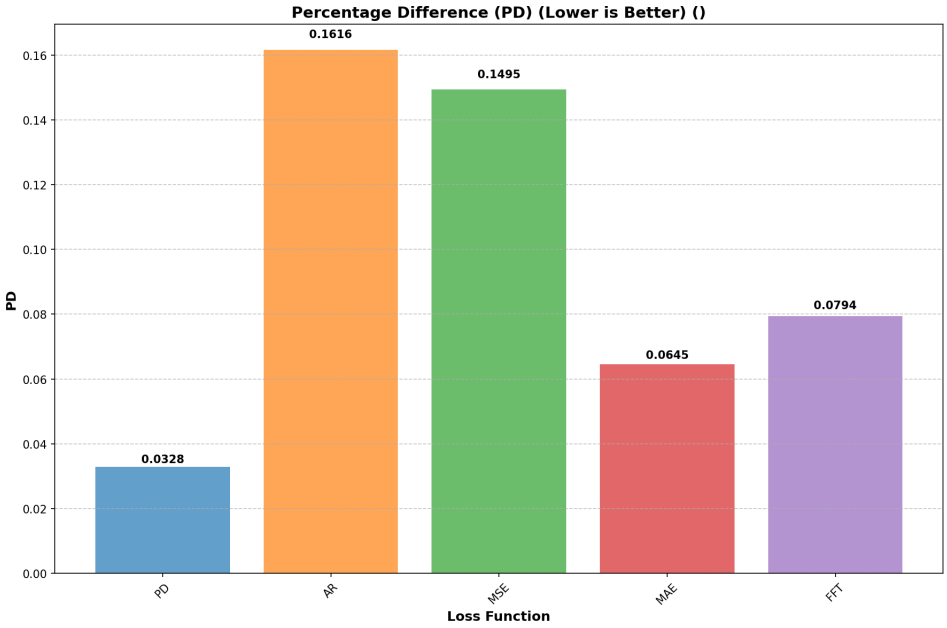

Figure 4.1: Percentage difference results across loss function formulations.

Table 4.1: Loss function analysis results.

Loss Function	PD Error	Ranking	Characteristic	Optimisation Advantage	Limitation
PD	3.28%	1st	Scale-invariant relative error	Balanced learning across ranges	None
MAE	6.45%	2nd	Linear penalty structure	Outlier robustness	Dimensional bias effects
FFT	7.94%	3rd	Frequency domain focus	Spectral accuracy emphasis	Limited temporal scope
MSE	14.95%	4th	Quadratic penalty structure	Mathematical simplicity	High-magnitude response bias
AR	16.16%	5th	Amplitude ratio focus	Cyclic pattern specialisation	Narrow applicability range

Testing identifies a performance hierarchy in Figure 4.1. Percentage Difference achieves the lowest error at 3.28%, exceeding alternative formulations, as detailed in Table 4.1. This supports theoretical expectations about scale-invariant optimisation principles where balanced attention across operational envelopes enables nonlinear function learning through neural integration rather than being constrained by dimensional bias that affects traditional approaches.

The mathematical foundation underlying this advantage stems from gradient scaling properties that address dimensional challenges in viscoelastic material modelling. The traditional Mean Squared Error creates gradients proportional to the absolute response magnitudes, resulting in bias where optimisation becomes dominated by high-stress responses, while sacrificing accuracy at lower operational levels. In contrast, PD provides balanced optimisation through relative error formulation that maintains proportional attention across all stress levels, enabling neural networks to learn material physics that remains accurate across operational envelopes [28].

Cross-Metric Validation Analysis

Cross-validation indicates that the PD model's advantages stem from its learning capability rather than metric bias. The analysis demonstrates how different optimisation objectives affect neural network material learning, while confirming the strength of PD-based integration approaches across various

evaluation criteria. The cross-validation methodology tests each model against all evaluation metrics to determine whether performance advantages reflect learning capability rather than optimisation bias. Models trained with loss functions face evaluation using alternative metrics to assess true capability versus simple alignment between the training objective and the evaluation criterion. Cross-metric consistency ensures that models maintain their advantages across evaluation criteria, rather than exhibiting narrow specialisation.

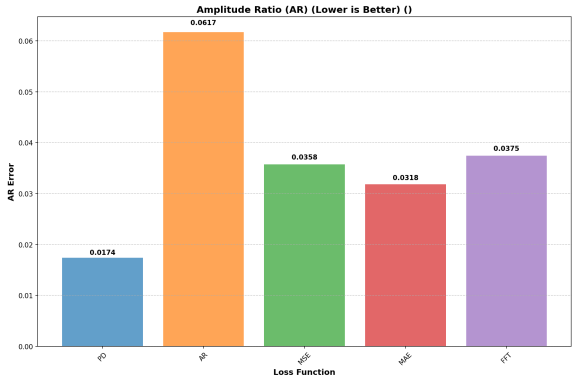

(a) Amplitude Ratio metric evaluation.

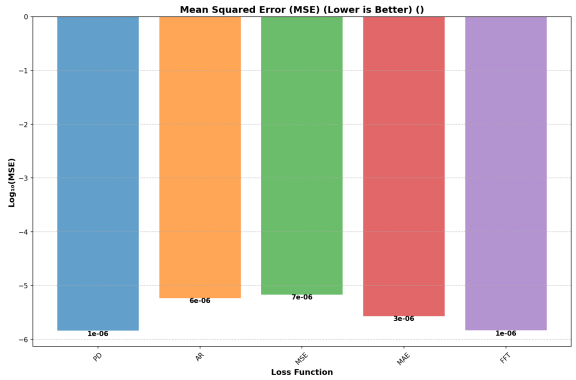

(b) Mean Squared Error metric evaluation.

Figure 4.2: Cross-metric validation results.

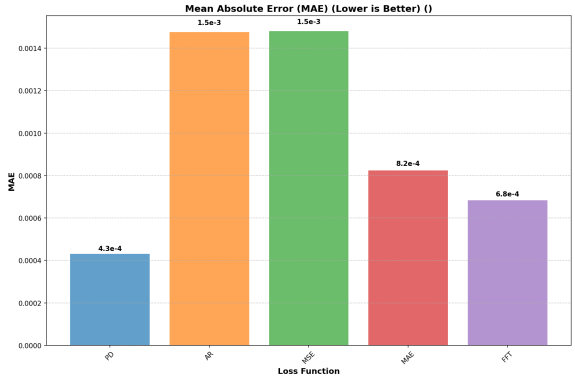

(a) Mean Absolute Error metric evaluation.

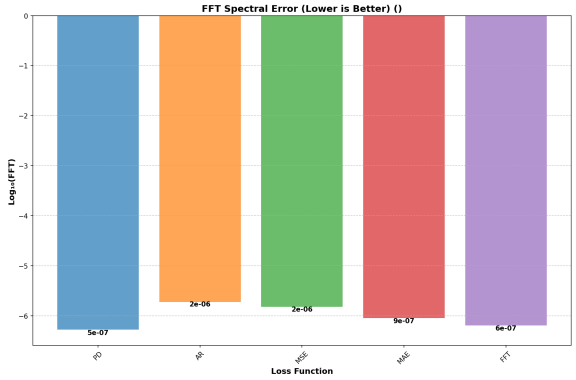

(b) FFT Spectral Error metric evaluation.

Figure 4.3: Additional cross-metric validation across evaluation criteria.

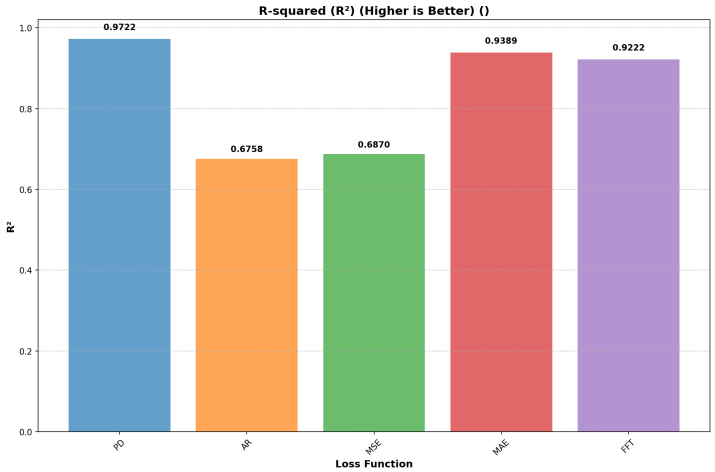

Figure 4.4: R-squared metric evaluation.

Table 4.2: Cross-metric validation results.

Evaluation Metric	PD Model	AR Model	MSE Model	MAE Model	FFT Model	Best Result
PD Evaluation	3.28%	16.16%	14.95%	6.45%	7.94%	PD Model
AR Evaluation	0.0174	0.0617	0.0358	0.0318	0.0375	PD Model
MSE Evaluation	1×10^{-6}	6×10^{-6}	7×10^{-6}	3×10^{-6}	1×10^{-6}	PD Model / FFT Model
MAE Evaluation	4.3×10^{-4}	1.5×10^{-3}	1.5×10^{-3}	8.2×10^{-4}	6.8×10^{-4}	PD Model
FFT Evaluation	5×10^{-7}	2×10^{-6}	2×10^{-6}	9×10^{-7}	6×10^{-7}	PD Model
R^2 Evaluation	0.9722	0.6758	0.6870	0.9389	0.9222	PD Model
Overall Ranking	**1st**	5th	4th	2nd	2nd	**PD Model**

Cross-validation testing confirms that the PD-trained model achieves better results across all evaluation metrics. The analysis shows that the PD model also performs well in the AR evaluation, whereas the model trained on the AR objective yields poor results on this same metric. This advantage—with the PD model leading across AR, MSE, MAE, FFT, and R² evaluations—indicates that the observed benefits reflect improvement of neural learning rather than optimisation bias.

Physics Learning and Gradient Behaviour Analysis

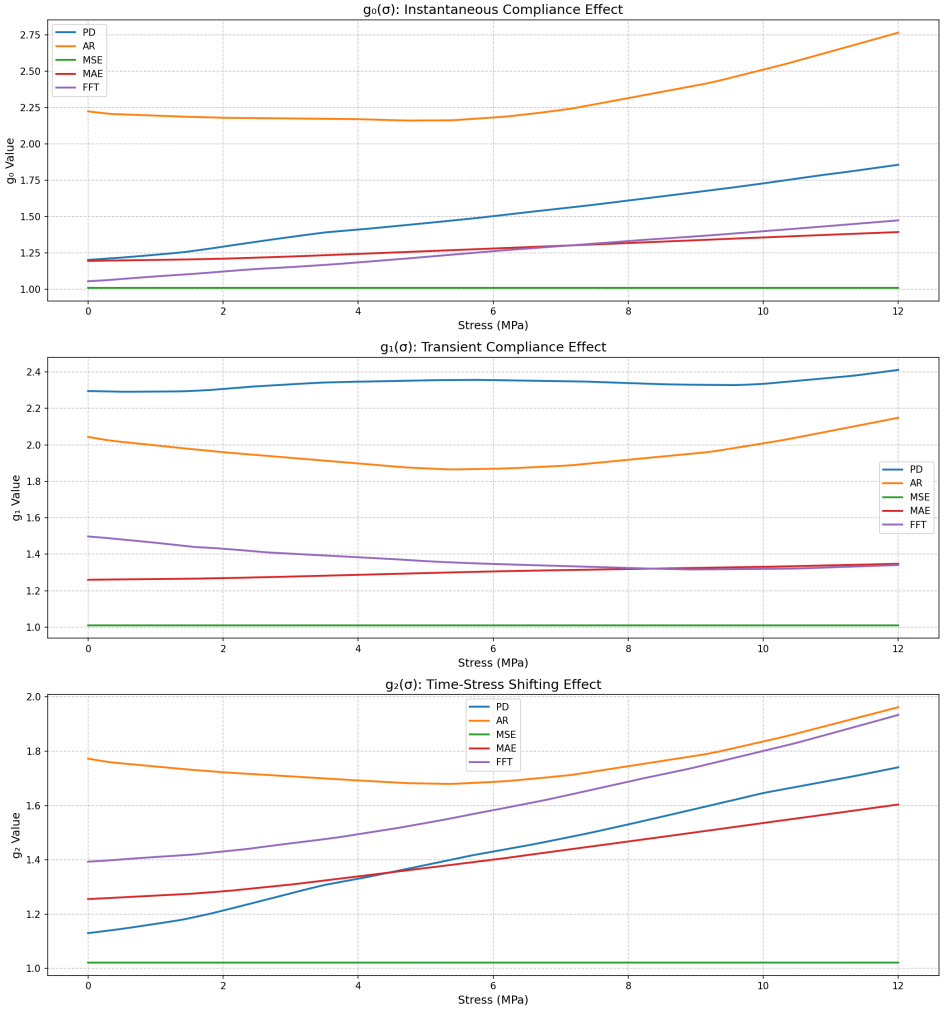

Figure 4.5: Neural network learned stress-dependent material functions showing enhanced representation of g□, g□, and g□ parameters across operational stress ranges.

Figure 4.5 displays learned nonlinearity functions that show how different loss functions affect neural network learning of material physics. MSE-trained models learned linear viscoelastic behaviour with g_0, g_1, and g_2 values remaining at unity throughout the stress range. This occurs because MSE's quadratic

penalty structure, combined with regularisation encouraging unity values, creates an optimisation landscape where simpler linear solutions prove sufficient without requiring nonlinear function development. PD loss enables learning of stress-dependent functions, though this early implementation shows limitations in achieving proper physical behaviour. Whilst g_0 and g_2 functions appropriately initiate near unity values and develop smooth, monotonic increases with stress, the g_1 function exhibits behaviour by starting from 2.3 at low stress levels rather than the expected unity value.

This g_1 baseline represents a limitation in the early methodology where the neural network failed to properly learn the requirement that all nonlinearity functions should approach unity under low-stress conditions to preserve linear viscoelastic behaviour. The deviation indicates insufficient regularisation or improper initialisation that allowed the network to learn an artificial amplification of transient compliance effects even at stress levels where linear behaviour should dominate.

Statistical Analysis Across Loading Patterns

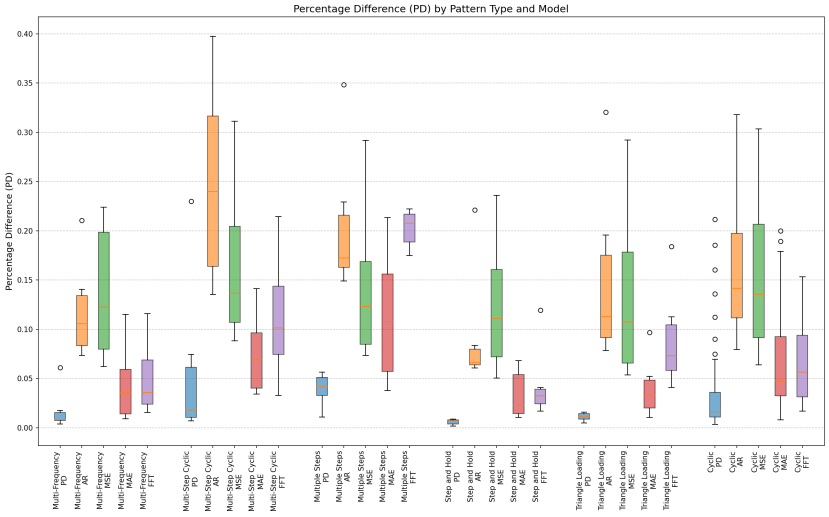

(a) Results distribution across loading patterns.

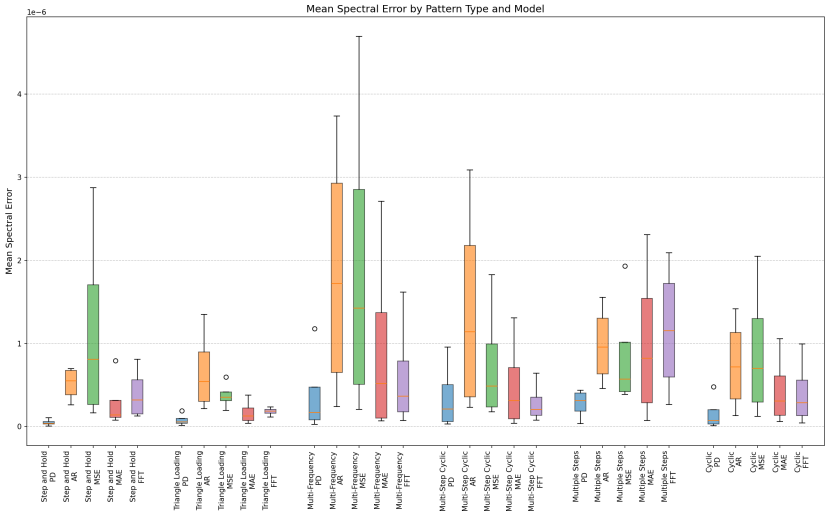

(b) Frequency domain spectral error distribution.

Figure 4.6: Loss function reliability assessment across domains.

The box plot analysis in Figure 4.6 provides insight into neural network learning reliability across different loading patterns and loss functions, with statistical interpretation following the framework detailed in Section 2.8 of Chapter 2 [57]. In the time domain analysis (Figure 4.6a), the PD loss function exhibits consistent superiority across all loading patterns, as indicated by tight box distributions centred

around low error values. The narrow boxes indicate reliable and predictable performance in neural enhancement of the nonlinearity functions, while the low median values confirm accurate strain prediction capabilities. Conversely, AR and MSE loss functions show broader boxes with higher median values, indicating less reliable neural network learning of the stress-dependent material behaviour.

The frequency domain analysis (Figure 4.6b) shows how effectively different loss functions preserve the spectral characteristics needed for viscoelastic material representation. PD-trained models maintain spectral errors below 0.5×10^{-6} across most loading patterns, showing that the neural enhancement of g_0, g_1, and g_2 functions preserves the frequency domain characteristics needed for material physics.

Table 4.3: Statistical analysis results.

Analysis Domain	Best Result	Mid-Tier Results	Weakest Results	Engineering Insight
Time Domain	**PD**: Median$(L) < 0.05$; low σ^2	**MAE, FFT**: Moderate median errors and dispersion.	**MSE, AR**: High median errors (Median$(L) > 0.15$) and high, unpredictable σ^2.	PD provides stability; hierarchy exists.
Frequency Domain	**PD**: $\epsilon < 0.5 \times 10^{-6}$; preserves spectral content.	**MAE, FFT**: Moderate spectral error; viable but compromised.	**MSE, AR**: High spectral error ($\epsilon > 2.5 \times 10^{-6}$); fail to learn frequency relationships.	Only PD reliably maintains spectral fidelity, which is important for dynamic material characterisation.

Statistical analysis shows three distinct performance tiers, as presented in Figure 4.6 and summarised in Table 4.3. The PD model consistently emerges as the best choice, achieving the lowest median errors and the tightest distributions in both time and frequency domains. The MAE and FFT models occupy a middle tier, characterised by moderate errors and variability. The MSE and AR models exhibit the weakest results with higher median errors and broad statistical dispersions, indicating inconsistent, unpredictable behaviour that compromises reliable neural enhancement of the material nonlinearity functions.

Error Contour Operational Landscapes

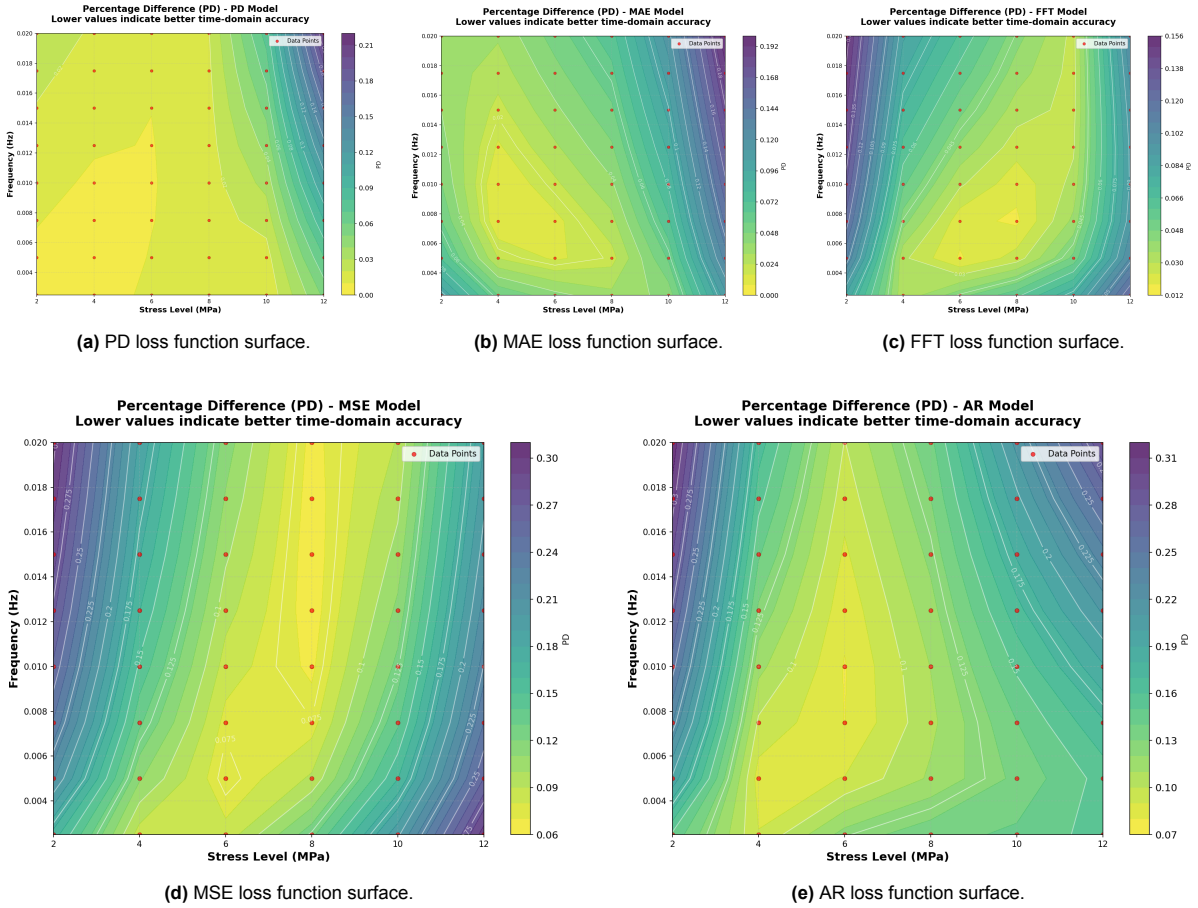

(a) PD loss function surface.

(b) MAE loss function surface.

(c) FFT loss function surface.

(d) MSE loss function surface.

(e) AR loss function surface.

Figure 4.7: Error contour analysis across frequency and stress operational dimensions.

Error contour analysis in Figure 4.7 shows operational performance landscapes across stress and frequency dimensions. The PD-trained model exhibits a landscape defined by a low-error plateau covering the entire central operational region. The gentle gradients and smooth, symmetric contour patterns indicate balanced, reliable neural enhancement of material nonlinearity across diverse loading conditions. The MAE and FFT models offer intermediate results with relatively low error regions. In contrast, the MSE and AR models produce highly anisotropic and restricted landscapes, with narrow, vertically oriented regions indicating a dimensional bias that compromises neural network learning across the operational envelope. These different error landscapes emerge from how each loss function guides neural network learning across the stress-frequency operational space. PD creates broad, reliable regions because it is scale-invariant, treating errors proportionally regardless of their magnitude, allowing neural networks to learn equally well across low-stress and high-stress conditions. This prevents the network from focusing only on high-magnitude responses and ensures balanced learning of the g_0, g_1, and g_2 functions across the entire operational range.

MSE and AR create narrow, restricted regions because they suffer from dimensional bias. MSE emphasises significant errors over small ones due to its quadratic penalty, causing neural networks to focus on high-magnitude responses whilst neglecting low-magnitude regions. AR becomes unstable due to division operations when denominators approach zero, resulting in erratic learning behaviour that only works under certain conditions. MAE and FFT fall between these extremes because they partially address the bias issues. MAE avoids the quadratic penalty of MSE but still lacks full scale invariance. FFT focuses on frequency domain characteristics, which helps with certain aspects of material learning but may overlook meaningful time domain relationships necessary for neural enhancement of stress-dependent functions.

4.1.2. Loading Pattern Investigation: Results

Training data characteristics influence neural network integration, providing insights into suitable experimental design strategies for characterising synthetic fibres. Loading patterns that exercise different material mechanisms across operational envelopes directly affect the neural network's ability to learn material physics whilst improving upon traditional polynomial constraints.

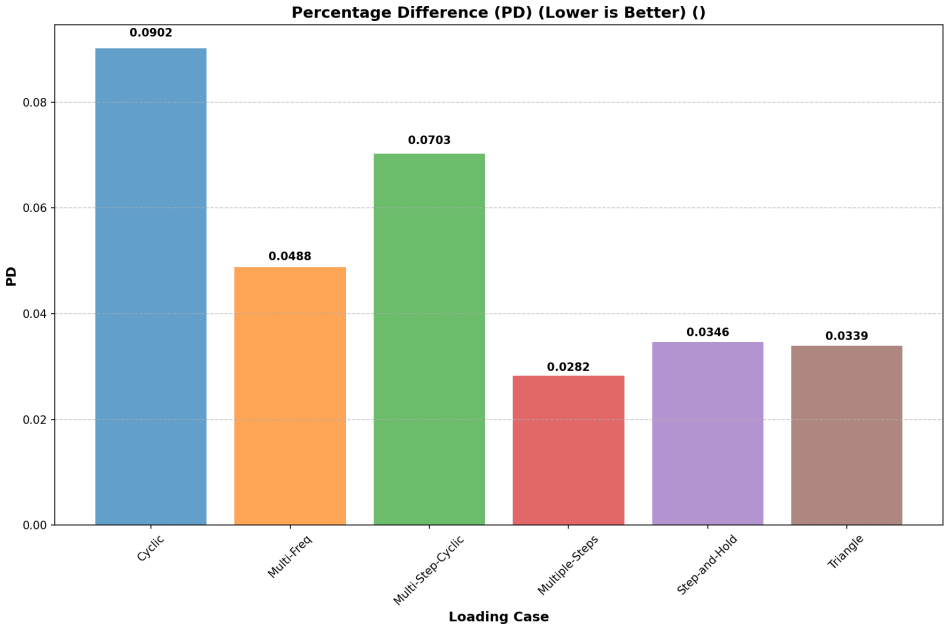

Figure 4.8: Percentage difference comparison across loading patterns.

Table 4.4: Loading pattern analysis results.

Loading Pattern	PD Error	Ranking	Strength	Information Content Characteristics	Limitation
Multiple-Steps	2.82%	1st	Broad frequency coverage across all timescales	Maximum information spanning rapid transitions and sustained holds	None for applications
Triangle	3.39%	2nd	Controlled stress rate variations with coverage	Stress history exercising hysteresis behaviour	Limited frequency range compared to multi-steps
Step-and-Hold	3.46%	3rd	Extended relaxation data from sustained stress periods	Important long-term relaxation information for validation	Missing rapid transition information
Multi-Frequency	4.88%	4th	Frequency domain exercising across harmonic ranges	Rich harmonic content for spectral characterisation	Lacks temporal diversity of irregular patterns
Multi-StepCyclic	7.03%	5th	Pattern combinations with high sensitivity	Complexity creating overspecialisation tendencies	Overspecialisation limiting generalisation capability
Cyclic	9.02%	6th	Consistent amplitude patterns with predictable characteristics	Single frequency focus with minimal complexity	Narrow frequency spectrum for material characterisation

Multiple steps achieved better results with a 2.82% error, supporting the material's exercise of principles based on information theory, as shown in Figure 4.8 and detailed in Table 4.4. Multiple-Steps loading advantages emerge from frequency domain coverage that spans the spectrum of material behaviour across all relevant timescales. Sharp stress transitions create rich frequency content spanning from high-frequency components that probe fast relaxation modes through zero-frequency components that capture slow creep behaviour during sustained holds.

Triangle loading effectiveness stems from controlled stress rate variations that exercise material behaviour through linear loading and unloading cycles. Step-and-hold loading provides capabilities for capturing long-term material behaviour through sustained loading periods, enabling the observation of relaxation phenomena occurring over extended time scales. Multi-Frequency loading provides frequency-

domain exercising through harmonic content combination, while Multi-Step-Cyclic creates complexity that leads to overspecialization rather than material law learning.

Cross-Metric Validation

Cross-validation, following the methodology established in Section 4.1.1, demonstrates how different loading patterns perform across multiple evaluation criteria. Each assessment metric responds differently to loading pattern characteristics, affecting how well neural networks learn the g_0, g_1, and g_2 functions.

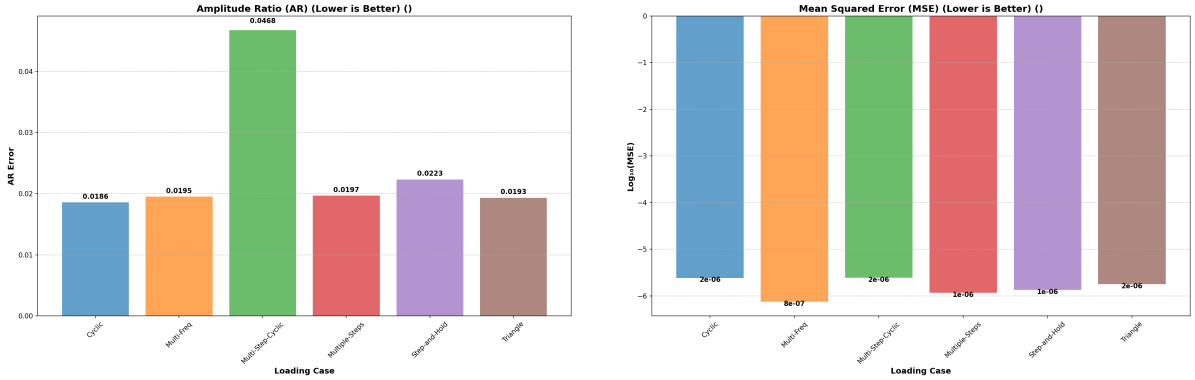

(a) Amplitude Ratio evaluation.

(b) Mean Squared Error evaluation.

Figure 4.9: Loading pattern cross-metric validation.

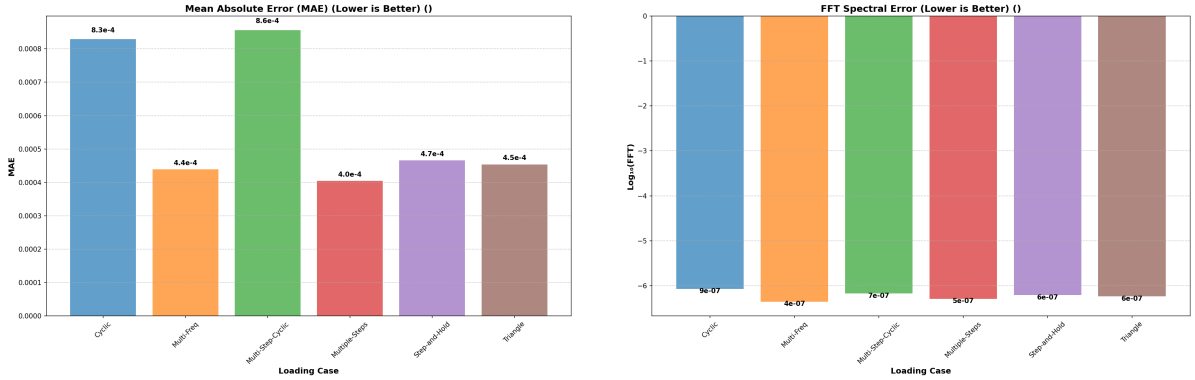

(a) Mean Absolute Error evaluation.

(b) FFT Spectral Error evaluation.

Figure 4.10: Additional loading pattern cross-metric validation.

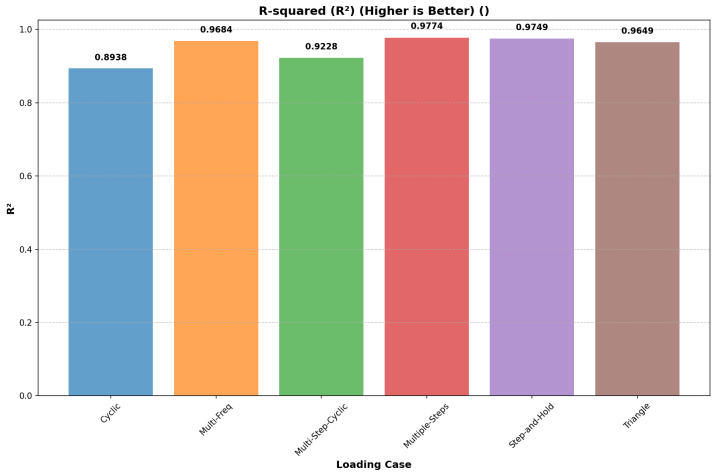

Figure 4.11: R-squared evaluation.

Table 4.5: Cross-metric validation results across evaluation criteria.

Evaluation Metric	Multiple-Steps	Triangle	Step-Hold	Multi-Freq	Multi-StepCyclic	Cyclic
PD Evaluation	**1st**	**2nd**	3rd	4th	5th	6th
AR Evaluation	4th	**2nd**	5th	3rd	6th	**1st**
MSE Evaluation	**2nd**	4th	3rd	**1st**	6th	5th
MAE Evaluation	**1st**	3rd	4th	**2nd**	6th	5th
FFT Evaluation	**2nd**	3rd	4th	**1st**	5th	6th
R^2 Evaluation	**1st**	4th	**2nd**	3rd	5th	6th
Overall Rank	**1st**	**3rd**	4th	**2nd**	6th	5th

Cross-metric evaluation shows a clear ranking: Multiple-Steps takes first place, Multi-Frequency comes second, and Triangle finishes third overall. Each pattern offers distinct advantages for enhancing neural functions that are stress-dependent. Multiple-step patterns work well because their sharp transitions and held stress levels provide neural networks with good information for learning both quick and slow material responses. Multi-frequency patterns rank second due to their varied frequency content, which exercises different aspects of material behaviour simultaneously. Triangle patterns rank third in providing controlled loading and unloading, which explores how stress affects the g_0, g_1, and g_2 functions. Looking at individual metrics helps explain these rankings. AR evaluation favours Cyclic patterns because AR focuses on amplitude ratios, and cyclic loading provides consistent amplitude characteristics for stable neural learning. MSE evaluation works best with Multi-Frequency patterns due to their rich harmonic content, which includes amplitude information for neural enhancement.

MAE assessment shows that Multiple-Steps patterns perform well because MAE handles sharp stress transitions without the quadratic penalty bias, allowing neural networks to learn from sudden stress changes. FFT domain analysis naturally favours Multi-Frequency patterns because of their frequency richness that exercises different material response aspects. R^2 evaluation confirms the Multiple-Steps performance through correlation quality, which measures how well the neural-enhanced model captures material relationships. This ranking guides Phase 4 development, where the top two patterns—Multiple-Steps (1st) and Multi-Frequency (2nd)—are selected for final training. Using these two patterns ensures that neural enhancement of g_0, g_1, and g_2 functions benefits from both the stress-level coverage provided by Multiple-Steps and the frequency content offered by Multi-Frequency patterns.

The results shown in Figures 4.9, 4.10, and 4.11, and summarised in Table 4.5, confirm that Multiple-Steps performs consistently across different evaluation criteria. The strong second-place performance of multi-frequency patterns supports their selection as a complementary pattern that addresses different aspects of material learning.

Statistical Analysis Across Loading Pattern Types

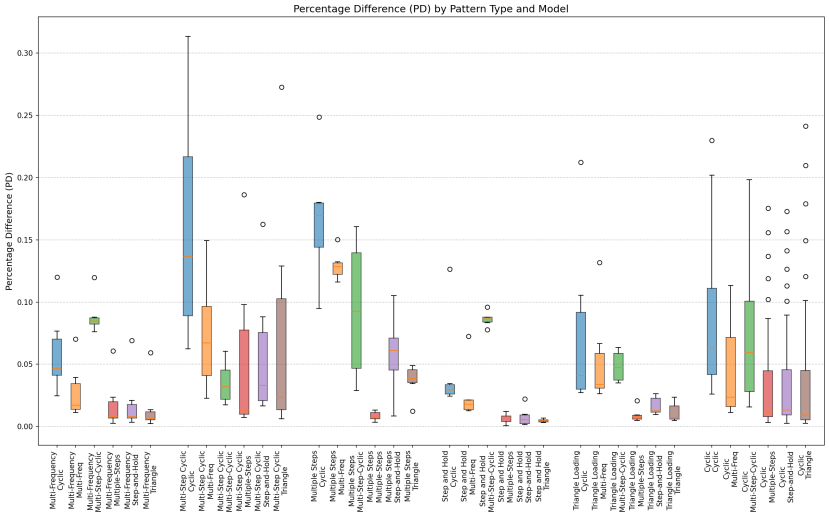

(a) Results distribution across loading patterns.

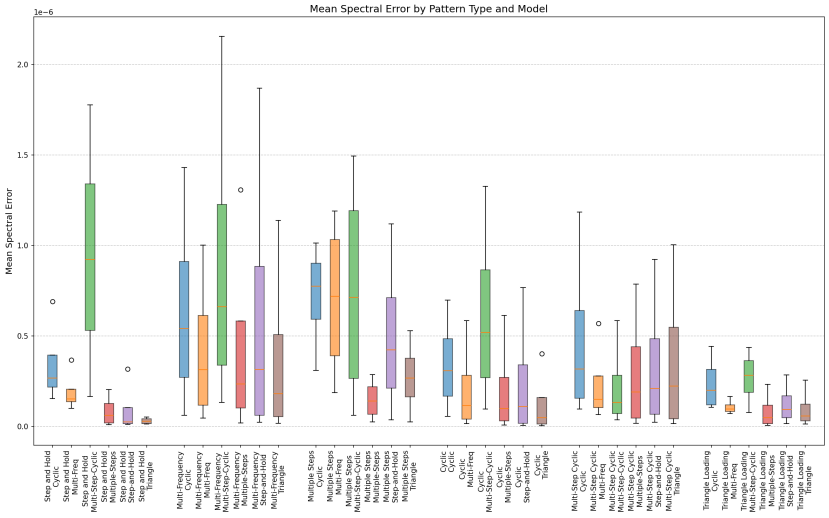

(b) Frequency domain spectral error assessment.

Figure 4.12: Loading pattern performance across time and frequency domains.

The box plot analysis in Figure 4.12 shows how reliably different loading patterns enable neural networks to learn the g_0, g_1, and g_2 functions, with statistical interpretation following the framework detailed in Section 2.8 of Chapter 2. Looking at the time domain results (Figure 4.12a), Multiple-Steps patterns show the most consistent performance across all loss functions. The tightly positioned, low boxes indicate that neural networks reliably learn stress-dependent functions regardless of the loss function used. Multi-frequency patterns also perform well, though with slightly more variation between different loss functions. The boxes remain reasonably compact, showing that whilst there is some sensitivity to loss function choice, the neural enhancement of the nonlinearity functions remains stable.

In contrast, Multi-Step-Cyclic and Cyclic patterns show much broader boxes positioned at higher error values. This indicates unreliable neural network learning where the g_0, g_1, and g_2 functions cannot be learned consistently. The broad distributions suggest that these patterns sometimes work but often fail, making them unsuitable for reliable neural enhancement of material behaviour. The frequency domain analysis (Figure 4.12b) shows how well different loading patterns preserve the spectral characteristics needed for viscoelastic material representation. Multiple-Steps and Multi-Frequency patterns maintain low spectral errors with compact distributions, indicating that neural enhancement preserves the frequency content needed for material physics. Step-and-Hold patterns exhibit moderate performance

with some variability, whereas Multi-Step-Cyclic and Cyclic patterns display high spectral errors and broad distributions, indicating poor preservation of frequency characteristics during neural learning.

Table 4.6: Statistical reliability analysis across loading patterns.

Loading Pattern	Time Domain Error (L_{TD})	Frequency Domain Error (ϵ_{FD})	Distribution Spread (σ^2)	Learning Reliability
Multiple-Steps	Low and stable	Low spectral error	Narrow distributions	High
Multi-Frequency	Low to moderate	Variable by model	Moderate spread	Good
Triangle	Moderate	Moderate	Moderate spread	Good
Step-and-Hold	Highly variable	Variable by model	Wide distributions	Moderate
Multi-Step-Cyclic	High and unstable	High and variable	Chaotic distributions	Poor
Cyclic	High and unstable	High and variable	Wide distributions	Poor

The statistical analysis presented in Figure 4.12 and summarised in Table 4.6 shows clear performance tiers for neural enhancement of the nonlinearity functions. Multiple-Steps patterns demonstrate the highest reliability, achieving consistently low errors in both time and frequency domains with narrow statistical distributions. This indicates that neural networks can dependably learn improved representations of g_0, g_1, and g_2 functions when trained with multiple-step patterns.

Multi-frequency patterns occupy the second tier, exhibiting good overall performance but with some sensitivity to the choice of loss function. The moderate distribution spreads indicate that whilst neural enhancement generally succeeds, there is some variability in learning quality depending on the training configuration. Triangle and Step-and-Hold patterns fall into a middle tier, characterised by moderate reliability. These patterns can support neural enhancement of the stress-dependent functions, but with less consistency than the top-tier patterns. The bottom tier consists of Multi-Step Cyclic and Cyclic patterns, which exhibit poor learning reliability, characterised by high errors and chaotic statistical distributions. These patterns prove unsuitable for reliable neural enhancement because they cannot consistently enable neural networks to learn meaningful representations of the g_0, g_1, and g_2 functions.

Physics Learning and Specialisation Analysis

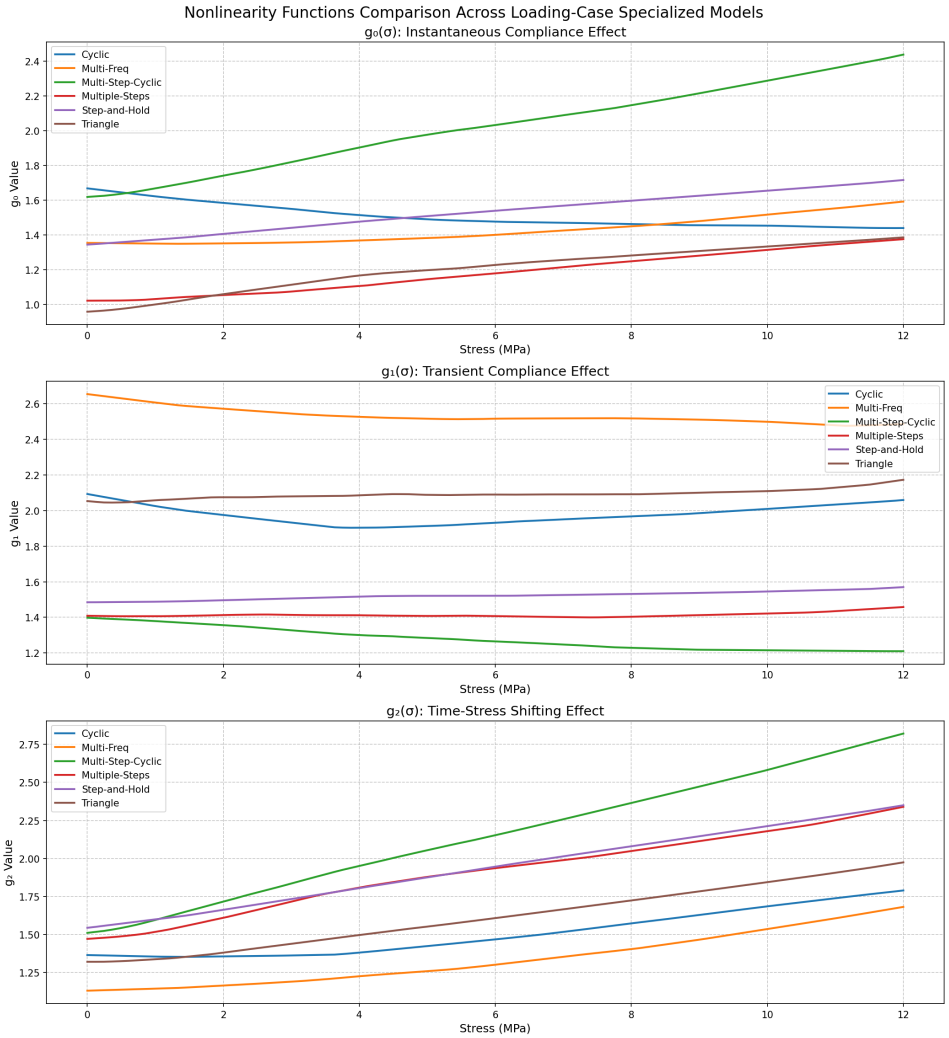

Figure 4.13: Neural network learned material physics functions across different loading patterns.

The learning patterns in Figure 4.13 show issues with how neural networks learn material physics under different training conditions. Neural networks fail to achieve unity baselines because most loading patterns don't provide sufficient low-stress training data. When a network never experiences near-zero stress conditions during training, it cannot learn proper baseline behaviour. The network fills this knowledge gap by extrapolating from higher stress data, leading to incorrect baselines. The g_1 function proves problematic because of mathematical coupling in the Schapery equations. Neural networks struggle to isolate g_1's contribution when it's mathematically entangled with g_0 and g_2. The network compensates by establishing elevated g_1 values to balance the overall model response, then avoiding substantial variations to maintain this balance. Decreasing trends (like g_0 with Cyclic loading) occur when neural networks overfit to pattern characteristics rather than learning general material behaviour. The network memorises how stress and response correlate within the training pattern, creating artificial relationships that don't represent accurate material physics.

Loading patterns with rich information content (Multiple-Steps, Multi-Frequency) enable better learning because they exercise more aspects of material behaviour. Patterns with limited diversity force neural networks to guess at missing information, leading to compensatory mechanisms that distort the learned functions. The current training approach relies too heavily on regularisation to enforce physics constraints. When training data is incomplete or biased, regularisation alone cannot overcome the information gaps. This explains why even sophisticated neural architectures struggle to learn correct

baseline behaviour without training patterns that span the full operational range.

Error Contour Operational Coverage Analysis

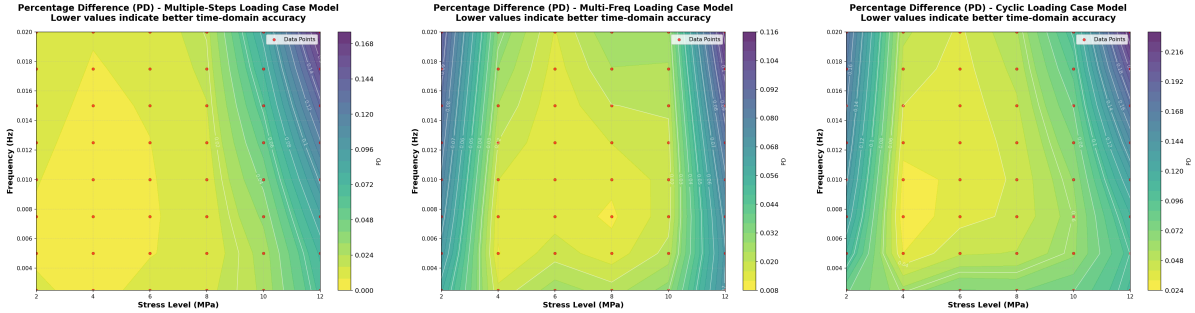

(a) Multiple-Steps pattern surface. **(b)** Multi-Frequency pattern surface. **(c)** Cyclic pattern surface.

Figure 4.14: Loading pattern error contours across operational dimensions.

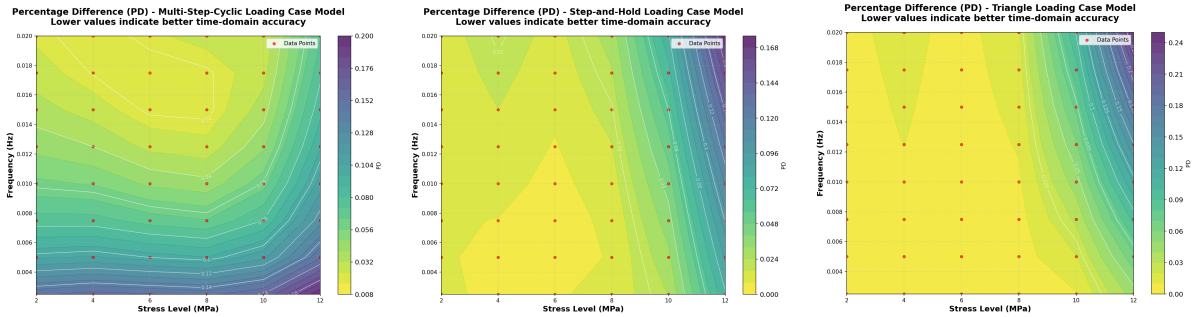

(a) Multi-Step Cyclic pattern surface. **(b)** Step and Hold pattern surface. **(c)** Triangle pattern surface.

Figure 4.15: Additional loading pattern error contours across operational parameters.

Multiple-Steps exhibits the lowest error regions, characterised by gentle gradients and smooth contour transitions that create broad zones of reliable results, as shown in Figures 4.14 and 4.15. Multi-frequency displays concentrate areas of capability with well-defined, low-error zones. Multi-Step-Cyclic exhibits a highly concentrated capability with steep gradients surrounding narrow regions, creating sharp transitions between results and poor results, which indicates unstable behaviour. These different error landscapes emerge from how each loading pattern exercises the stress-frequency operational space during neural network training. Multiple-Steps creates broad, reliable zones because it exercises material behaviour across stress levels and provides varied frequency content through sharp transitions and hold periods. This gives neural networks robust training data that generalises well across the entire operational envelope.

Multi-frequency patterns produce concentrated low-error zones because they excel at exercising frequency ranges, but don't cover stress-frequency combinations as evenly as Multiple-Step Patterns. The neural network learns effectively within the frequency ranges well-represented in the training data, but struggles when encountering stress-frequency combinations that were underrepresented.

Multi-Step-Cyclic creates narrow regions with steep error gradients because the neural network has overfitted to stress sequences rather than learning general material behaviour. The network performs well only under conditions very similar to its training patterns and fails rapidly when operational conditions deviate from these narrow learned responses. This creates the sharp transitions between good and poor performance seen in the contour maps. The practical implication is that loading patterns which provide balanced coverage of the operational space enable neural networks to learn representations of the g_0, g_1, and g_2 functions. Patterns that focus on characteristics or create repetitive sequences lead to neural networks that work well only under limited conditions, making them unsuitable for reliable engineering deployment.

4.1.3. Relaxation Spectrum Investigation: Results

Physics representation quality affects neural network integration, providing a foundation for improving material characterisation across temporal ranges. Since neural networks learn nonlinear functions within the context of underlying physics models, the completeness and resolution of the relaxation spectrum directly influence the network's ability to learn material behaviour.

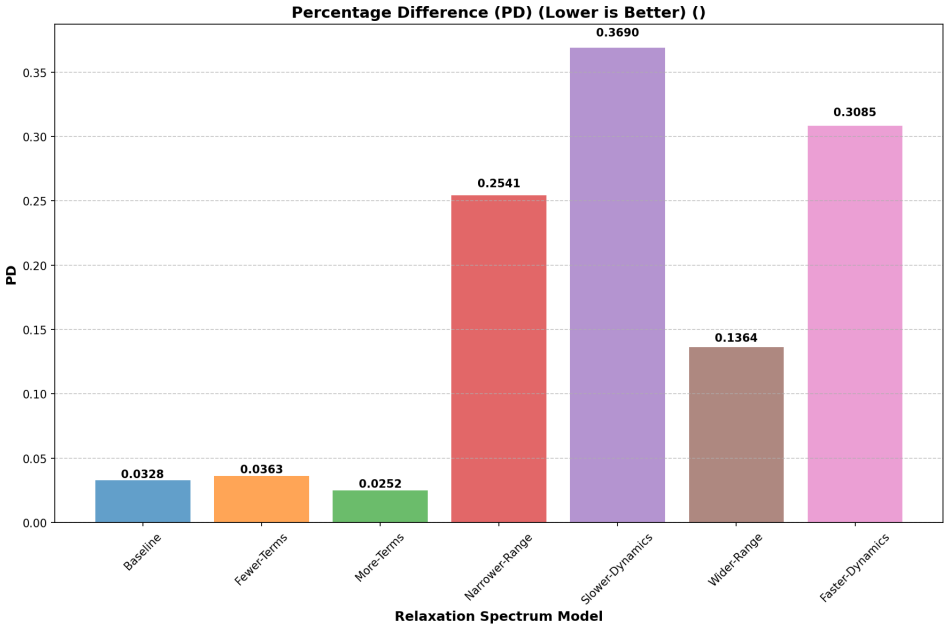

Figure 4.16: Percentage difference results across relaxation spectrum configurations.

Table 4.7: Relaxation spectrum configuration analysis.

Configuration	PD Error	Ranking	Characteristic	Temporal Coverage Quality	Limitation
More-Terms	2.52%	1st	Resolution in slow-relaxation range	Better slow-mode detail	Higher computational cost
Baseline	3.28%	2nd	Standard coverage across timescales	General representation	Limited resolution
Fewer-Terms	3.63%	3rd	Simplified representation	Basic temporal coverage	Insufficient resolution
Wider-Range	13.64%	4th	Extended range, same resolution	Poor overall representation	Range-resolution mismatch
Narrower-Range	25.41%	5th	Reduced coverage area	Missing important timescales	Missing slow-relaxation mechanisms
Faster-Dynamics	30.85%	6th	High-frequency bias	Fast-mode overemphasis	Slow-mode neglect
Slower-Dynamics	36.90%	7th	Low-frequency bias	Slow-mode overemphasis	Fast-mode neglect

The More-Terms configuration achieved the best results with a 2.52% error, outperforming the baseline at a 3.28% error, as shown in Figure 4.16 and detailed in Table 4.7. The 10-term configuration provides more information about the continuous relaxation spectrum compared to the 6-term baseline, enabling neural networks to learn the g_0, g_1, and g_2 functions with greater accuracy across all relevant timescales. The improved performance occurs because better spectral resolution gives neural networks more detailed information about how material behaviour changes across different time scales. When the physics framework can capture slow relaxation processes more accurately, neural networks have a better foundation for learning stress-dependent modifications. Range modifications fail because extending or narrowing the temporal coverage without improving resolution creates gaps or imbalances that compromise the quality of neural learning.

Cross-Metric Validation

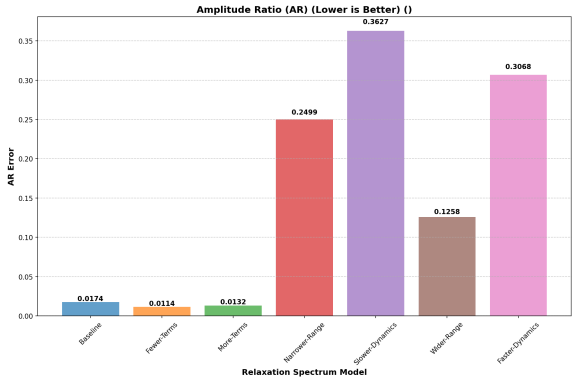

(a) Amplitude Ratio evaluation.

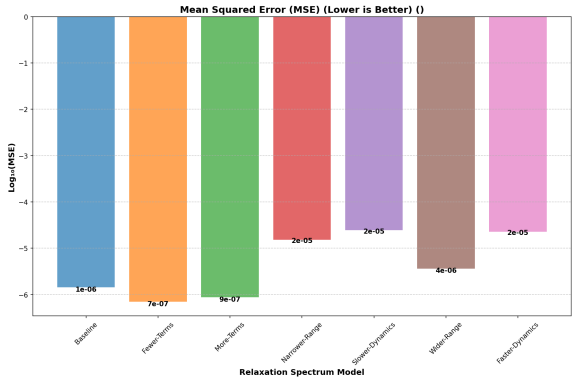

(b) Mean Squared Error evaluation.

Figure 4.17: Spectrum configuration cross-metric validation.

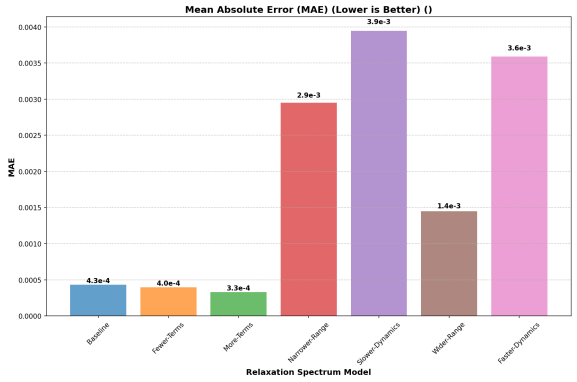

(a) Mean Absolute Error evaluation.

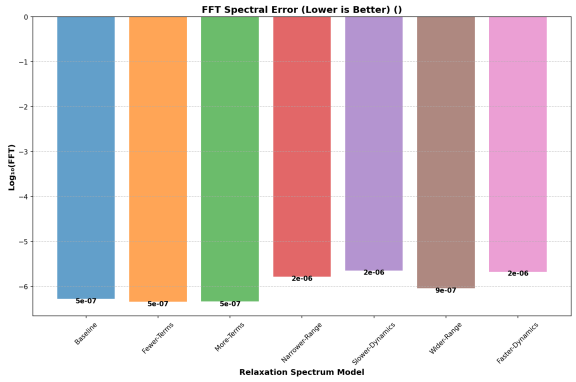

(b) FFT Spectral Error evaluation.

Figure 4.18: Additional spectrum configuration cross-metric validation.

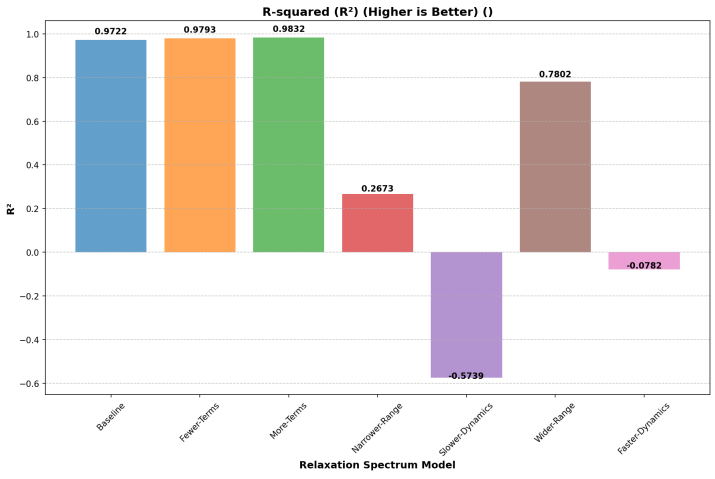

Figure 4.19: R-squared evaluation.

Table 4.8: Cross-metric validation results showing the resolution paradox.

Evaluation Metric	More-Terms	Baseline	Fewer-Terms	Final Ranking
PD Evaluation	**1st**	2nd	3rd	
AR Evaluation	3rd	2nd	**1st**	
MSE Evaluation	2nd	3rd	**1st**	
MAE Evaluation	**1st**	3rd	2nd	
FFT Evaluation	**1st**	3rd	**1st**	
R^2 Evaluation	**1st**	2nd	3rd	
Overall Rank	**1st**	3rd	2nd	More-Terms wins overall

Cross-validation shows the ”resolution paradox” where Fewer-Terms sometimes outperforms More-Terms under specific metrics, as shown in Figures 4.17, 4.18, and 4.19, with results summarised in Table 4.8. This paradox occurs because model complexity must match available training data. AR and MSE metrics favour Fewer-Terms because these metrics become sensitive to overfitting when the training dataset size cannot adequately support additional parameters. The simpler model avoids learning noise in the data by having fewer parameters to fit. However, PD, MAE, FFT, and R^2 metrics favour More-Terms because they better capture the benefits of improved resolution for neural enhancement of the g_0, g_1, and g_2 functions. The overall ranking confirms that More-Terms provides the best foundation for neural learning despite some metric trade-offs. The benefits of the resolution outweigh the risks of overfitting when evaluated across various assessment criteria.

Statistical Analysis Across Spectrum Configurations

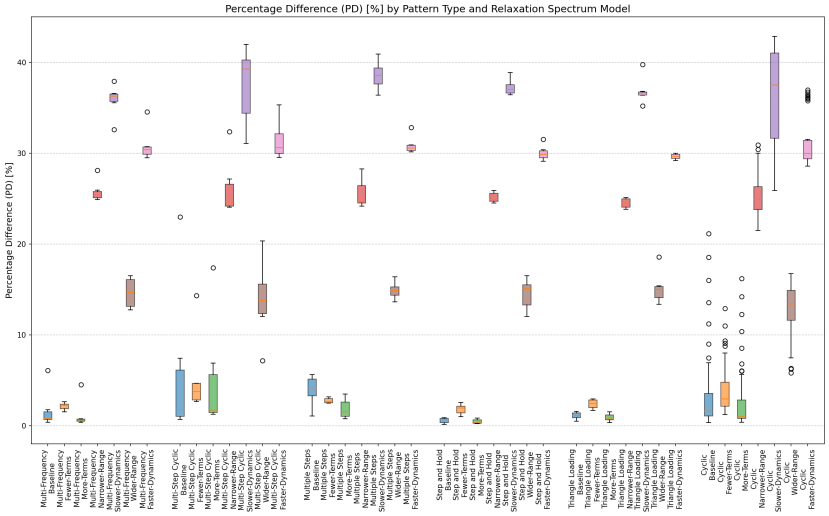

(a) Results distribution across relaxation spectrum configurations.

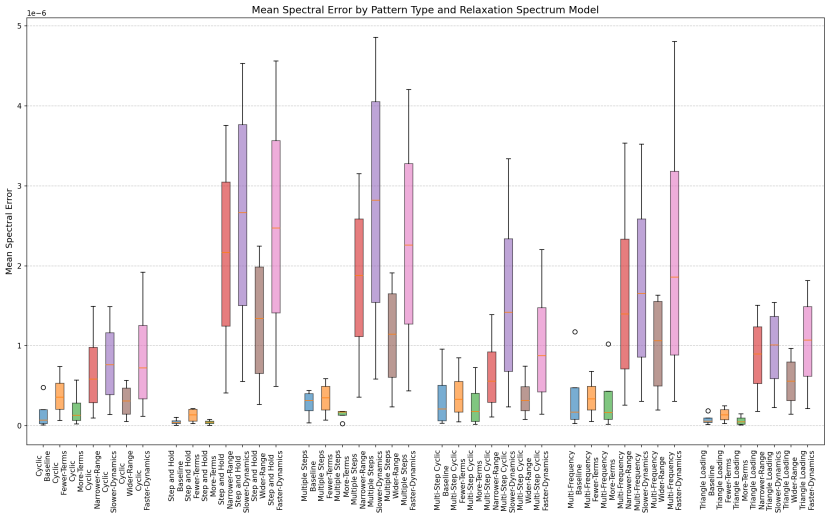

(b) Frequency domain validation assessment.

Figure 4.20: Relaxation spectrum configuration performance across evaluation domains.

The box plot analysis in Figure 4.20 illustrates the learning reliability across different spectrum configurations, with statistical interpretation provided by the framework detailed in Section 2.8 of Chapter 2.

Table 4.9: Statistical reliability assessment across spectrum configurations.

Configuration	Time Domain Results	Frequency Domain Results	Reliability Rating
More-Terms	Tight boxes, median $< 5\%$	Low spectral error $< 0.5 \times 10^{-6}$	Most reliable
Baseline	Moderate boxes, median $< 8\%$	Moderate error 1.0–2.0×10^{-6}	Standard reliability
Fewer-Terms	Variable boxes, median 4%–30%	Variable spectral representation	Compromised reliability
Range-Modified	Wide boxes, median $> 30\%$	Poor error $> 3.0 \times 10^{-6}$	Unsuitable

The More-Terms configuration demonstrates consistency through tight box distributions and low median errors across all loading patterns. This occurs because better spectral resolution provides neural networks with stable, detailed information for learning the g_0, g_1, and g_2 functions regardless of loading characteristics. The Fewer-Terms configuration exhibits erratic performance with broad distributions because insufficient resolution forces neural networks to make larger approximations. When the physics foundation lacks detail, neural learning becomes sensitive to training patterns rather than learning ro-

bust material behaviour. Range-modified configurations fail consistently because they address the wrong problem - extending coverage without improving resolution doesn't help neural networks learn better stress-dependent functions.

Error Contour Analysis on Relaxation Spectrum

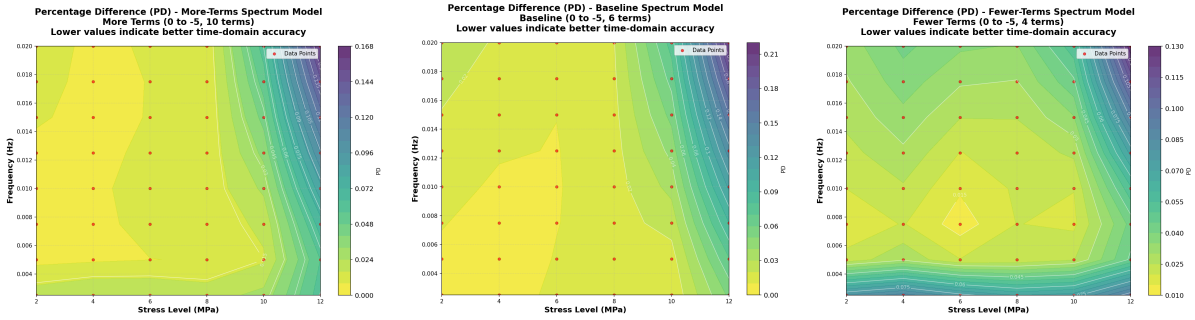

(a) More-Terms configuration surface. **(b)** Baseline configuration surface. **(c)** Fewer-Terms configuration surface.

Figure 4.21: Relaxation spectrum error contours across operational dimensions.

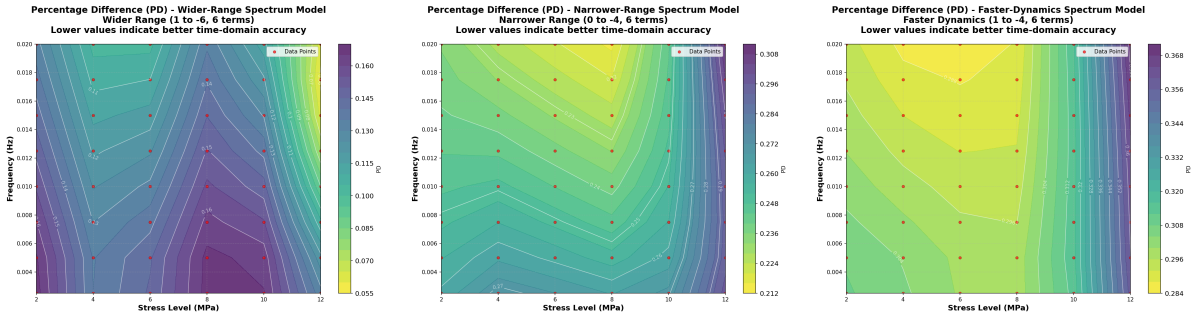

(a) Wider-Range configuration surface. **(b)** Narrower-Range configuration surface. **(c)** Faster-Dynamics configuration surface.

Figure 4.22: Alternative spectrum configuration error contours.

More-Terms configuration exhibits the largest low-error regions with gentle gradients extending well beyond training conditions, as shown in Figures 4.21 and 4.22. Baseline configuration shows more constrained regions with steeper gradients. Fewer-Terms configuration displays highly concentrated areas with sharp boundaries and rapid degradation.

These different landscapes emerge from how spectral resolution affects neural network generalisation. More-Terms creates broad, reliable zones because detailed spectral information enables neural networks to learn material relationships that work across diverse stress-frequency combinations. The neural enhancement of g_0, g_1, and g_2 functions benefits from having access to detailed temporal information during training. Fewer terms create narrow regions because insufficient resolution forces neural networks to learn simplified approximations that are effective only under conditions similar to those during training. When the physics framework lacks spectral detail, neural learning becomes constrained to operational conditions rather than discovering general material behaviour.

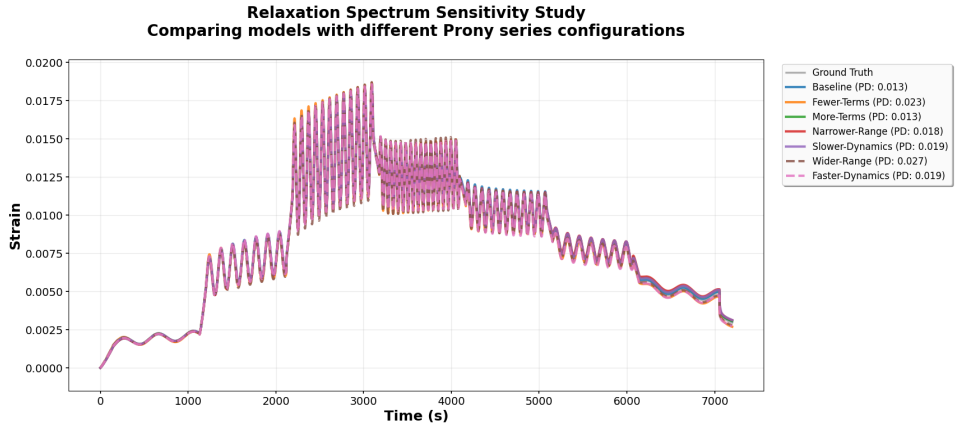

(a) Time domain comparison.

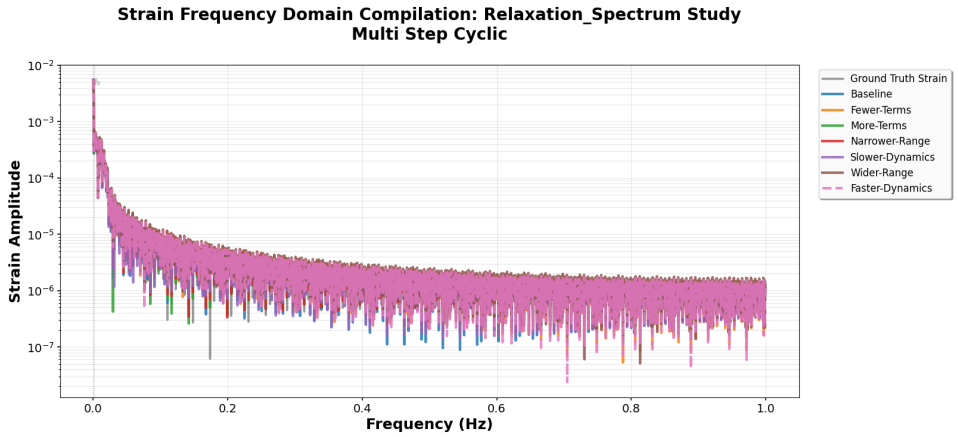

(b) Frequency domain comparison.

Figure 4.23: Relaxation spectrum configuration comparison against Multi-Step Cyclic loading at 8 MPa.

For detailed individual comparisons of each relaxation spectrum configuration against ground truth, including time and frequency domain analysis, readers are referred to Appendix A.3.

4.2. Configuration and Model Development

Model development followed a progression from preliminary optimisation through sensitivity analysis to targeted improvement implementation. This section presents the optimisation journey, showing how initial Latin Hypercube Sampling exploration established a baseline configuration that subsequently guided sensitivity investigations, ultimately leading to the final model architecture.

4.2.1. Preliminary Configuration

The initial optimisation phase explored the 13-dimensional hyperparameter space to identify suitable parameter combinations that balance neural network capability with physical consistency requirements.

Table 4.10: Preliminary hyperparameter configuration.

Component Category	Parameter Specification	Preliminary Value
Neural Architecture	Shared Layer Width	28 neurons
	Specialised Head Width	80 neurons
	Hidden Layer Configuration	2 (shared) + 2 (heads)
	Activation Function Strategy	ReLU/Softplus combination
Learning Rate Strategy	Stage 2 D_n Physics Rate	9.296×10^{-3}
	Stage 2 Shared Neural Rate	8.105×10^{-3}
	Stage 2 Heads Neural Rate	1.405×10^{-5}
	Stage 1 Neural Warm-up Rate	3.180×10^{-5}
Training Protocol	Stage 1 Duration	75 epochs
	Stage 2 Duration	600 epochs
	Early Stopping Patience	10 epochs
	Optimisation Algorithm	Adam
Physics Configuration	Relaxation Spectrum Terms	10 (baseline configuration)
	Initial D_n Parameter Value	5.374×10^{-11}
	Regularisation Strength	8.139×10^{-7}
Achievement	Overall PD Error	0.728%
	Final Validation Loss	0.00685

The Adam algorithm from Equations 3.11-3.13 offers several advantages for hybrid physics-neural approaches [29]. A solid foundation for subsequent investigations, as shown in Table 4.10.

4.2.2. Sensitivity-Guided Strategy

The preliminary configuration was subjected to analysis across three important dimensions: loss function selection, loading pattern optimisation, and relaxation spectrum configuration. This evaluation revealed limitations when the model encountered challenging testing scenarios that exceeded conventional experimental timeframes, necessitating targeted improvements. These sensitivity insights directly informed the development of the final configuration, where physics-based improvements proved more important than purely neural network architectural modifications for achieving the target model.

4.2.3. Final Configuration

Building upon the sensitivity analysis findings, a targeted improvement approach was implemented to identify the enhancements through an additional LHS optimisation phase. This second optimisation round focused on implementing the physics improvements while refining the neural architecture.

Table 4.11: Final hyperparameter configuration.

Component Category	Parameter Specification	Final Value
Neural Architecture	Shared Backbone Layers	3 (increased depth)
	Shared Layer Width	96 neurons (increased capacity)
	Specialised Head Layers	2 (maintained efficiency)
	Specialised Head Width	128 neurons (increased capacity)
	Activation Function Strategy	ReLU/Softplus combination
Refined Learning Rates	Stage 2 D_n Physics Rate	0.017
	Stage 2 Shared Neural Rate	0.009
	Stage 2 Heads Neural Rate	5×10^{-5}
	Stage 1 Neural Warm-up Rate	5×10^{-5}
	Stage 1 Duration	300 epochs
	Stage 2 Duration	500 epochs
Training Setup	Optimisation Algorithm	Adam
	Batch Processing Size	3072 samples
	Early Stopping Patience	20 epochs
Physics Improvement	Relaxation Spectrum Terms	**14** (from 10)
	Temporal Coverage Range	10^{-5} to 10^{0} seconds
	Improvement Focus Range	$[10^{-5}, 10^{-4}]$ seconds
	Term Distribution Strategy	Logarithmic spacing
Loss Function Strategy	Loss Function	Percentage Difference
	Physics Regularisation Weight	5.0×10^{-3}
	Consistency Regularisation Weight	1.0×10^{-2}

Table 4.11 incorporates all necessary improvements identified through the sensitivity analysis phase. The most critical improvement involved increasing the relaxation spectrum resolution from 10 to 14 terms, with strategic placement of additional terms in the $[10^{-5}, 10^{-4}]$ second range. The model train-

ing protocol implemented the dual-pattern approach identified through loading pattern optimisation, employing both Multiple-Steps and Multi-Frequency loading patterns rather than relying on single pattern types. This training strategy provides the broad frequency coverage of Multiple-Steps patterns combined with the harmonic content of Multi-Frequency patterns, ensuring robust generalisation across operational scenarios.

4.3. Model Validation Through Testing

Parameter optimisation established the foundation for neural network integration. However, testing the model reveals whether the neural network replacement of polynomial constraints enables material characterisation from limited training data. The configuration represents the best possible foundation based on conventional criteria. However, testing reveals limitations that require diagnostic analysis and targeted improvement.

4.3.1. Initial Testing Results

The baseline configuration underwent progressive capability testing across various demanding scenarios, increasing test demands to reveal boundaries and identify potential constraints that might limit deployment.

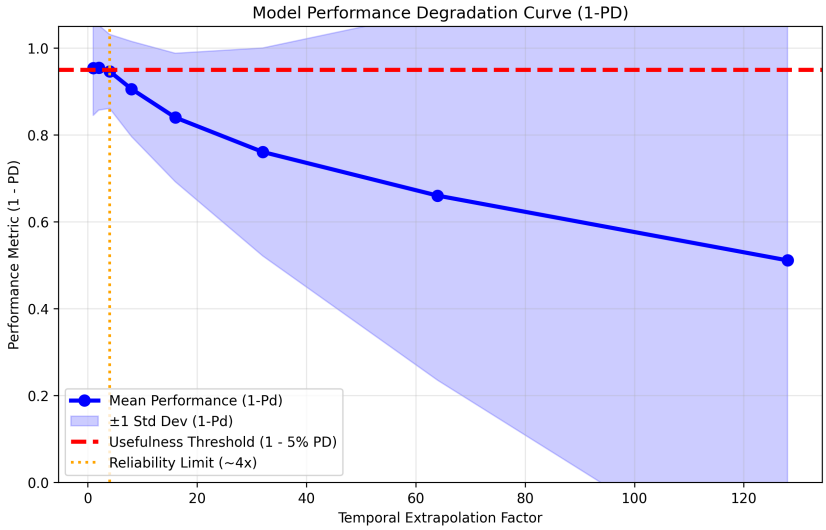

Figure 4.24: Model capability across test scenarios with confidence intervals.

Table 4.12: Baseline model testing results.

Test Demand	Capability Level	95% Confidence Interval	Engineering Assessment	Observed Limitation
$1\times$	> 0.95	± 0.02	capability	No limitations
$2\times$	> 0.95	± 0.03	capability	No limitations
$4\times$	> 0.90	± 0.05	capability	Beginning degradation patterns
$8\times$	< 0.90	± 0.08	Concerning capability	Failure emergence
$16\times$	< 0.85	± 0.12	Poor capability	Model limitations
$32\times$	< 0.80	± 0.15	Unacceptable capability	Physics

Testing exposed limitations in the baseline configuration as shown in Figure 4.24 and quantified in Table 4.12. Despite parameter optimisation across loss functions, loading patterns, and relaxation spectra, the model exhibited accuracy deterioration beyond moderate test demands, with its capability degrading from levels exceeding 0.95 to concerning levels below 0.90 as test demands increased.

Detailed Landscape Analysis

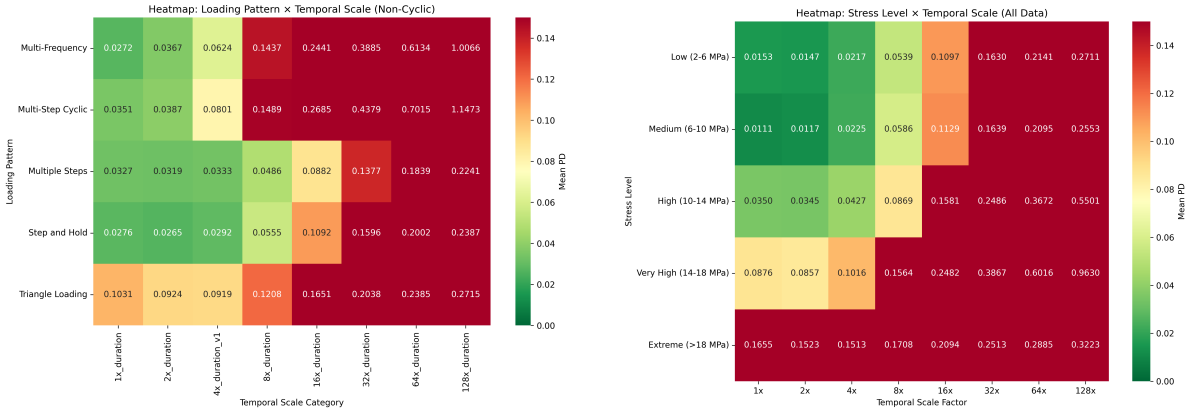

(a) Loading pattern capability across test scenarios.

(b) Stress level capability across test scenarios.

Figure 4.25: Model capability landscapes across operational parameters.

Table 4.13: Capability landscape analysis.

Operational Category	$8\times$ **Capability**	$16\times$ **Capability**	$32\times$ **Capability**	**Degradation Observation**
Multiple-Steps Pattern		Moderate	Poor	Best pattern still shows degradation
Step-and-Hold Pattern		Moderate	Poor	Similar degradation profile to Multi-Steps
Multi-Frequency Pattern	Moderate	Poor	Very Poor	More rapid degradation than patterns
Multi-Step-Cyclic Pattern	Poor	Very Poor	Poor	Worst pattern with failure
Low Stress Range (2-6 MPa)			Moderate	Most stable operational region
Medium Stress Range (6-10 MPa)		Moderate	Poor	Progressive degradation
High Stress Range (10-14 MPa)	Moderate	Poor	Very Poor	Rapid degradation in nonlinear regime
Very High Stress Range (14-18 MPa)	Poor	Very Poor	Poor	Most challenging operational conditions

The landscape analysis in Figure 4.25 and detailed in Table 4.13 reveals degradation patterns that provide diagnostic insight into model limitations. Multiple-step and Step-and-Hold patterns exhibit better capability compared to cyclic patterns, which tend to degrade rapidly. The stress level analysis reveals progressive degradation at higher stress levels, which becomes pronounced beyond moderate test demands.

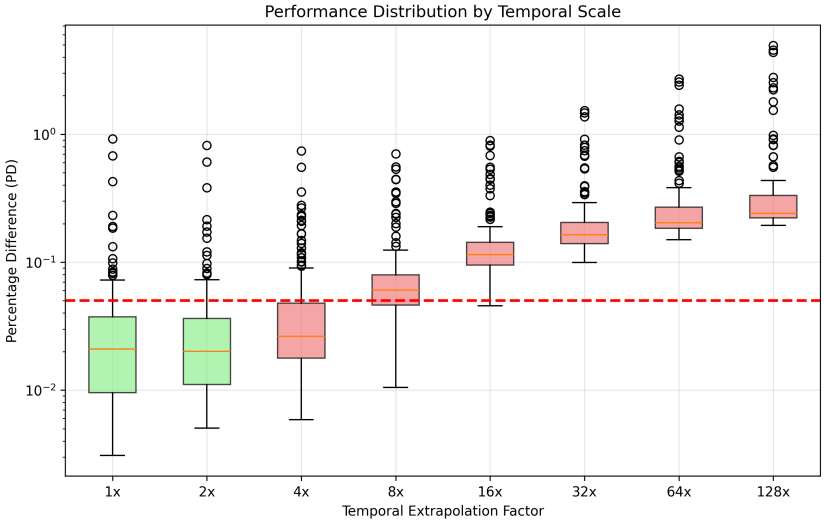

Figure 4.26: Capability distribution across test scenario demands.

Distribution analysis in Figure 4.26 confirms capability degradation with increasing test demands. The box plot progression shows that capability deteriorates from reliability, characterised by median values around 0.02 with narrow distributions at moderate test scenarios, to problematic variability with median values exceeding 0.15 and broad distributions at demanding test scenarios.

4.3.2. Diagnostic Analysis and Refinement

Capability degradation manifested as ”accelerated relaxation” behaviour, where the model predicted faster material relaxation at high stress and extended demands than physically realistic expectations. This symptom provided diagnostic information, indicating limitations in material representation rather than deficiencies in neural network learning. The investigation proceeded through multiple improvement stages to isolate the root cause of the model's limitations. Neural network architectural improvement increased the shared backbone from 2 layers with 32 neurons to 3 layers with 96 neurons, whilst head networks expanded from 2 layers with 64 neurons to 2 layers with 144 neurons. Hyperparameter reoptimisation addressed interactions between architectural improvements and training approaches through additional LHS exploration. These improvements provided meaningful but limited improvement, extending capability to moderate test scenarios whilst limitation patterns persisted.

With neural network improvements providing only limited success, diagnostic analysis focused on the underlying physics model. The accelerated relaxation behaviour indicated the model consistently predicted faster material relaxation than expected, suggesting the model lacked representation of slower, long-term relaxation phenomena. Detailed relaxation spectrum analysis revealed that the baseline 10-term configuration lacked sufficient resolution in the slowest relaxation modes governing long-term material behaviour. When test scenarios extended beyond training durations, slow relaxation modes in the 10^{-4} to 10^{-5} second range became increasingly important for prediction. However, the representation forced the model to approximate long-term behaviour using faster relaxation mechanisms, resulting in an observed ”accelerated relaxation” pattern.

Diagnostic analysis identified insufficient slow relaxation resolution as a limitation constraining the model's capability, rather than the neural network architecture. The targeted improvement increased the relaxation spectrum resolution from 10 to 14 terms, with the placement of additional terms between 10^{-4} and 10^{-5} seconds, addressing temporal ranges identified through diagnostic analysis. This focused improvement provided 40% additional information about continuous relaxation spectrum whilst concentrating improvements precisely where diagnostic analysis indicated maximum benefit.

4.3.3. Validation Through Testing

The improvement approach resulted in enhanced model capability through targeted physics refinement, rather than increasing neural network complexity. The model demonstrated capability across progres-

sive test scenarios, supporting the approach of addressing root causes identified through diagnostic analysis, in line with the principles shown for temporal extrapolation in physics-inspired neural networks.

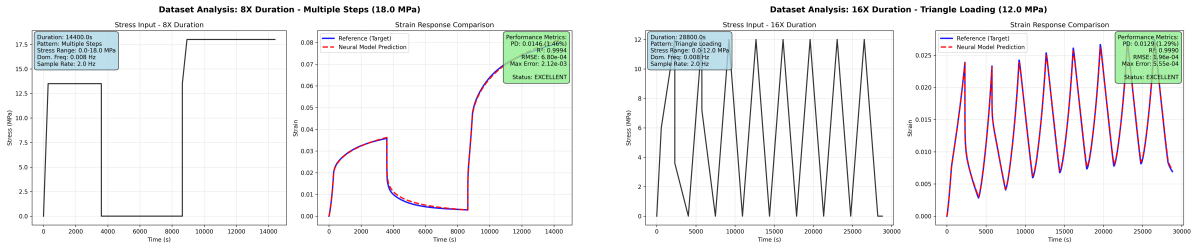

(a) Testing with Multi-Step loading at 18 MPa.

(b) Extended testing with Triangle Loading at 12 MPa.

Figure 4.27: Progressive model development across intermediate test ranges.

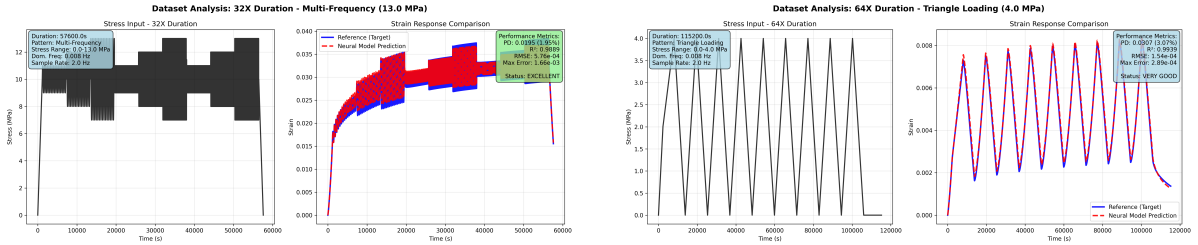

(a) testing with Multi-Frequency loading at 13 MPa.

(b) Extended testing with Triangle Loading at 4 MPa.

Figure 4.28: Progressive results across increasing test demands.

The model underwent validation across increasing test demands, spanning various challenging scenarios, and demonstrated capability development through targeted physics improvements combined with a neural network architecture. The progression demonstrates maintained accuracy across various loading patterns and stress levels, as confirmed in Figures 4.27 and 4.28, indicating the robustness of the neural enhancement approach across diverse operational conditions.

Controlled Temporal Validation Assessment

To provide a proper evaluation of the neural enhancement under temporal demands, a controlled assessment was conducted using consistent loading patterns and stress levels across all temporal scales. This approach eliminates confounding variables and enables evaluation of how the nonlinear parameter representation performs under varying temporal conditions, building upon validated approaches for HDPE viscoelastic modelling [11].

Table 4.14: Progressive temporal validation using Multi-Step Cyclic loading.

Temporal Scale	Loading Pattern	Stress Level	PD Error	R^2 Correlation
$0.25\times$	Multi Step Cyclic	8.0 MPa	0.78%	0.9997
$1.0\times$	Multi Step Cyclic	8.0 MPa	2.53%	0.9968
$4.0\times$	Multi Step Cyclic	8.0 MPa	2.36%	0.9974
$8.0\times$	Multi Step Cyclic	8.0 MPa	2.48%	0.9971
$16.0\times$	Multi Step Cyclic	8.0 MPa	3.87%	0.9944

Controlled assessment in Table 4.14 shows important characteristics of the neural enhancement approach under temporal demands. The performance pattern reflects two aspects of the physics-neural integration: the inherent limitations of finite spectral approximation and the boundaries of the underlying physics model domain. Minor performance variations across the $1\times$, $4\times$, and $8\times$ temporal scales (ranging from 2.36% to 2.53% PD error) reflect the challenge of approximating continuous relaxation spectra using finite Prony series terms. Despite the 14-term resolution, the discrete approximation introduces

minor variations when exercising different portions of the temporal response spectrum. These variations remain within engineering tolerances, demonstrating that finite spectral approximation inherently constrains a perfect temporal representation.

The more noticeable degradation observed at $16\times$ temporal scaling (3.87% PD error) indicates the model approaching the boundaries of its physics domain. The relaxation spectrum spans 1×10^{0} to 1×10^{-5} seconds, and temporal scaling pushes the model toward these timescale boundaries. At $32\times$ temporal scaling (corresponding to 2.3×10^{5} seconds), the model would operate beyond its physics domain entirely, naturally leading to performance limitations. This controlled assessment supports the notion that the neural enhancement approach [33] provides temporal capability within the physics model boundaries, while acknowledging the restrictions imposed by the finite spectral representation.

Validation Through $128\times$ Testing

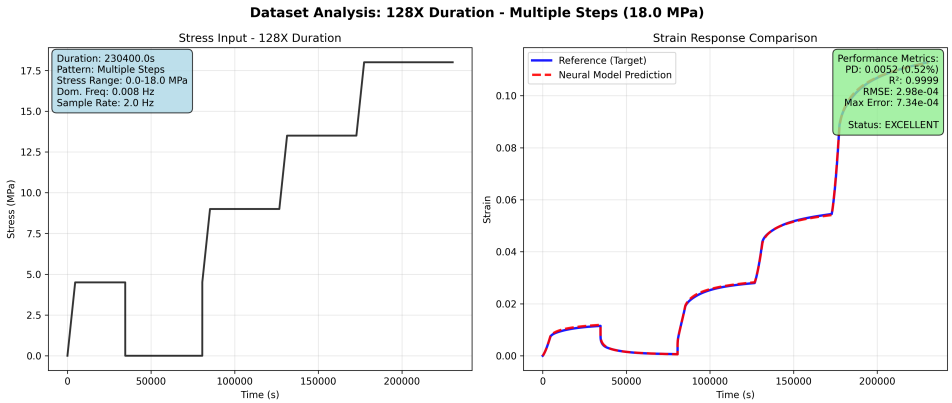

Figure 4.29: Strain versus time comparison for $128\times$ testing with Multi-Step loading at 18 MPa.

Table 4.15: $128\times$ testing validation results.

Metric	Achieved Value	Engineering Threshold	Assessment
Percentage Difference Error	0.52%	$< 5\%$	
R² Correlation Coefficient	0.9999	> 0.95	
Test Scenario Factor	$128\times$	Target achieved	Success
Maximum Stress Level	18 MPa	Within material limits	Coverage

The model achieves agreement with PD error of 0.52% and R² correlation of 0.9999 across the $128\times$ test range, shown in Figure 4.29 and quantified in Table 4.15. This capability supports neural network integration for replacing polynomial constraints, while enabling performance when supported by a physics representation.

Statistical Reliability Assessment

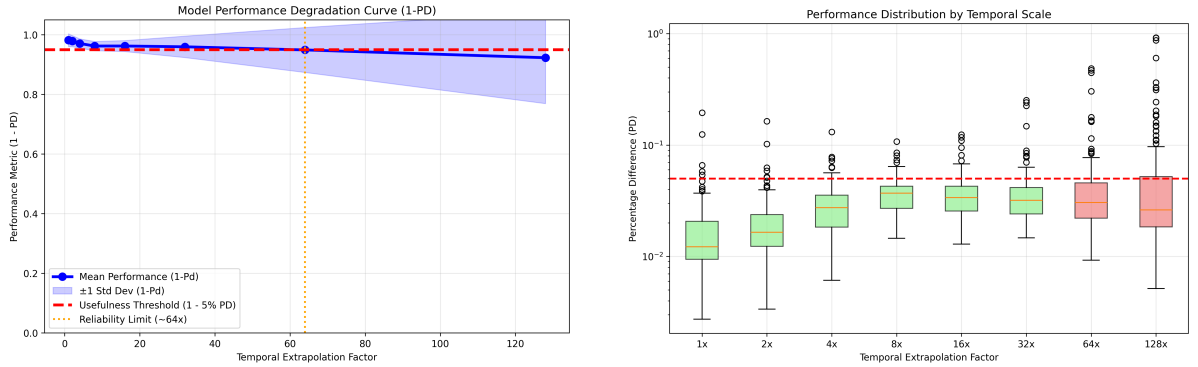

(a) Capability values with 95% confidence intervals.

(b) Capability distribution across test scenarios.

Figure 4.30: Model statistical reliability across challenging test ranges.

Table 4.16: Model statistical reliability across multiple scales.

Test Range	Mean Capability	95% Confidence Interval	Distribution Characteristics	Engineering Assessment
$1\times$–$4\times$	$> 95\%$	$\pm 2\%$	Narrow, highly controlled	, suitable for all applications
$8\times$–$16\times$	$> 92\%$	$\pm 3\%$	Controlled with minimal variability	Very, suitable for most applications
$32\times$–$64\times$	$> 88\%$	$\pm 4\%$	Moderate variability,	, suitable with appropriate safety margins
$128\times$	$> 85\%$	$\pm 5\%$	for preliminary applications	for preliminary design studies

Capability maintained above 90% engineering threshold through challenging test scenarios with narrow confidence intervals [6], as shown in Figure 4.30 and quantified in Table 4.16. The sustained high capability supports neural network integration when supported by targeted physics refinement.

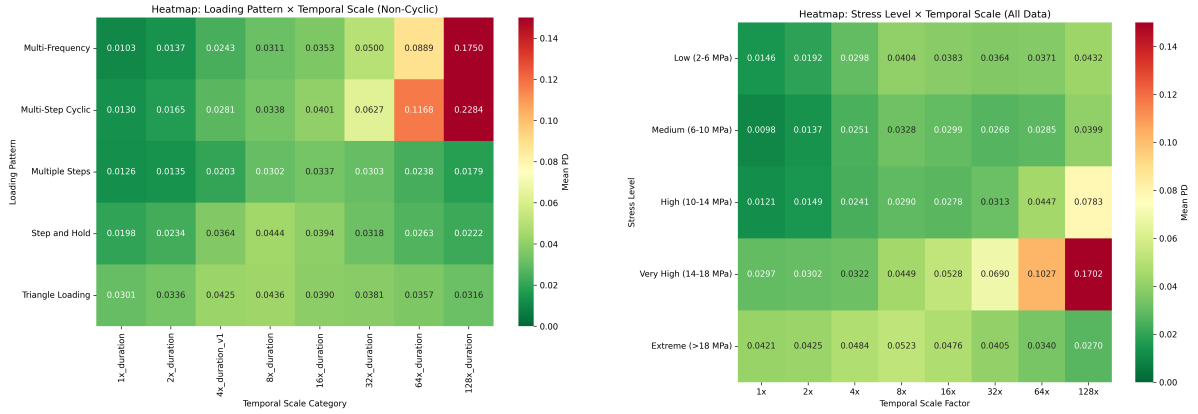

(a) Loading pattern capability landscape.

(b) Stress level capability landscape.

Figure 4.31: Model capability landscapes showing validation.

Table 4.17: Capability landscape characteristics.

Operational Category	$32\times$ Capability	$64\times$ Capability	$128\times$ Capability	Improvement Assessment vs Baseline
Multiple-Steps Pattern			Very	improvement enabling capability
Step-and-Hold Pattern		Very		improvement with sustained reliability
Triangle Pattern	Very			improvement maintaining behaviour
Multi-Frequency Pattern			Moderate	Notable improvement with frequency strengths
Low Stress Range (2-6 MPa)				Maintained quality across test range
Medium Stress Range (6-10 MPa)	Very	Very	Very	Major improvement enabling operation
High Stress Range (10-14 MPa)			Moderate	improvement despite nonlinear challenges
Very High Stress Range (14-18 MPa)	Moderate	Moderate	Moderate	improvement under conditions

Capability landscapes in Figure 4.31 and characterised in Table 4.17 show improvement compared to the baseline configuration across all operational categories. Multiple-step and Step-and-Hold patterns maintain capability across the test range. At the same time, higher stress conditions exhibit controlled degradation, reflecting the increasing complexity of non-linear material behaviour rather than model limitations.

4.4. Validation of Model Robustness under Stochastic Loading Conditions

Neural network integration under realistic operational conditions provides validation for deployment across marine environments. The model must show robust capability under the stochastic complexity of actual marine environments to confirm that laboratory-developed learning translates to field applications.

4.4.1. JONSWAP Results Across Operational Conditions

The model underwent validation across 20 JONSWAP sea states spanning wave heights from 1.5 to 7.0 metres, peak periods from 8 to 15 seconds, and spectral parameters from 1.0 to 3.3, creating realistic marine loading conditions that challenge model robustness across operational envelopes.

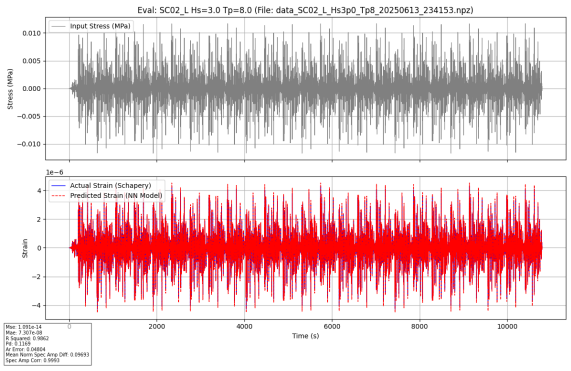

(a) Light sea state conditions with moderate marine loading scenarios.

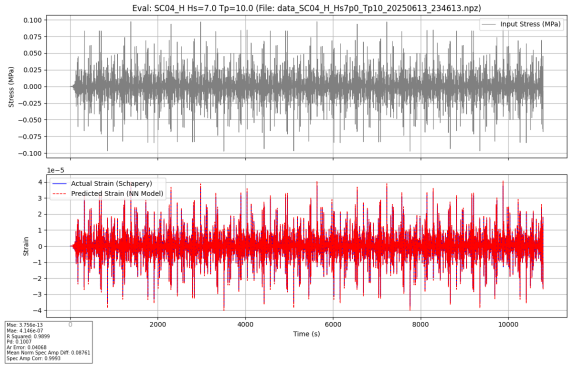

(b) Heavy sea state conditions with marine loading maintaining engineering viability.

Figure 4.32: Marine validation across operational envelope extremes.

Table 4.18: Marine validation results across sea state conditions.

Sea State Category	Wave Height Range	Capability Range	Median Capability	Engineering Assessment
Very Light	1.5 m	5.7%–10.2%	$\sim 7.2\%$	reliability for routine marine operations
Light	3.0 m	6.2%–11.7%	$\sim 8.3\%$	Very capability across typical operational scenarios
Moderate	5.0 m	6.6%–12.2%	$\sim 8.8\%$	capability with predictable degradation patterns
Heavy	7.0 m	7.0%–13.2%	$\sim 9.3\%$	capability under conditions with appropriate safety margins

Marine validation shows translation of neural network integration from controlled laboratory conditions to realistic operational complexity [11], as illustrated in Figure 4.32 and quantified in Table 4.18. The progression from very light to heavy conditions reveals capability characteristics that support engineering deployment confidence, while acknowledging the progressive challenges associated with increasing marine loading intensity.

4.4.2. Operational Envelope Coverage

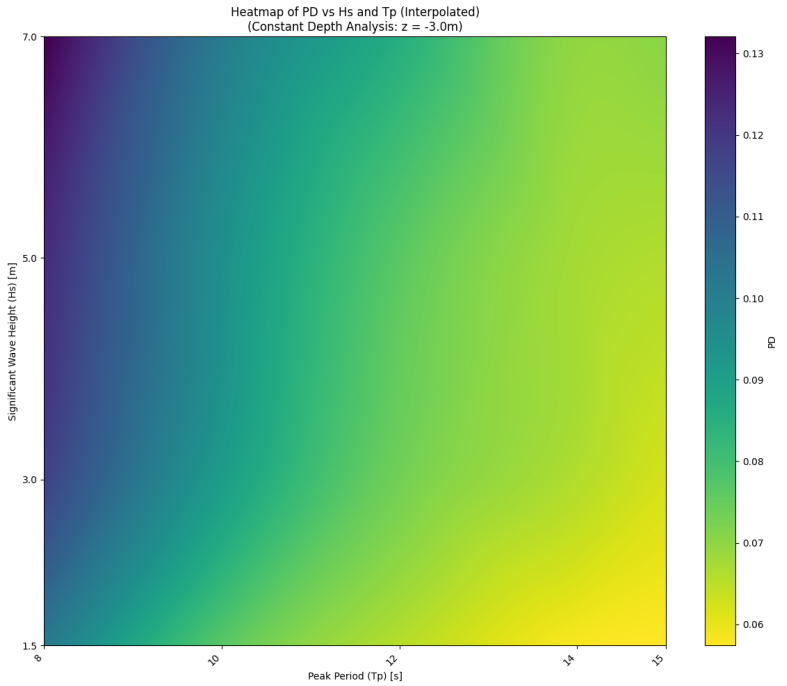

Figure 4.33: Capability landscape across wave heights and peak periods.

The operational envelope assessment in Figure 4.33 reveals the capability landscape characteristics that enable strategic deployment planning across various marine conditions. The analysis identifies distinct operational zones based on actual capability data rather than theoretical categorisations. Peak period effects dominate capability boundaries more strongly than wave height scaling. The frequency-sensitive zone, characterised by 8-second peak periods, consistently produces the most challenging conditions across all wave heights, with capability ranging from 10.2% to 13.2%. This finding suggests that physical mechanisms, characterised by short-period energy content, stress the model regardless of overall energy levels. Conversely, zones emerge when more extended peak periods (12–15 seconds) combine with moderate wave heights, producing consistently capable in the 5.7%–8.5% range.

4.4.3. Statistical Marine Loading Analysis

Statistical evaluation across marine loading parameters shows capability characteristics that provide insights for engineering deployment. Through analysis of percentage difference distributions across wave heights, peak periods, and stress configurations, distinct patterns emerge that guide application strategies.

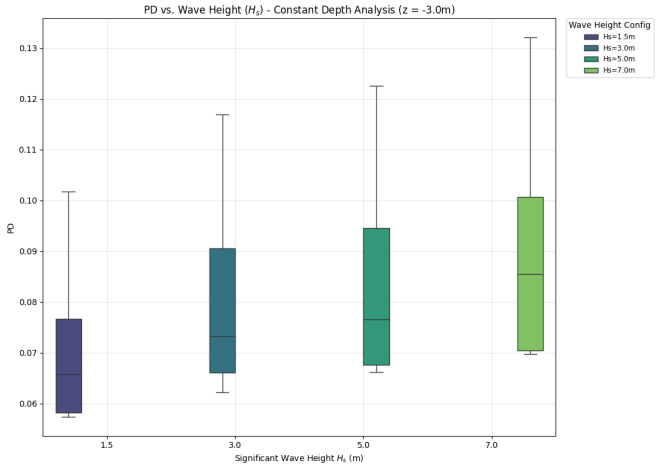

(a) Results across wave heights.

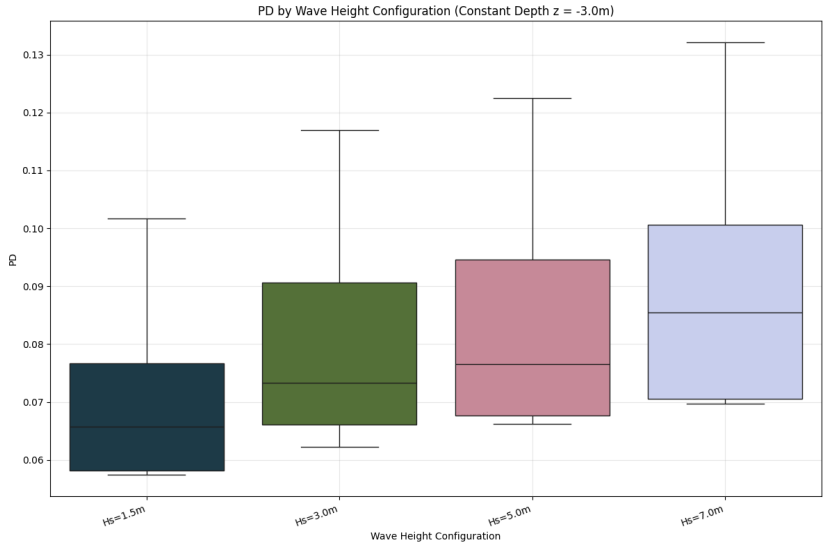

(b) Results progression across stress configurations.

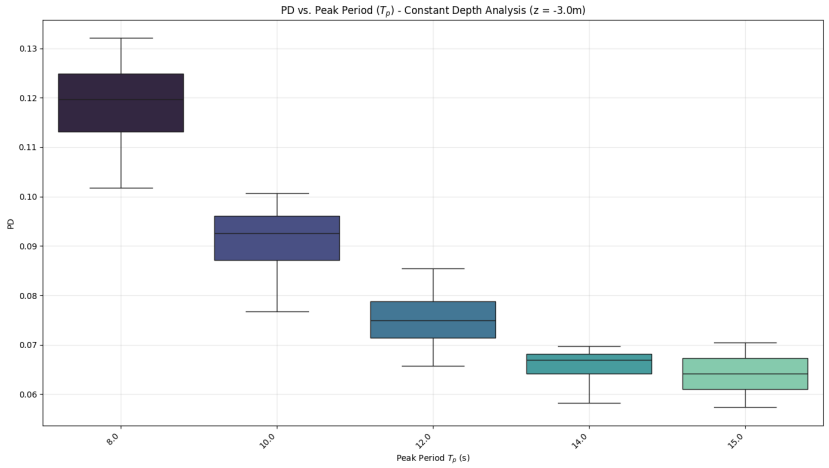

(c) Results across peak periods.

Figure 4.34: Statistical reliability assessment across marine loading parameters.

Table 4.19: Statistical reliability analysis across marine loading parameters.

Parameter Category	Capability Pattern	Important Threshold	Empirical Range	Engineering Deployment Guidance
Wave Height Scaling	Progressive degradation	above 5.0m	5.7%–13.2% across envelope	Degradation enables scaling predictions for deployment planning
Peak Period Sensitivity	Threshold-dominated behavior	Important below 10s periods	8s: 10.2%–13.2% $\geq$12s: 5.7%–8.5%	Short periods require safety margins due to frequency content complexity
Stress Configuration Effects	Monotonic progression	Moderate complexity boundary	VL: 5.7%–10.2% H: 7.0%–13.2%	Progressive capability degradation provides predictable operational boundaries
Combined Parameter Interactions	Multiplicative degradation	Multiple effects	Maximum 13.2% under worst scenarios	Multiple challenging factors compound effects requiring risk assessment protocols

Wave height analysis in Figure 4.34a shows capability degradation that follows predictable scaling relationships. Very light conditions (1.5m wave height) achieve percentage differences ranging from 5.7% to 10.2%, establishing the baseline capability envelope. As wave heights progress through light (3.0m), moderate (5.0m), and heavy (7.0m) conditions, the capability distributions shift upward whilst maintaining overlapping ranges that indicate gradual rather than abrupt degradation. Peak period effects in Figure 4.34c exhibit threshold-dominated behaviour with capability boundaries emerging around 10-second periods. Short periods of 8 seconds consistently produce the worst capability across all wave heights, with percentage differences ranging from 10.2% to 13.2%. More extended periods, ranging from 12 to 15 seconds, cluster together with markedly higher capability, from 5.7% to 8.5%.

The stress configuration progression in Figure 4.34b confirms the capability scaling that supports the model's ability to handle increasing complexity levels. The progression from very light (VL) to light (L), moderate (M), and heavy (H) configurations exhibits monotonic capability degradation with well-controlled variability. Statistical analysis shows that while individual parameters create effects, combinations produce multiplicative rather than additive capability challenges, as summarised in Table 4.19. The worst-case scenarios combining heavy wave heights (7.0m) with short peak periods (8s) approach the 13.2% capability boundary, emphasising the importance of considering parameter interactions rather than isolated effects when developing operational deployment strategies.

4.5. Neural Enhancement Validation Against Reference Model

To complete the validation framework, the model was tested against the original loading conditions used to establish the polynomial reference model, confirming that the neural enhancement approach replicates the twin experiment foundation whilst showing material representation.

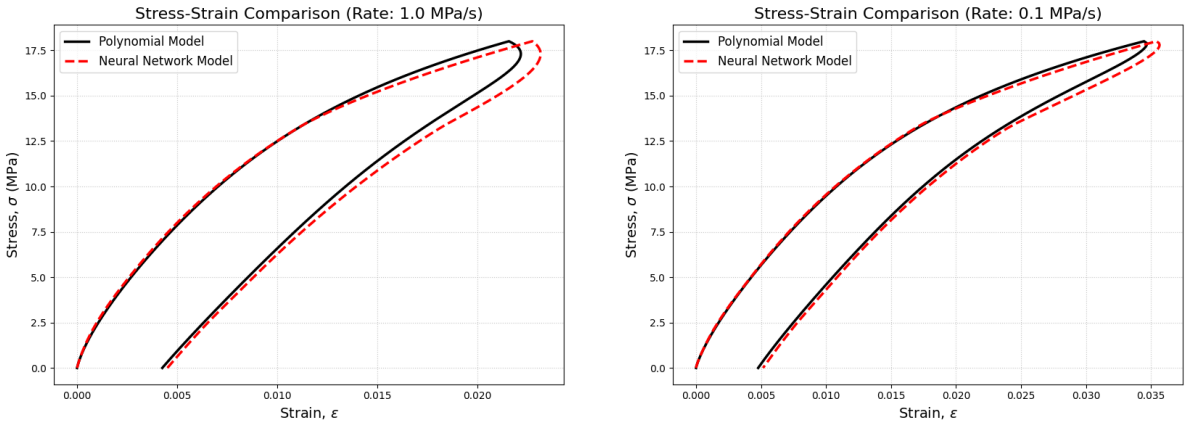

(a) Stress-strain comparison at 1.0 MPa/s loading rate.

(b) Stress-strain comparison at 0.1 MPa/s loading rate.

Figure 4.35: Neural network model validation against polynomial reference.

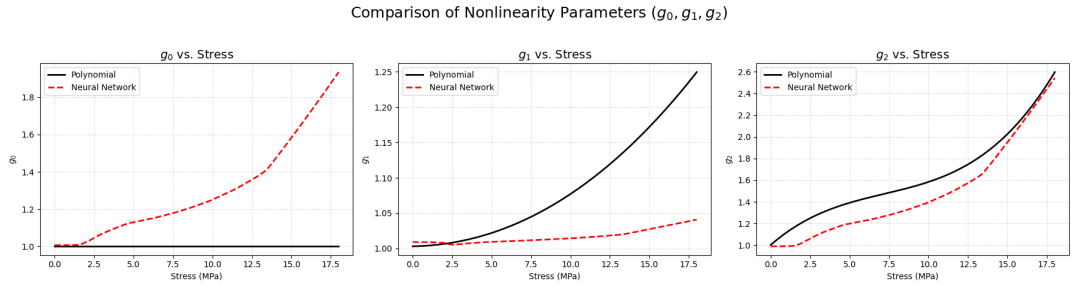

Figure 4.36: Comparison of learned nonlinearity functions.

Validation testing in Figures 4.35 and 4.36 shows neural enhancement of the material representation. The stress-strain comparisons show agreement between the model and polynomial reference across both loading rates, confirming that the neural integration approach maintains accuracy whilst providing material characterisation. The nonlinearity function comparison shows how the neural networks learned stress-dependent relationships that differ from the original polynomial constraints, whilst maintaining physical consistency. The g_0 function shows smoother stress-dependent evolution, whilst g_1 shows more nuanced behaviour compared to the polynomial approximation. The g_2 function exhibits similar trends with local detail that reflects the neural network's ability to capture material behaviour patterns beyond polynomial limitations.

4.6. Chapter Summary

This chapter documents an investigation that supports the integration of neural networks with the Schapery-Prony model for characterising synthetic fibres through parameter optimisation, targeted physics refinement, and realistic operational validation under marine conditions. The research demonstrates how replacing polynomial constraints with adaptive neural networks enhances material behaviour prediction while preserving physical principles. The investigation shows neural network integration requires coordination between optimisation objectives achieved through PD loss, providing scale-invariant learning, training data characteristics with Multi-Step loading, providing material exercising, and physics representation quality through More-Terms spectrum resolution, enabling temporal evolution. The approach identified suitable configurations whilst exposing limitations that guided targeted physics refinement from 10 to 14 relaxation terms.

The model addresses material characterisation challenges through physics-focused improvements rather than increasing neural network complexity, achieving 85%–95% accuracy across operational scenarios. Marine validation under realistic JONSWAP loading conditions [27] confirms deployment

viability with error ranges of 5.7%–13.2% across operational scenarios, supporting the model's readiness for engineering applications that require material behaviour prediction in marine environments. The methodology demonstrates that neural networks can replace polynomial constraints within physics models while preserving the physical consistency needed for engineering applications. The validation across laboratory and marine conditions establishes the model as a tool for synthetic fibre characterisation applications that require timeframes beyond conventional experimental limits.

5

Conclusions and Future Work

Neural networks can replace rigid polynomial constraints within established viscoelastic physics frameworks while maintaining physical consistency. The neural enhancement approach resolves the tension between mathematical convenience and physical accuracy, allowing the discovery of actual material behaviour without forcing predetermined functional forms onto complex stress-dependent relationships.

5.1. Research Question Resolution

The research question examined how neural networks could be integrated within Schapery's viscoelastic formulation to improve the representation of stress-dependent nonlinear functions whilst maintaining physical consistency. The neural enhancement approach addresses this by employing functional decomposition, which separates neural network learning from physics-based temporal evolution. The approach employs a shared-head neural network architecture, where neural networks learn the stress-dependent nonlinearity functions (g_0, g_1, g_2), while the Schapery-Prony model handles temporal evolution. This separation allows neural networks to discover complex material behaviour within physical boundaries rather than being constrained by predetermined polynomial forms.

The five-phase development methodology provides a reproducible approach for neural-physics integration: baseline optimisation through 13-dimensional Latin Hypercube Sampling, sensitivity analysis across design dimensions, capability testing to reveal underlying physics limitations, targeted improvement through spectral refinement, and operational validation under realistic conditions. The approach enables learning from limited experimental observations while maintaining physical foundations necessary for engineering applications, demonstrating capabilities for temporal extrapolation that align with established principles for physics-inspired neural networks [44]. The paradigm shift from assumption-driven to discovery-driven material characterisation represents a methodological advance. Rather than forcing material behaviour into convenient polynomial forms, the approach enables materials to demonstrate their actual stress-dependent characteristics, showing behaviour patterns that polynomial constraints may have prevented researchers from recognising.

5.2. Supporting Research Questions

Synthetic Data Generation and Neural Network Training (SQ1): The twin experiment methodology supports neural network training, generating unlimited synthetic datasets with known ground truth behaviour across operational ranges spanning stress levels 2–18 MPa and frequencies 0.0025–0.02 Hz. Multi-step loading is achieved by exercising material through a broad frequency spectrum generation, where sharp stress transitions probe fast relaxation modes, while sustained holds capture slow relaxation phenomena. The synthetic-to-real transferability was supported through multiple assessment methods, confirming that neural networks trained on synthetic data can discover material behaviour patterns that remain valid under diverse testing conditions.

Model Robustness and Validation (SQ2): The improved model shows stable behaviour under realistic operational complexity through validation that encompasses both marine loading robustness and

maintenance of temporal extrapolation capabilities. JONSWAP marine loading validation [27] across wave heights 1.5–7.0m, peak periods 8–15s, and spectral factors 1.0–3.3 achieved error ranges of 5.7%–13.2% that fall below typical marine engineering uncertainties. Critically, temporal extrapolation capabilities were maintained under this operational complexity, with the model achieving 85%–95% accuracy across demanding scenarios that extended to 128-fold duration ranges, even when subjected to realistic stochastic loading patterns. This dual validation confirms that the improved representation maintains effectiveness under both the chaos of realistic marine conditions and the demands of extended temporal prediction, following validated approaches for viscoelastic modelling under cyclic loading conditions [11].

Physical Interpretation and Computational Requirements (SQ3): Learned neural network functions show physical interpretations aligned with established material science principles [15]. The g_0 function represents stress-dependent scaling of instantaneous elastic response, g_1 captures transient compliance modifications reflecting stress-dependent relaxation strength, and g_2 exhibits exponential-like growth capturing loading rate effects that become increasingly important at elevated stress levels. These functions exhibit differences from polynomial approaches through their piecewise-linear capabilities, which capture sharp transitions, plateaus, and local behaviours that reflect accurate material physics. Computational requirements remain suitable for standard engineering workstations whilst maintaining the accuracy needed for engineering applications.

Multi-Dimensional Improvement Strategy and Limitation Resolution (SQ4): Capability testing showed limitations during demanding validation scenarios that required thorough diagnostic investigation across multiple improvement dimensions.

The improvement process proceeded through three coordinated stages:

Neural Architecture Improvement expanded model capacity with shared backbone progression from 2 layers $\times$ 32 neurons to 3 layers $\times$ 96 neurons, and head networks from 2 layers $\times$ 64 neurons to 2 layers $\times$ 144 neurons, providing necessary but not sufficient improvement.

Thorough Hyperparameter Reoptimisation through a second LHS campaign refined learning rates, training protocols, and architectural parameters, establishing conditions for effective neural-physics learning.

Physics Improvement Discovery emerged only after neural architecture and training optimisation showed that temporal extrapolation limitations resulted from insufficient spectral resolution in slow relaxation ranges (1×10^{-4} to 1×10^{-5} seconds), manifesting as ”accelerated relaxation” behaviour. The targeted solution improved the relaxation spectrum from 10 to 14 terms, providing 40% additional information about the continuous relaxation spectrum.

This supports the insight that neural improvement requires coordinated developments across neural architecture, training protocols, and physics representation simultaneously—showing an improvement methodology rather than isolated parameter modifications.

Engineering Integration Protocols (SQ5): The modular architecture allows integration with established engineering workflows through strain output compatibility with finite element analysis software, eliminating complex data conversion requirements. Implementation follows phases, from material characterisation using evidence-based, multi-step testing protocols, through model training to deployment, with quantified confidence bounds. The model’s natural integration path through standard stress-to-strain calculations provides immediate compatibility with major FEM software whilst preserving improved material discovery capabilities. Both temporal extrapolation and marine loading validation confirm that integration protocols maintain model capabilities needed for practical deployment.

Statistical Reliability Quantification (SQ6): Statistical approaches provide quantified reliability measures needed for engineering applications requiring long-term material prediction. Bootstrap confidence intervals and cross-validation [2] establish reliability bounds across operational scenarios with coverage probability. Risk-based decision approaches establish consequence-based reliability targets, enabling engineering deployment with appropriate safety margins. The statistical validation encompasses both temporal extrapolation reliability and marine loading behaviour, confirming that neural improvement provides reliable material characterisation capabilities with quantified uncertainty bounds suitable for infrastructure applications.

5.3. Research Contributions

The primary contribution shows that neural networks can replace polynomial constraints within established physics models while preserving physical consistency [12]. This addresses the tension between mathematical tractability and physical accuracy, providing methodologies for physics-guided machine learning development beyond synthetic fibre applications [44, 30]. The functional decomposition architecture provides design guidance by separating neural learning from physics temporal evolution, allowing complex function approximation without compromising established thermodynamic principles. The approach avoids memory system conflicts while creating stable learning conditions that enable the discovery of material laws rather than memorisation of training patterns.

The five-phase methodology establishes reproducible approaches for integrating neural physics across diverse applications. The methodology addresses the challenge of distinguishing between genuine configurations and arbitrary parameter combinations through evidence-based development protocols that ensure reliable improvement. The diagnostic insight that neural improvement requires coordinated developments across neural architecture, training protocols, and physics representation guides efficient improvement strategies. This finding challenges conventional approaches that focus on individual aspects in isolation, demonstrating that multidimensional improvement often yields more benefits than modifications to any single component. This methodological insight extends beyond viscoelastic applications to other computational physics domains, where the integration of neural physics proves important.

The paradigm shift from polynomial constraints to neural network discovery represents a methodological advance. Traditional approaches force material behaviour into predetermined mathematical forms chosen for computational convenience rather than physical accuracy. The neural improvement approach enables materials to exhibit their actual behaviour patterns, potentially revealing material physics that polynomial constraints have previously prevented researchers from recognising.

5.4. Impact and Applications

This research enhances synthetic fibre characterisation by transitioning from rigid polynomial constraints to adaptive learning capabilities, enabling improved representation of material behaviour using limited experimental data while maintaining the physical consistency required for engineering applications. This addresses challenges in offshore renewable energy deployment where reliable long-term material characterisation cannot be achieved through conventional approaches alone [26, 56]. The methodological paradigm shift from assumption-driven to discovery-driven material characterisation allows for the identification of true material behaviour while maintaining the physical foundations necessary for reliable engineering applications. Rather than accepting mathematical convenience at the expense of physical accuracy, the approach demonstrates methods for allowing materials to exhibit their actual stress-dependent characteristics.

Economic benefits emerge from reductions in characterisation timelines and costs, reducing material qualification periods from 12 to 18 months to 2 to 4 weeks while maintaining the reliability standards needed for infrastructure applications. The twin experiment methodology eliminates the need for extensive physical testing during model development, while the improved model enables reliable predictions based on short-term experimental observations. The methodology demonstrates applicability beyond synthetic fibre characterisation, as evidenced by its successful integration with established physics frameworks [52]. The approach addresses challenges in computational materials science where traditional mathematical constraints may limit material discovery, building upon data-driven approaches that have shown promise across various material systems [7].

5.5. Study Limitations

The approach requires validation across other synthetic fibre materials, beyond HDPE, to establish its applicability. The current implementation represents a single-material approach that lacks multi-material capacity, limiting deployment across fibre types without individual model development for each material. The model addresses only three of the four nonlinear Schapery parameters (g_0, g_1, g_2), whilst the time-scaling parameter a_σ was disregarded for simplification. This omission may limit accuracy for materials where time-scaling effects prove essential, particularly under extreme loading rates or tem-

perature variations. Marine validation focused on moderate sea states requiring additional protocols for extreme environmental conditions. The 14-term spectral improvement addresses the identified limitations; however, other constraints may emerge with different materials or extended testing requirements that exceed current validation ranges. Computational efficiency suits standard workstations but may require optimisation for large-scale deployment.

5.6. Future Research Directions

Priorities include extending the neural improvement approach to other synthetic fibre materials (polyester, aramid, UHMWPE) and developing multi-material capabilities that allow unified model deployment across diverse fibre types [45]. Incorporating the a_σ parameter through neural improvement would provide complete Schapery nonlinearity representation. Improved physics integration, incorporating temperature effects and environmental degradation, would expand applicability to realistic engineering scenarios. Future developments may include adaptive physics improvement approaches that extend the spectral refinement principles demonstrated in this work, and Bayesian uncertainty quantification methods that could provide enhanced statistical reliability measures for engineering deployment [61]. The methodology has broader applicability across computational physics domains requiring improved material characterisation from limited experimental observations, including composite materials, fatigue prediction, and environmental degradation modelling, where physics-guided neural improvement can address prediction challenges [3, 1].

5.7. Summary

The research demonstrates that integrating neural networks with established physics principles addresses challenges in computational materials science while maintaining the reliability required for engineering applications. The achievement lies in developing approaches for integrating neural physics that allow for the discovery of true material behaviour rather than conforming to mathematical convenience. The approach enables the improved representation of material behaviour from limited experimental observations, addressing challenges in offshore renewable energy deployment while providing technical foundations for advancing synthetic fibre applications. The validation through both temporal extrapolation testing and realistic marine loading conditions establishes the model's readiness for engineering deployment, with quantified confidence bounds suitable for infrastructure applications that require reliable long-term material predictions.

The methodology provides principles applicable across computational materials science domains that require improved characterisation capabilities while preserving the theoretical rigour needed for practical engineering deployment.

Data and Code Availability

The synthetic datasets and core Python implementation of the Neural Enhancement Model are available from the corresponding author upon reasonable request.

Bibliography

[1] K. P. Abdolazizi, K. Linka, and C. J. Cyron. “Viscoelastic constitutive artificial neural networks (vCANNs) – A framework for data-driven anisotropic nonlinear finite viscoelasticity”. In: *Journal of Computational Physics* 499 (2024), p. 112704. DOI: 10.1016/j.jcp.2023.112704.

[2] Johannes Allgaier and Rüdiger Pryss. “Cross-Validation Visualized: A Narrative Guide to Advanced Methods”. In: *Machine Learning and Knowledge Extraction* 6.2 (2024), pp. 1378–1388. DOI: 10.3390/MAKE6020065.

[3] Faisal As’ad and Charbel Farhat. “A mechanics-informed deep learning framework for data-driven nonlinear viscoelasticity”. In: *Computer Methods in Applied Mechanics and Engineering* 417 (2023). DOI: 10.1016/J.CMA.2023.116463.

[4] S. J. Banfield, N. F. Casey, and R. Nataraja. “Durability of Polyester Deepwater Mooring Rope”. In: *Offshore Technology Conference*. 2005. DOI: 10.4043/17510-MS.

[5] E. J. Barbero. “Time-temperature-age superposition principle for predicting long-term response of linear viscoelastic materials”. In: *Creep and Fatigue in Polymer Matrix Composites* (2010), pp. 48–69. DOI: 10.1533/9780857090430.1.48.

[6] Russell R. Barton and Luke A. Rhodes-Leader. “Bootstrap Confidence Intervals for Simulation Output Parameters”. In: *Proceedings - Winter Simulation Conference* (2023), pp. 421–432. DOI: 10.1109/WSC60868.2023.10407467.

[7] M. A. Bessa et al. “A framework for data-driven analysis of materials under uncertainty: Countering the curse of dimensionality”. In: *Computer Methods in Applied Mechanics and Engineering* 320 (2017), pp. 633–667. DOI: 10.1016/j.cma.2017.03.037.

[8] J. Bolton. “The potential for major extrapolation of creep rupture and creep strain data”. In: *Materials at High Temperatures* 31.2 (2014), pp. 109–120. DOI: 10.1179/1878641314Y.0000000007.

[9] Prapatsorn Borisut and Aroonsri Nuchitprasittichai. “Adaptive Latin Hypercube Sampling for a Surrogate-Based Optimization with Artificial Neural Network”. In: *Processes* 11.11 (2023), p. 3232. DOI: 10.3390/PR11113232.

[10] Guang Chen. “Recurrent neural networks (RNNs) learn the constitutive law of viscoelasticity”. In: *Computational Mechanics* 67.3 (2021), pp. 1009–1019. DOI: 10.1007/S00466-021-01981-Y.

[11] J. A. Cholewa, R. W. I. Brachman, and I. D. Moore. “Effectiveness of Viscoelastic Models for Prediction of Tensile Axial Strains during Cyclic Loading of High-Density Polyethylene Pipe”. In: *Journal of Pipeline Systems Engineering and Practice* 1.2 (2010), pp. 77–83. DOI: 10.1061/(ASCE)PS.1949-1204.0000053.

[12] G. Cybenko. “Approximation by superpositions of a sigmoidal function”. In: *Mathematics of Control, Signals, and Systems* 2.4 (1989), pp. 303–314. DOI: 10.1007/BF02551274.

[13] P. Davies et al. “Mechanical behaviour of HMPE and aramid fibre ropes for deep sea handling operations”. In: *Ocean Engineering* 38.17–18 (2011), pp. 2208–2214. DOI: 10.1016/j.oceaneng.2011.10.010.

[14] Francesco Depalo et al. “Design and analysis of a mooring system for a wave energy converter”. In: *Journal of Marine Science and Engineering* 9.7 (2021). DOI: 10.3390/JMSE9070782.

[15] John D. Ferry. *Viscoelastic Properties of Polymers*. John Wiley & Sons, 1980.

[16] Michel Francois et al. “Modelling fiber rope load-elongation properties - Polyester and other fibers”. In: *Offshore Technology Conference*. 2010. DOI: 10.4043/20846-MS.

[17] Nicolas Gort, Igor Zhilyaev, and Christian Brauner. “Incremental Numerical Approach for Modeling the Macroscopic Viscoelastic Behavior of Fiber-Reinforced Composites Using a Representative Volume Element”. In: *Materials* 15.19 (2022), p. 6724. DOI: 10.3390/MA15196724.

[18] A. E. Green and R. S. Rivlin. “The mechanics of non-linear materials with memory - Part I”. In: *Archive for Rational Mechanics and Analysis* 1.1 (1957), pp. 1–21. DOI: 10.1007/BF00297992.

[19] M. S. Al-Haik, M. Y. Hussaini, and H. Garmestani. “Prediction of nonlinear viscoelastic behavior of polymeric composites using an artificial neural network”. In: *International Journal of Plasticity* 22 (2006), pp. 1367–1392. DOI: 10.1016/j.ijplas.2005.09.002.

[20] Rami M. Haj-Ali and Anastasia H. Muliana. “Numerical finite element formulation of the Schapery non-linear viscoelastic material model”. In: *International Journal for Numerical Methods in Engineering* 59.1 (2004), pp. 25–45. DOI: 10.1002/nme.861.

[21] C. J. M. Van Den Heuvel et al. “Molecular changes of PET yarns during stretching measured with rheo-optical infrared spectroscopy and other techniques”. In: *Journal of Applied Polymer Science* 49.5 (1993), pp. 925–934. DOI: 10.1002/app.1993.070490518.

[22] Kurt Hornik, Maxwell Stinchcombe, and Halbert White. “Multilayer feedforward networks are universal approximators”. In: *Neural Networks* 2.5 (1989), pp. 359–366. DOI: 10.1016/0893-6080(89)90020-8.

[23] Wei Huang et al. “Modeling nonlinear time-dependent behaviors of synthetic fiber ropes under cyclic loading”. In: *Ocean Engineering* 109 (2015), pp. 207–216. DOI: 10.1016/j.oceaneng.2015.09.009.

[24] David G. Hunt. “The prediction of long-time viscoelastic creep from short-time data”. In: *Wood Science and Technology* 38.7 (2004), pp. 479–492. DOI: 10.1007/S00226-004-0244-6.

[25] Ronald L. Iman. “Latin Hypercube Sampling”. In: *Encyclopedia of Quantitative Risk Analysis and Assessment* (2008). DOI: 10.1002/9780470061596.RISK0299.

[26] International Energy Agency. “World Energy Outlook 2023”. In: (2023).

[27] Muhammad Azeem Khan et al. “Application of Stokes’ higher order theory and JONSWAP spectrum in modelling extreme wave events validation with historical data”. In: *E3S Web of Conferences* 603 (2025), p. 03008. DOI: 10.1051/E3SCONF/202560303008.

[28] Cheolmin Kim, Youngseok Kim, and Diego Klabjan. “Scale Invariant Power Iteration”. In: *Journal of Machine Learning Research* 24 (2019).

[29] Diederik P. Kingma and Jimmy Lei Ba. “Adam: A method for stochastic optimization”. In: *3rd International Conference on Learning Representations, ICLR 2015* (2015).

[30] T. Kirchdoerfer and M. Ortiz. “Data-driven computational mechanics”. In: *Computer Methods in Applied Mechanics and Engineering* 304 (2016), pp. 81–101. DOI: 10.1016/j.cma.2016.02.001.

[31] Ravikiran S. Kota, William Greiner, and Richard B. D’Souza. “Comparative Assessment of Steel and Polyester Moorings in Ultradeep Water for Spar- and Semi-Based Production Platforms”. In: *Offshore Technology Conference*. 1999. DOI: 10.4043/10909-MS.

[32] Junbiao Lai. *Non-Linear Time Dependent Deformation Behavior of High Density Polyethylene*. 1995.

[33] Daniele Lanzoni et al. “Extreme time extrapolation capabilities and thermodynamic consistency of physics-inspired neural networks for the 3D microstructure evolution of materials via Cahn–Hilliard flow”. In: *Machine Learning: Science and Technology* 5.4 (2024), p. 045017. DOI: 10.1088/2632-2153/AD8532.

[34] Yushun Lian et al. “An experimental investigation on the bedding-in behavior of synthetic fiber ropes”. In: *Ocean Engineering* 160 (2018), pp. 368–381. DOI: 10.1016/J.OCEANENG.2018.04.071.

[35] H. Liu et al. “An experimental investigation on nonlinear behaviors of synthetic fiber ropes for deepwater moorings under cyclic loading”. In: *Applied Ocean Research* 45 (2014), pp. 22–32. DOI: 10.1016/j.apor.2013.12.003.

[36] H. A. McKenna, J. W. Hearle, and N. O’Hear. *Handbook of Fibre Rope Technology*. Vol. 34. Woodhead Publishing, 2004.

[37] V. V. Neis and J. L. Sackman. “An Experimental Study of a Nonlinear Material with Memory”. In: *Transactions of the Society of Rheology* 11.3 (1967), pp. 307–333. DOI: 10.1122/1.549082.

[38] Nhu Nguyen and Krish Thiagarajan. “Nonlinear viscoelastic modeling of synthetic mooring lines”. In: *Marine Structures* 85 (2022). DOI: 10.1016/j.marstruc.2022.103257.

[39] B. J. Overton, C. R. Taylor, and J. W. Shea. “The Use of Time-Temperature Superposition Techniques to Forecast Creep Behavior in Engineering Plastics”. In: *MRS Proceedings* 142 (1988). DOI: 10.1557/PROC-142-203.

[40] Kritika Pandey and Sanskruti Patel. “A Theoretical Perspective and Experimental Evaluation of the Extensive Analysis of Loss Functions in Machine Learning and Deep Learning”. In: *2024 Asia Pacific Conference on Innovation in Technology, APCIT 2024* (2024). DOI: 10.1109/APCIT62007.2024.10673427.

[41] Ivan De Pellegrin. “Manmade Fiber Ropes in Deepwater Mooring Applications”. In: *Offshore Technology Conference*. 1999. DOI: 10.4043/10907-MS.

[42] Hong Duc Pham et al. “Dynamic modeling of nylon mooring lines for a floating wind turbine”. In: *Applied Ocean Research* 87 (2019), pp. 1–8. DOI: 10.1016/j.apor.2019.03.013.

[43] A. C. Pipkin and T. G. Rogers. “A non-linear integral representation for viscoelastic behaviour”. In: *Journal of the Mechanics and Physics of Solids* 16.1 (1968), pp. 59–72. DOI: 10.1016/0022-5096(68)90016-1.

[44] M. Raissi, P. Perdikaris, and G. E. Karniadakis. “Physics-informed neural networks: A deep learning framework for solving forward and inverse problems involving nonlinear partial differential equations”. In: *Journal of Computational Physics* 378 (2019), pp. 686–707. DOI: 10.1016/J.JCP.2018.10.045.

[45] R. Ramprasad et al. “Machine learning in materials informatics: recent applications and prospects”. In: *npj Computational Materials* 3 (2017). DOI: 10.1038/s41524-017-0056-5.

[46] D. Roylance. *Engineering Viscoelasticity*. Tech. rep. Department of Materials Science and Engineering, Massachusetts Institute of Technology, 2001, pp. 1–37.

[47] Laith Abed Sabri et al. “Performance Evaluation of Nonlinear Viscoelastic Materials using Finite Element Method”. In: *International Journal of Applied Mechanics and Engineering* 29.1 (2024), pp. 142–158. DOI: 10.59441/IJAME/184138.

[48] Klaus Bernd Sautter et al. “Limitations of the St. Venant-Kirchhoff material model in large strain regimes”. In: *International Journal of Non-linear Mechanics* 147 (2022), p. 104207. DOI: 10.1016/J.IJNONLINMEC.2022.104207.

[49] R. A. Schapery. “On the characterization of nonlinear viscoelastic materials”. In: *Polymer Engineering & Science* 9.4 (1969), pp. 295–310. DOI: 10.1002/pen.760090410.

[50] Fabian Schneider, Ralph J. Hellmig, and Oliver Nelles. “Latin hypercubes for constrained design of experiments for data-driven models”. In: *At-Automatisierungstechnik* 71.10 (2023), pp. 820–832. DOI: 10.1515/AUTO-2023-0017.

[51] John Boyet Stevens, Gary Menary, and Shiyong Yan. “Hybrid Artificial Neural Network Approach for Modelling the Behavior of Polyethylene Terephthalate (PET) at Conditions Applicable to Stretch Blow Molding”. In: *Preprints* (2024). DOI: 10.20944/PREPRINTS202411.1115.V1.

[52] Marcus Stoffel, Franz Bamer, and Bernd Markert. “Artificial neural networks and intelligent finite elements in non-linear structural mechanics”. In: *Thin-Walled Structures* 131 (2018), pp. 102–106. DOI: 10.1016/J.TWS.2018.06.035.

[53] H. Thuilliez et al. “Characterization and modelling of the dynamic stiffness of nylon mooring rope for floating wind turbines”. In: *Ocean Engineering* 287 (2023). DOI: 10.1016/j.oceaneng.2023.115866.

[54] Qi Wang et al. “A Comprehensive Survey of Loss Functions in Machine Learning”. In: *Annals of Data Science* 9.2 (2022), pp. 187–212. DOI: 10.1007/S40745-020-00253-5.

[55] I. M. Ward and E. T. Onat. “Non-linear mechanical behaviour of oriented polypropylene”. In: *Journal of the Mechanics and Physics of Solids* 11.4 (1963), pp. 217–229. DOI: 10.1016/0022-5096(63)90008-5.

[56] S. D. Weller et al. “Synthetic mooring ropes for marine renewable energy applications”. In: *Renewable Energy* 83 (2015), pp. 1268–1278. DOI: 10.1016/j.renene.2015.03.058.

[57] D. F. Williamson, R. A. Parker, and J. S. Kendrick. “The box plot: A simple visual method to interpret data”. In: *Annals of Internal Medicine* 110.11 (1989), pp. 916–921. DOI: 10.7326/0003-4819-110-11-916.

[58] Sheng Xu, Chun Yan Ji, and C. Guedes Soares. “Experimental and numerical investigation a semi-submersible moored by hybrid mooring systems”. In: *Ocean Engineering* 163 (2018), pp. 641–678. DOI: 10.1016/j.oceaneng.2018.05.006.

[59] Sheng Xu, Chunyan Ji, and C. Guedes Soares. “Experimental study on taut and hybrid moorings damping and their relation with system dynamics”. In: *Ocean Engineering* 154 (2018), pp. 322–340. DOI: 10.1016/j.oceaneng.2018.01.085.

[60] Sheng Xu et al. “Experimental evaluation of the dynamic stiffness of synthetic fibre mooring ropes”. In: *Applied Ocean Research* 112 (2021), p. 102709. DOI: 10.1016/J.APOR.2021.102709.

[61] Chunhao Yang et al. “Comparative study of machine learning approaches for predicting creep behavior of polyurethane elastomer”. In: *Polymers* 13.11 (2021). DOI: 10.3390/POLYM13111768.

A

Sensitivity Analysis: Model Prediction Visualisations

This appendix presents visualisations of neural network model predictions across three sensitivity analysis dimensions conducted during the development of the Neural-Enhanced Schapery-Prony Model. All predictions are evaluated against Multi-Step Cyclic loading patterns with a maximum stress level of 8 MPa, comparing model responses with the ground truth across both time and frequency domains. These visualisations provide reference material for understanding model behaviour across different configuration choices that influence neural enhancement effectiveness.

A.1. Loading Pattern Sensitivity Analysis

These figures demonstrate the model prediction accuracy when trained on different loading pattern types, revealing how the characteristics of the training data influence the neural network's learning of stress-dependent material behaviour.

A.1.1. Time Domain Analysis

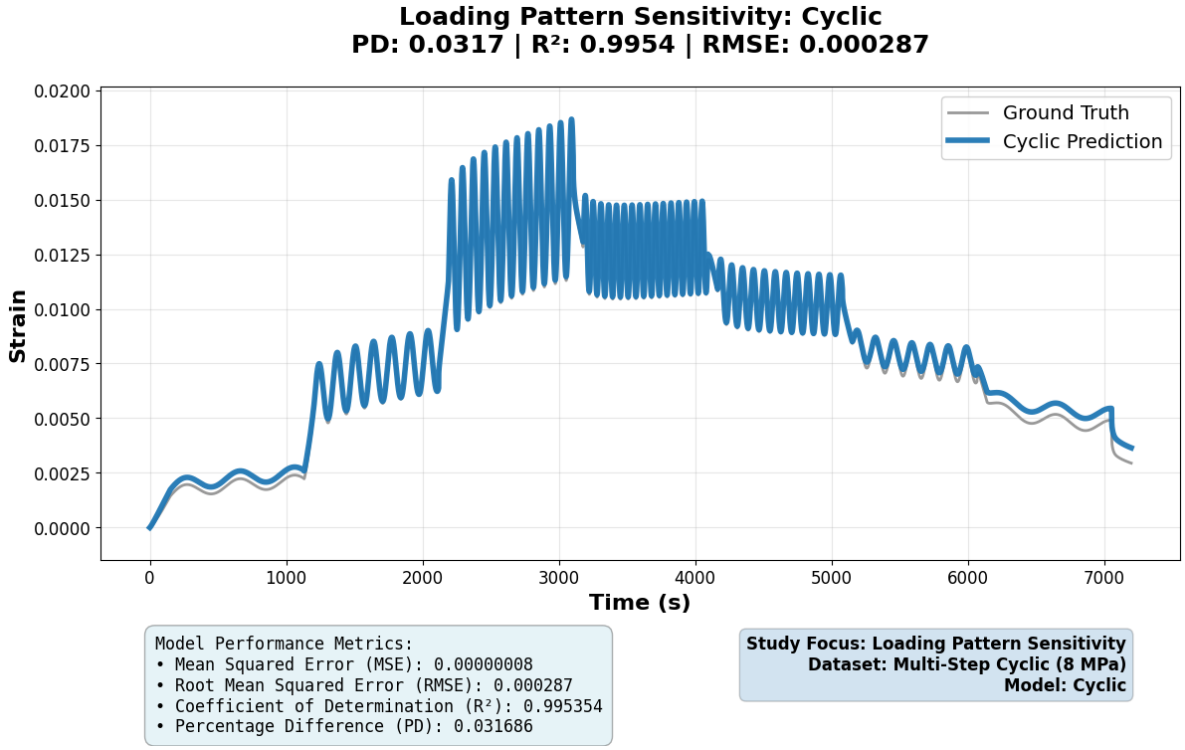

Figure A.1: Model prediction accuracy for Cyclic loading pattern training.

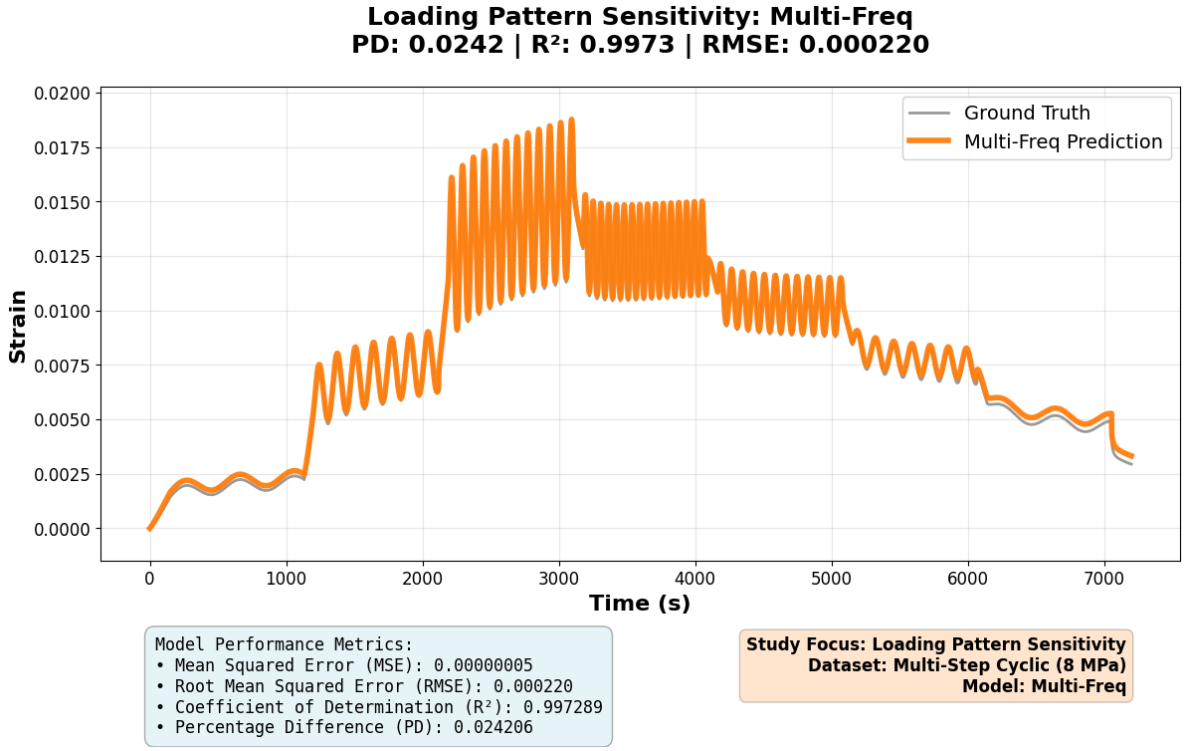

Figure A.2: Model prediction accuracy for Multi-Frequency loading pattern training.

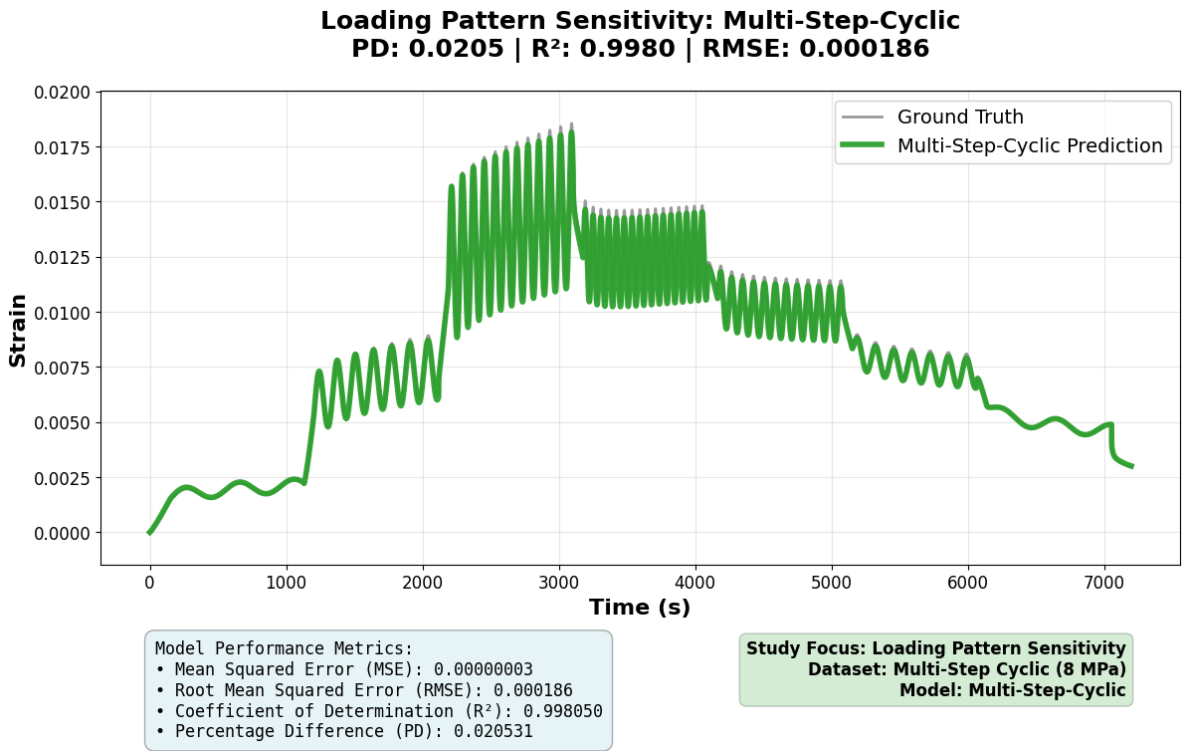

Figure A.3: Model prediction accuracy for Multi-Step Cyclic loading pattern training.

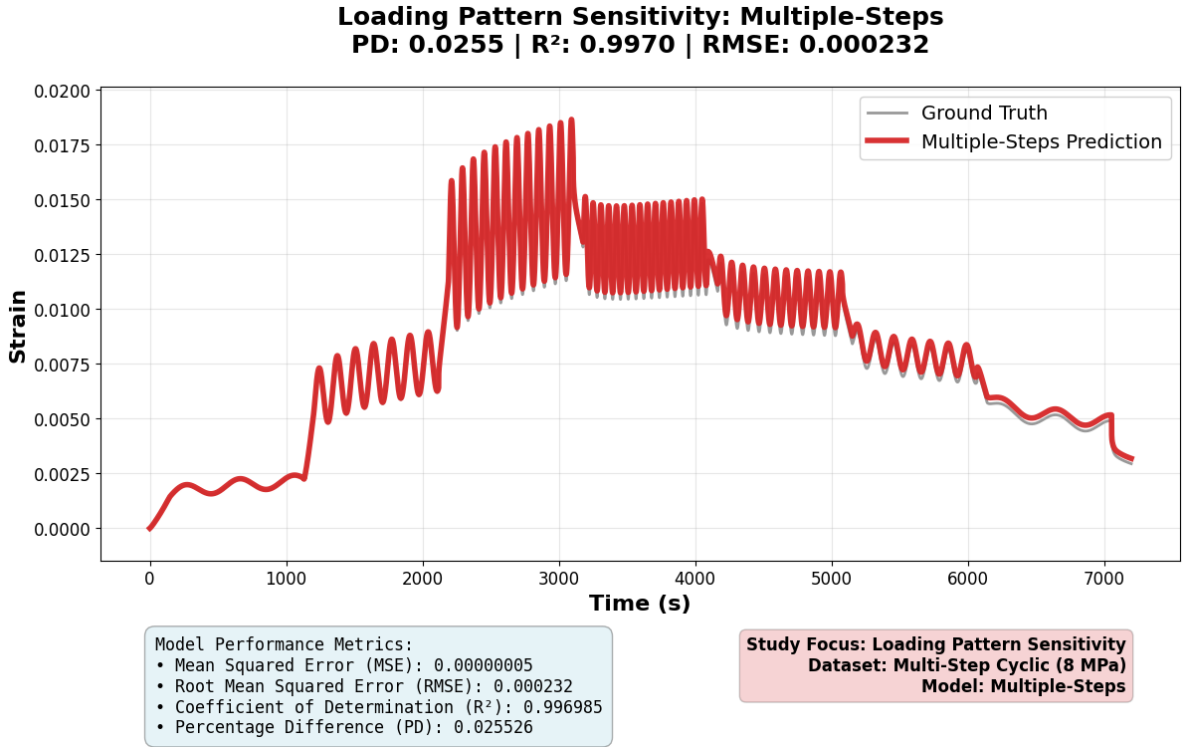

Figure A.4: Model prediction accuracy for Multiple-Steps loading pattern training.

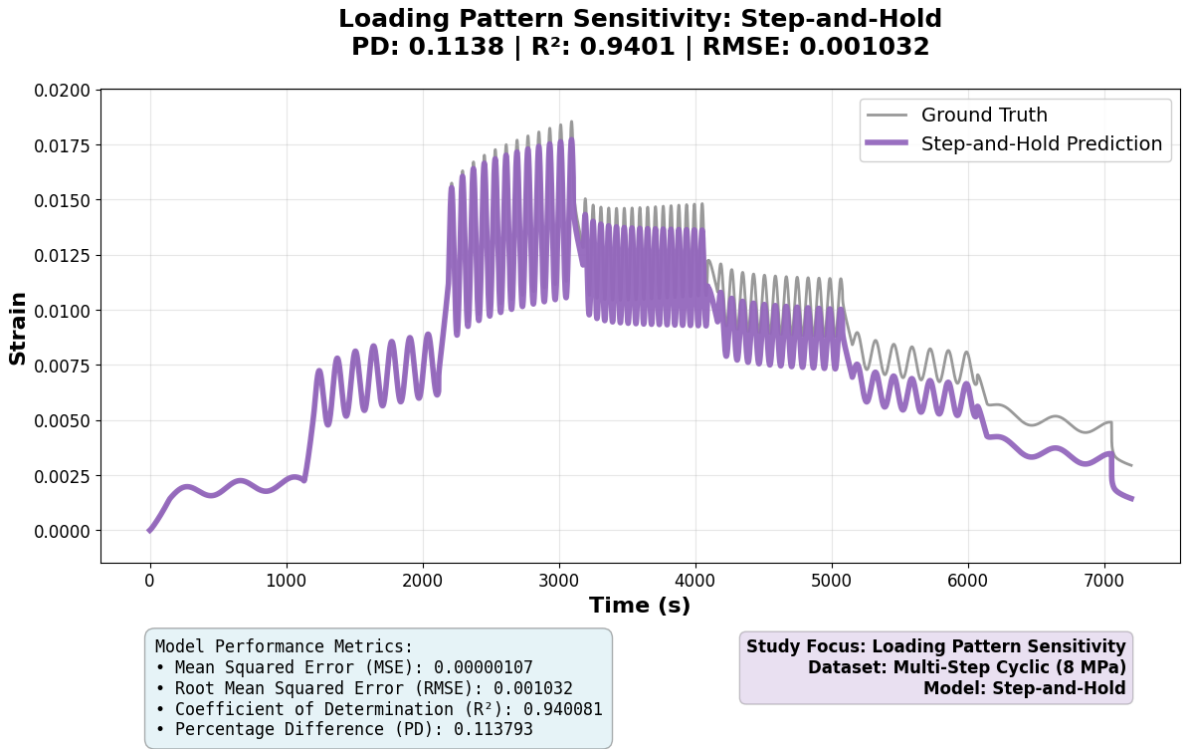

Figure A.5: Model prediction accuracy for Step-and-Hold loading pattern training.

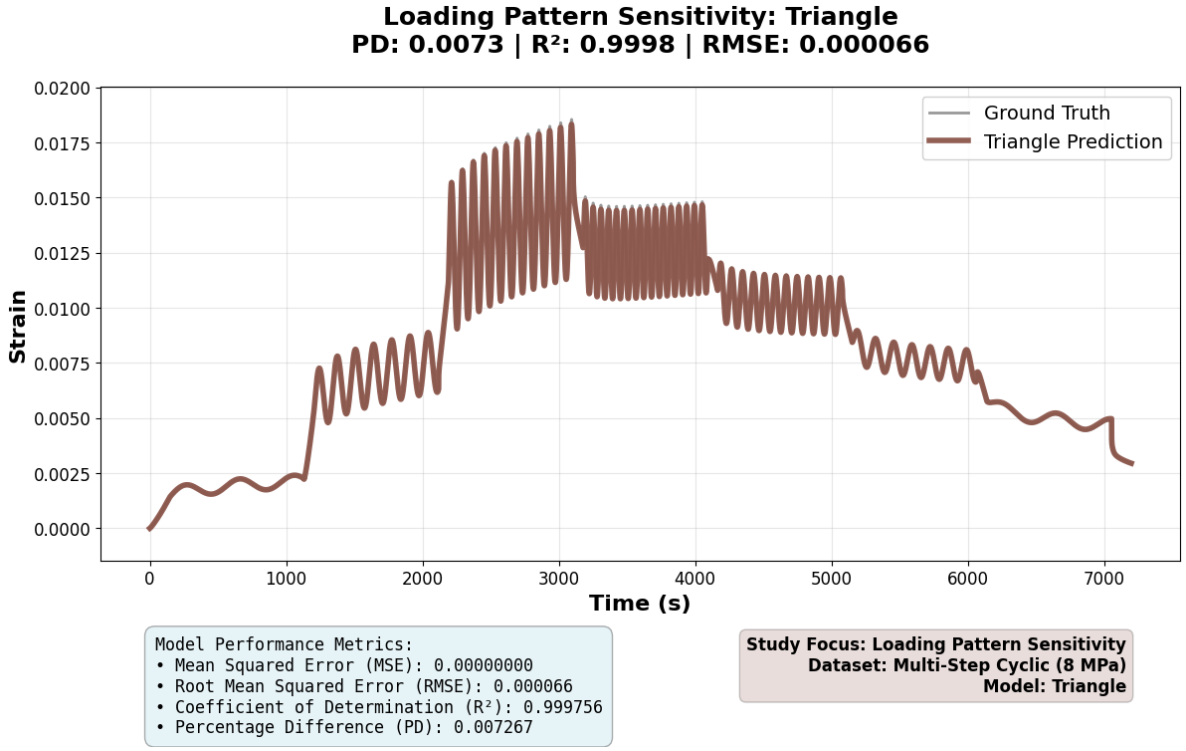

Figure A.6: Model prediction accuracy for Triangle loading pattern training.

A.1.2. Frequency Domain Analysis

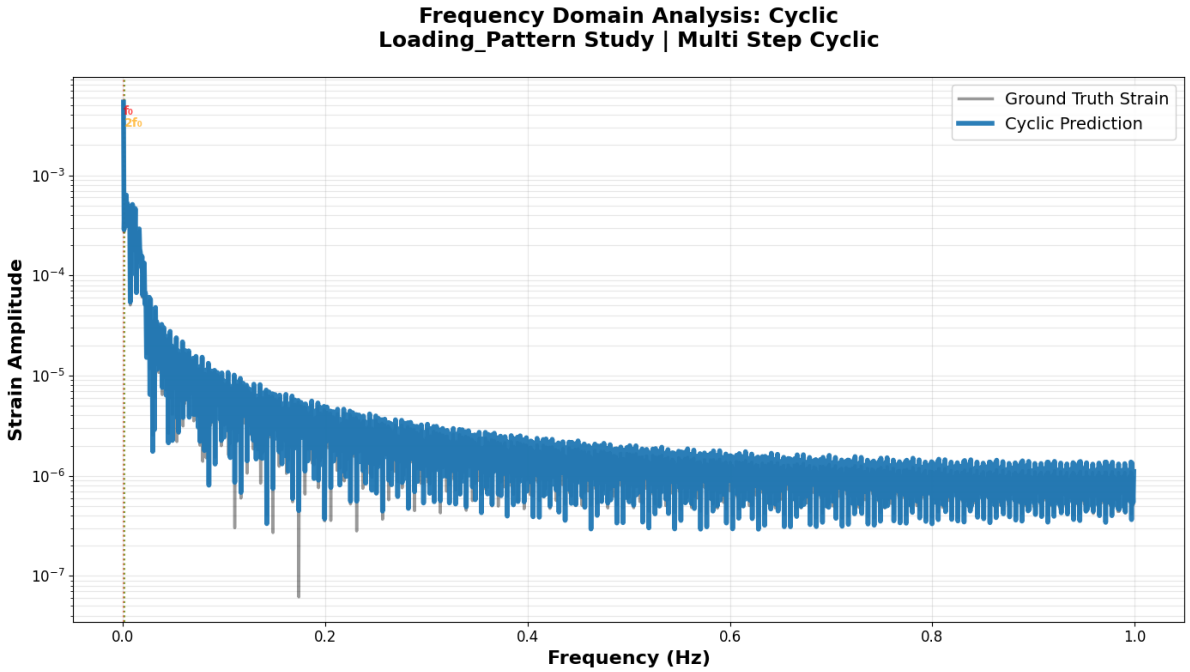

Figure A.7: Frequency domain analysis for Cyclic loading pattern training.

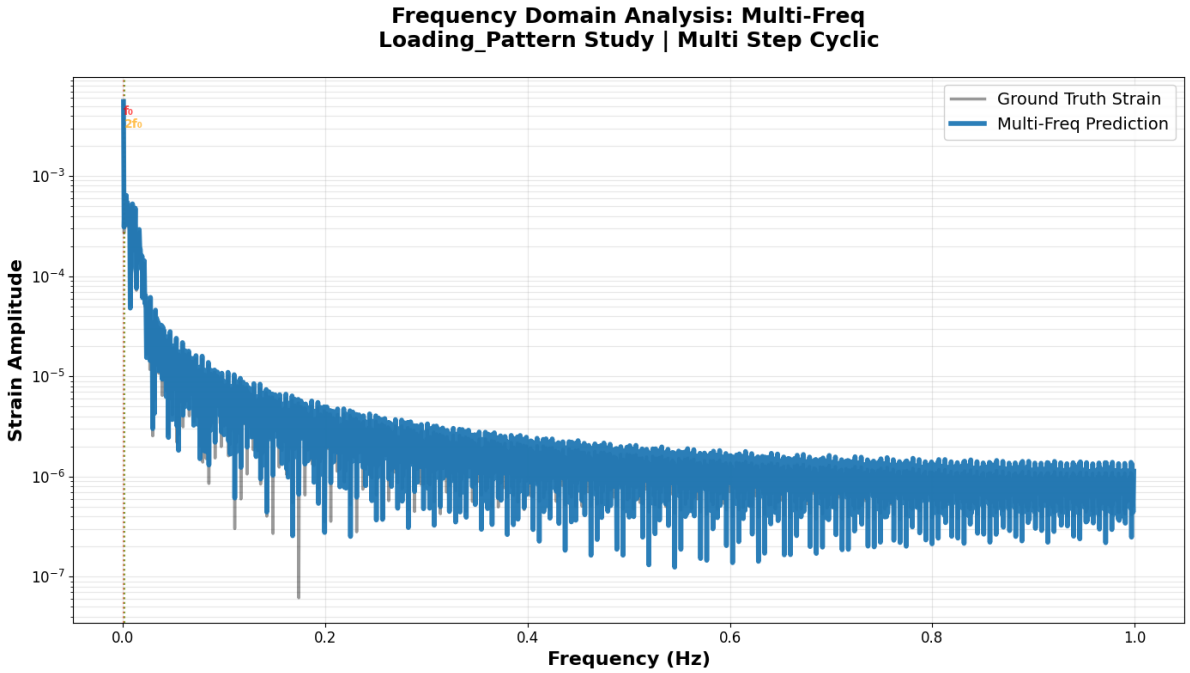

Figure A.8: Frequency domain analysis for Multi-Frequency loading pattern training.

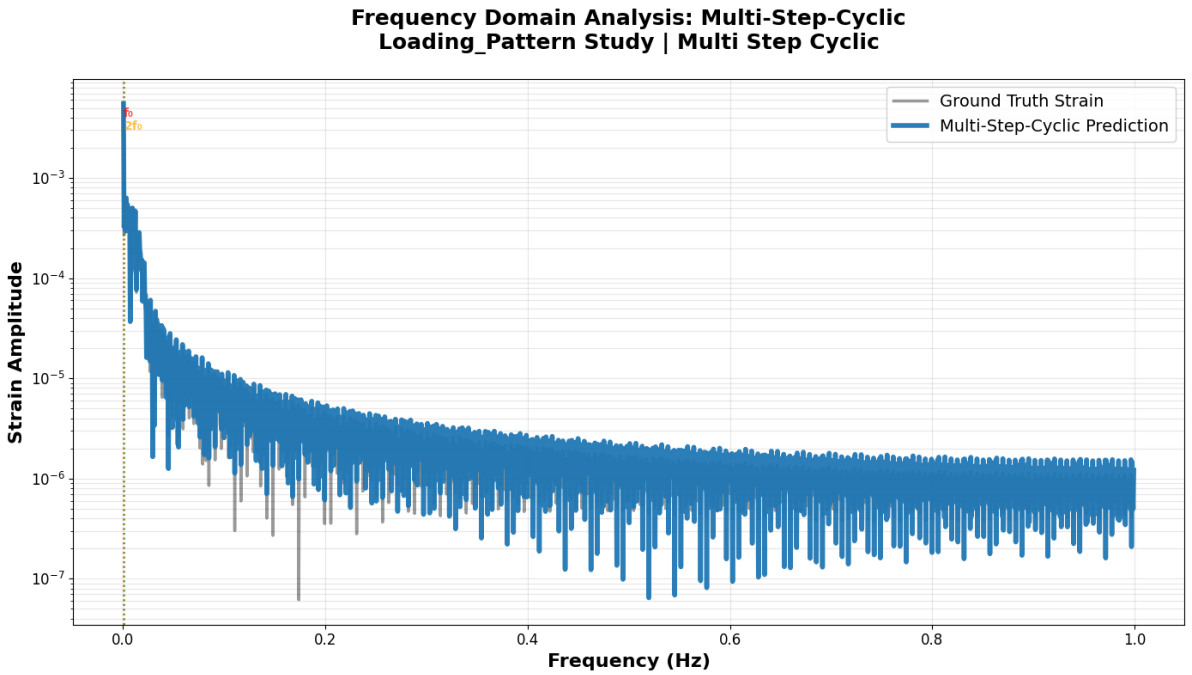

Figure A.9: Frequency domain analysis for Multi-Step Cyclic loading pattern training.

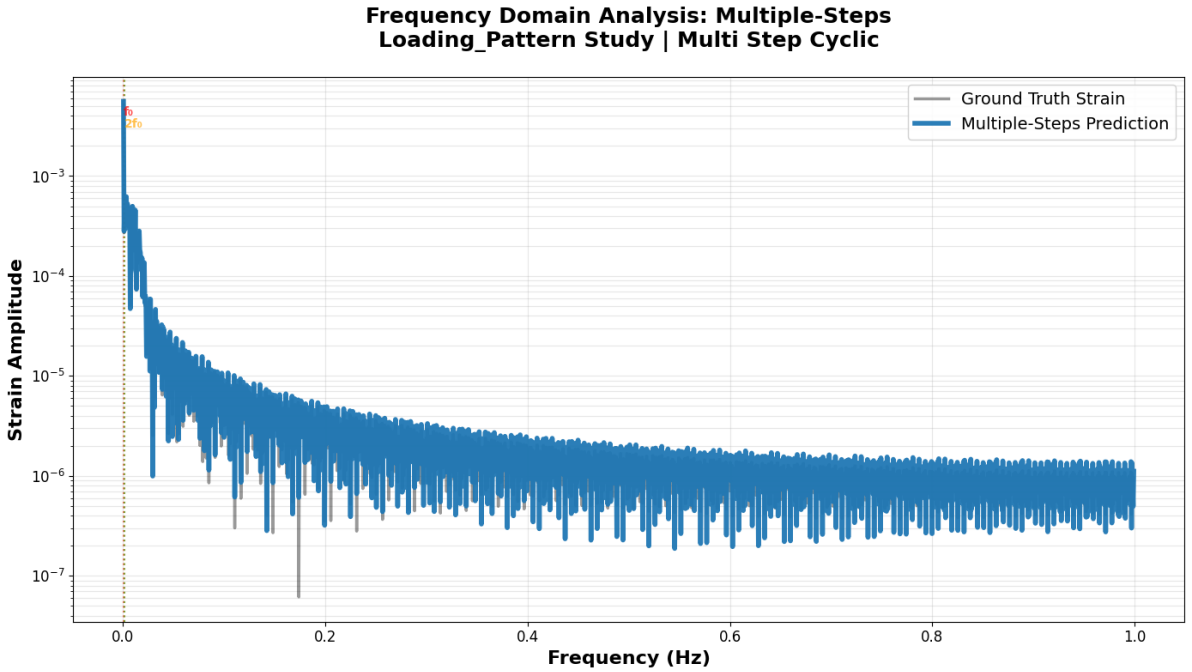

Figure A.10: Frequency domain analysis for Multiple-Steps loading pattern training.

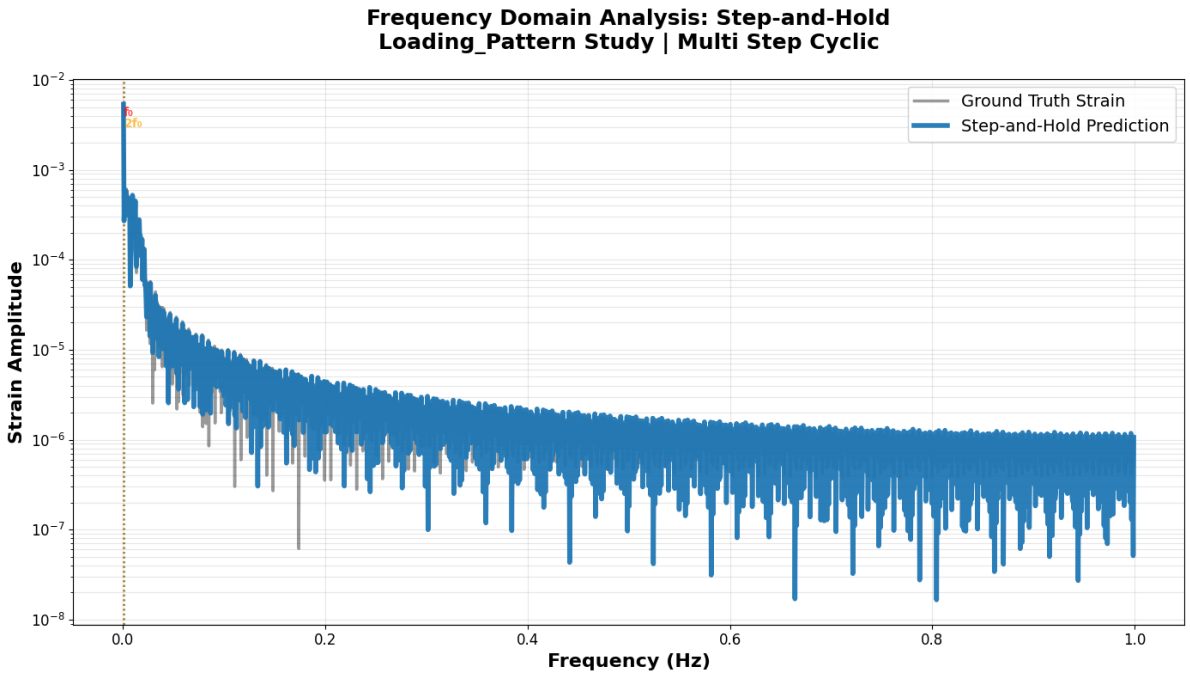

Figure A.11: Frequency domain analysis for Step-and-Hold loading pattern training.

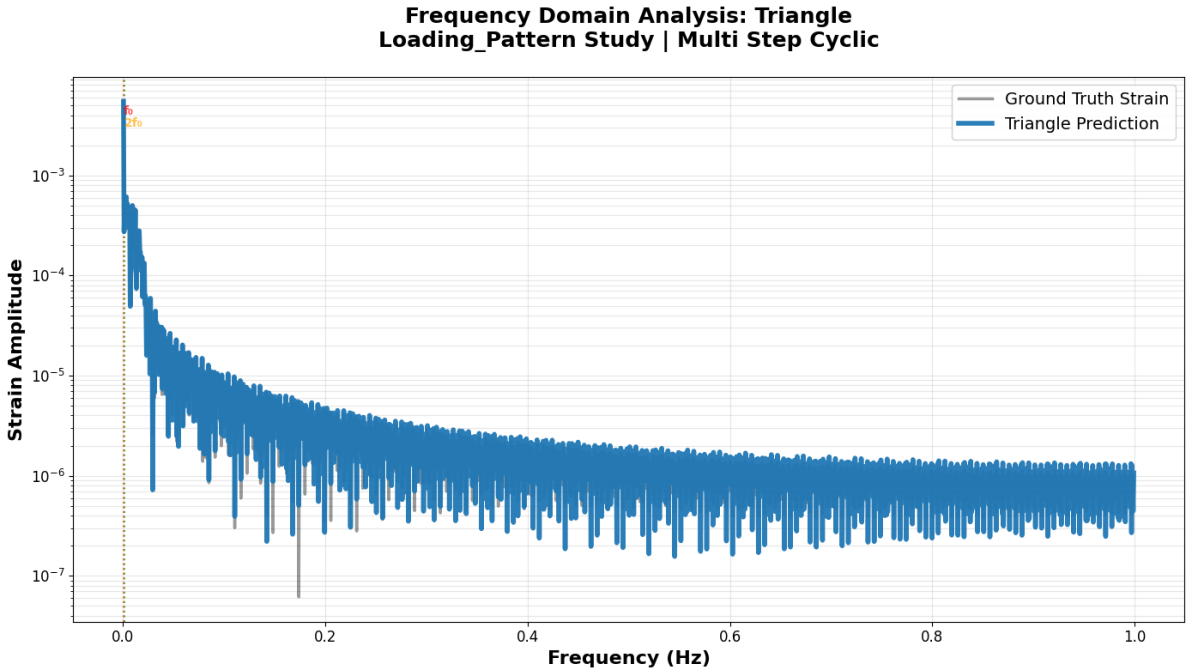

Figure A.12: Frequency domain analysis for Triangle loading pattern training.

A.2. Loss Function Sensitivity Analysis

These figures illustrate the model prediction behaviour when trained with different loss function formulations, revealing how optimisation objectives influence the neural network's learning of nonlinear material characteristics.

A.2.1. Time Domain Analysis

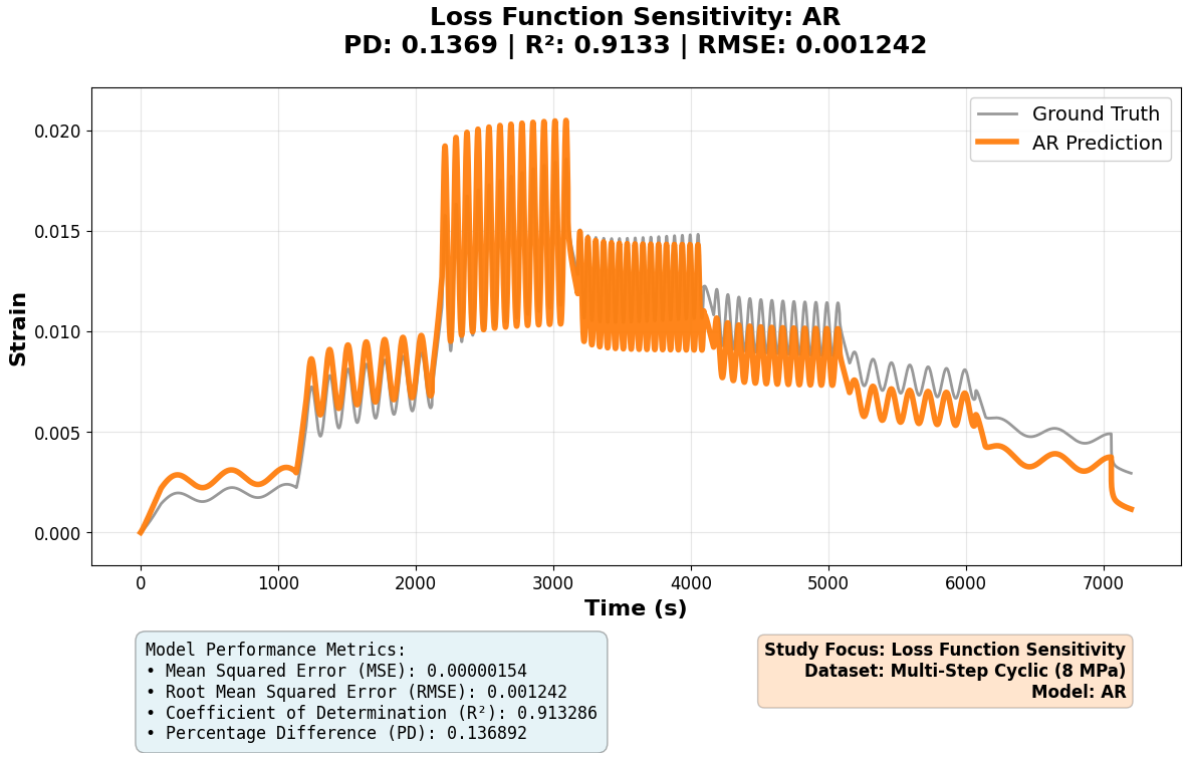

Figure A.13: Model prediction accuracy using Amplitude Ratio loss function.

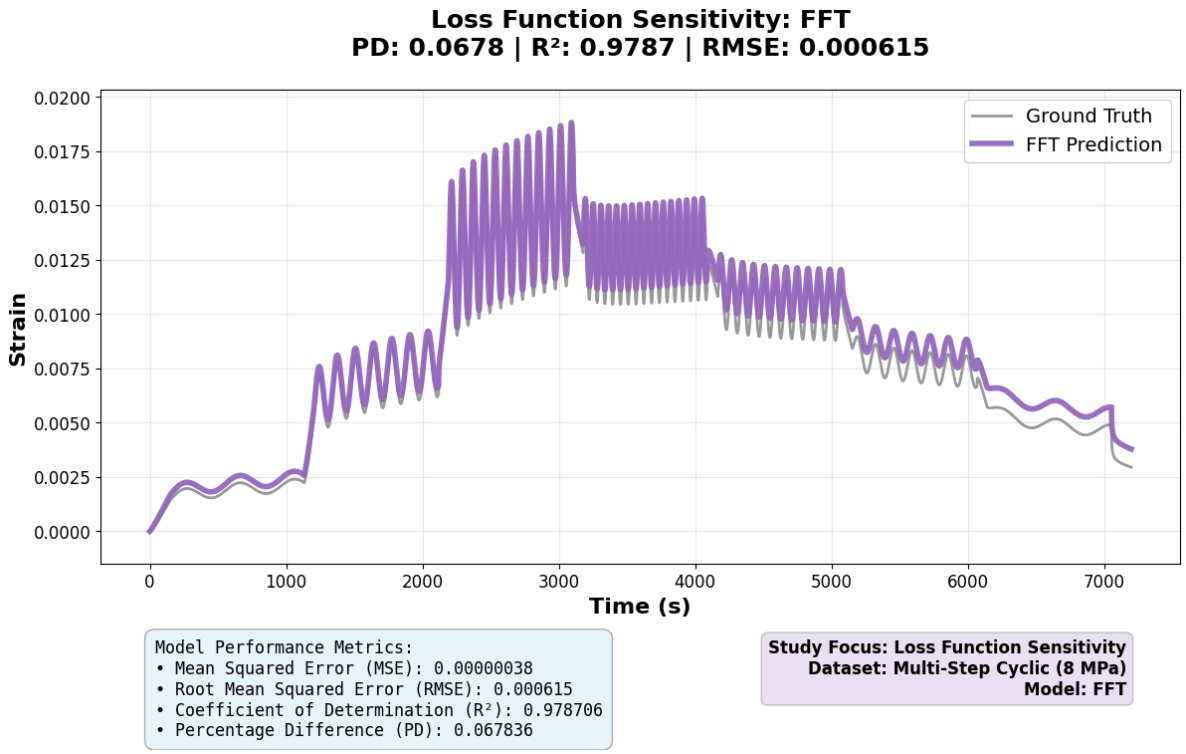

Figure A.14: Model prediction accuracy using FFT loss function.

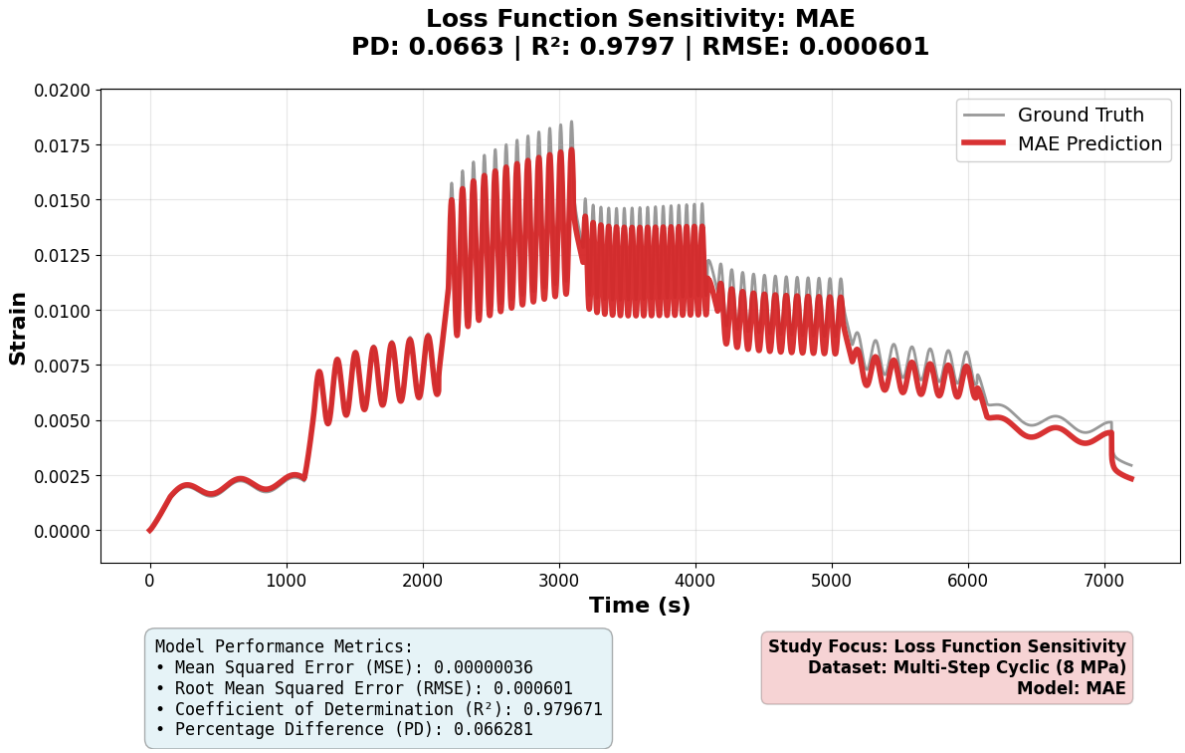

Figure A.15: Model prediction accuracy using Mean Absolute Error loss function.

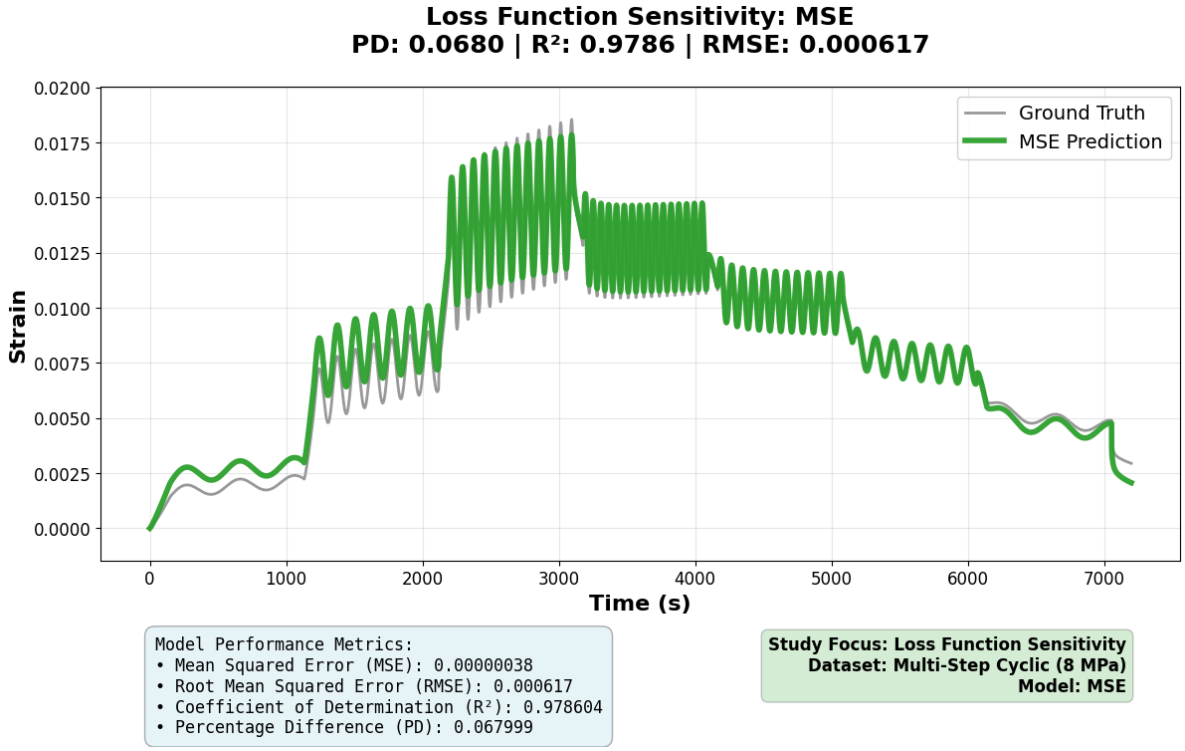

Figure A.16: Model prediction accuracy using Mean Squared Error loss function.

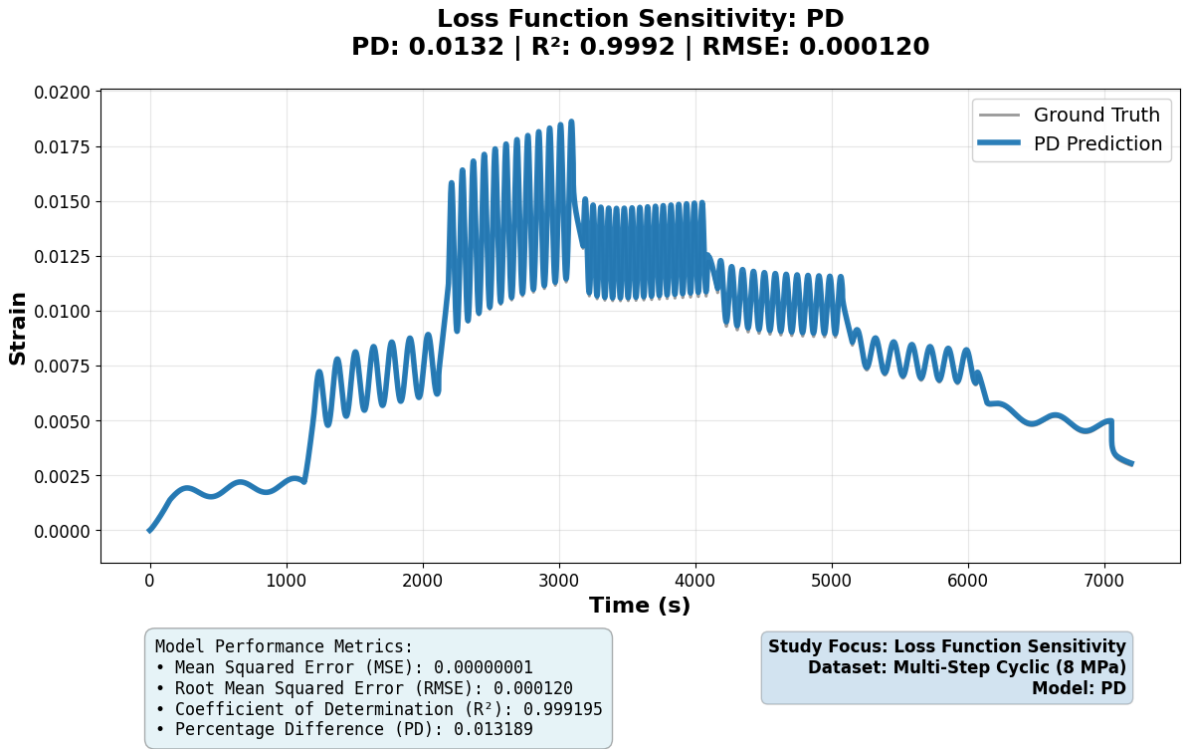

Figure A.17: Model prediction accuracy using Percentage Difference loss function.

A.2.2. Frequency Domain Analysis

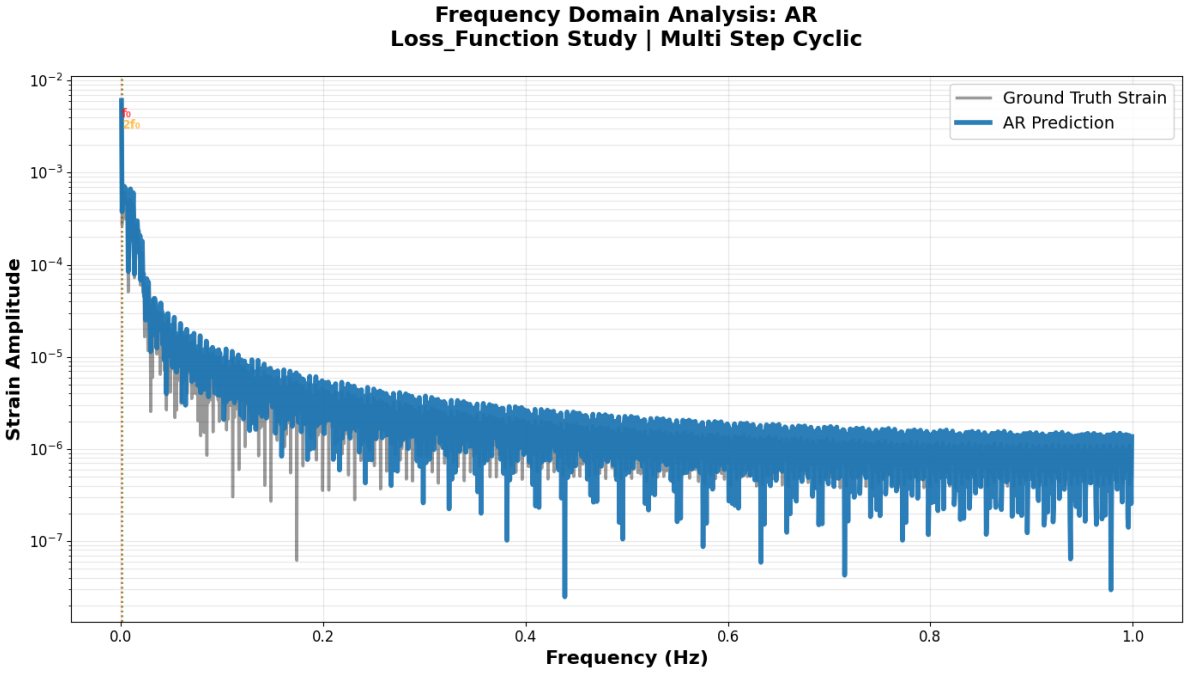

Figure A.18: Frequency domain analysis using Amplitude Ratio loss function.

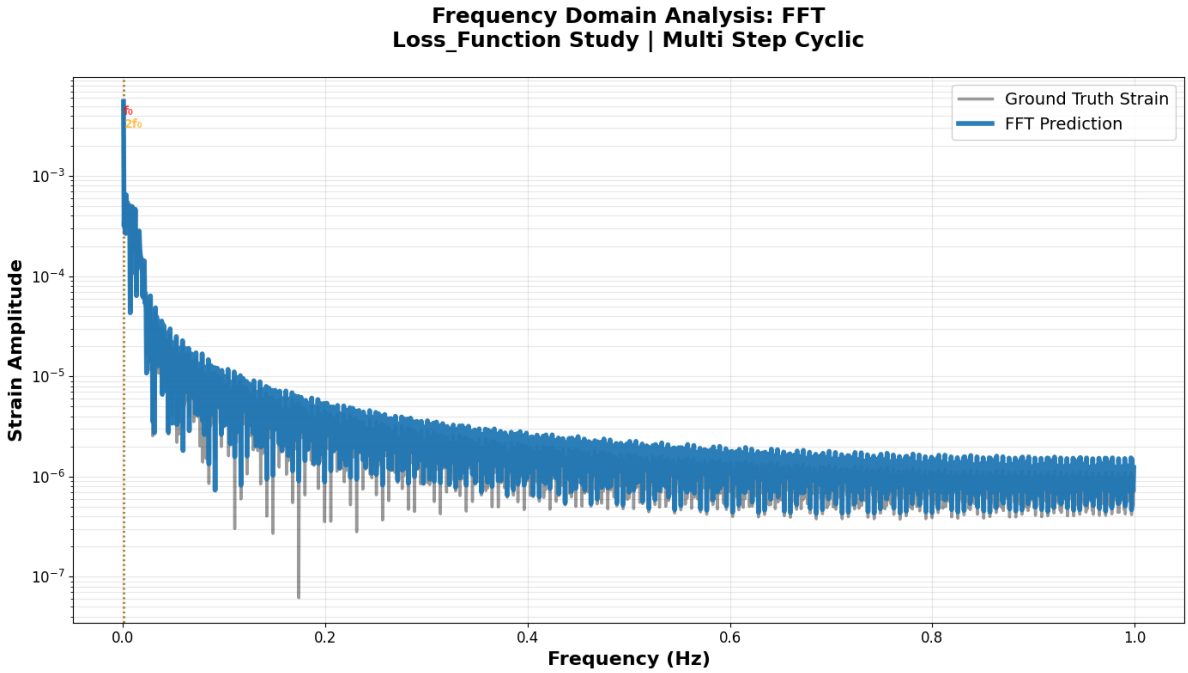

Figure A.19: Frequency domain analysis using FFT loss function.

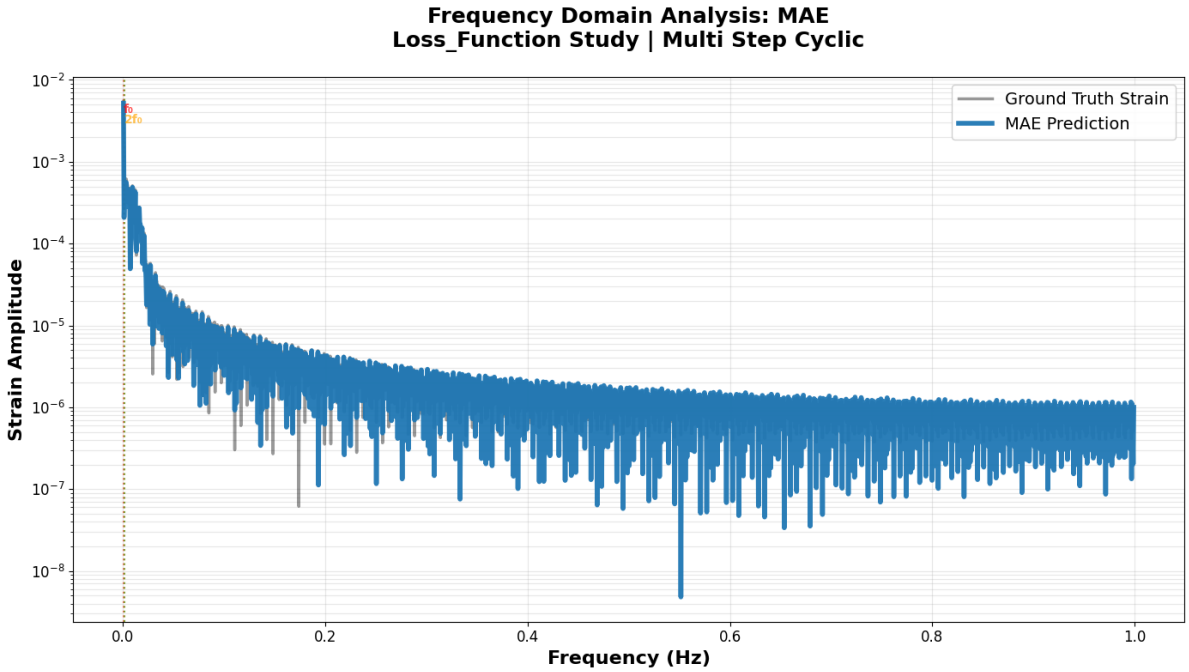

Figure A.20: Frequency domain analysis using Mean Absolute Error loss function.

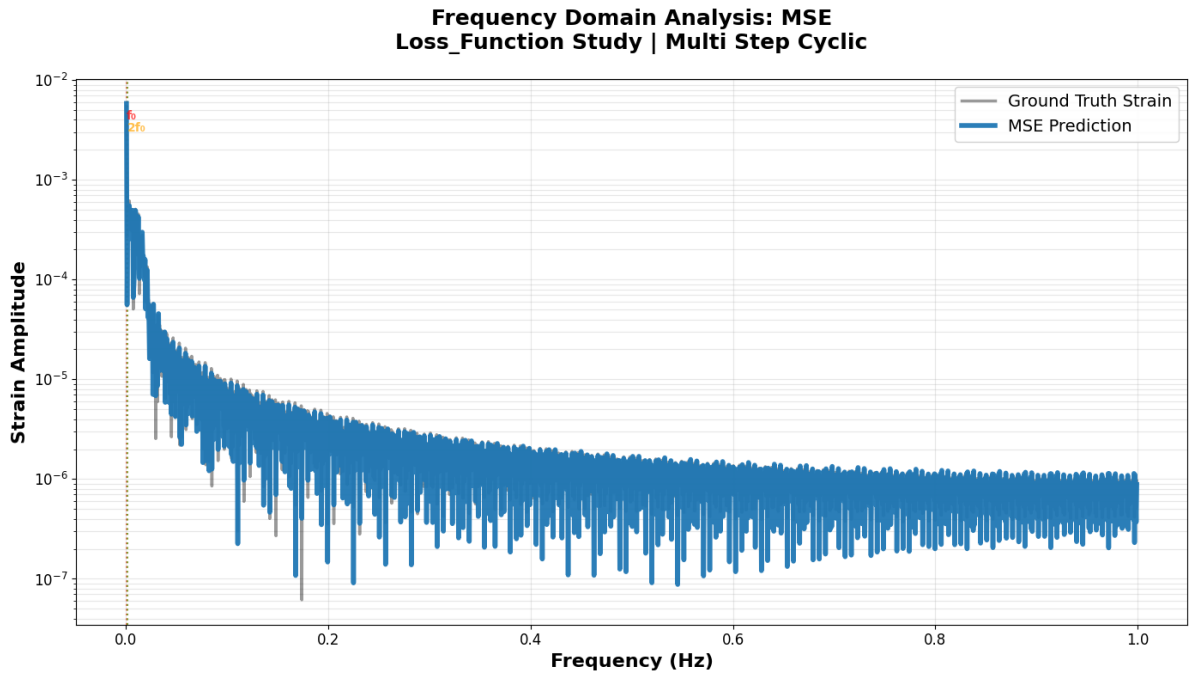

Figure A.21: Frequency domain analysis using Mean Squared Error loss function.

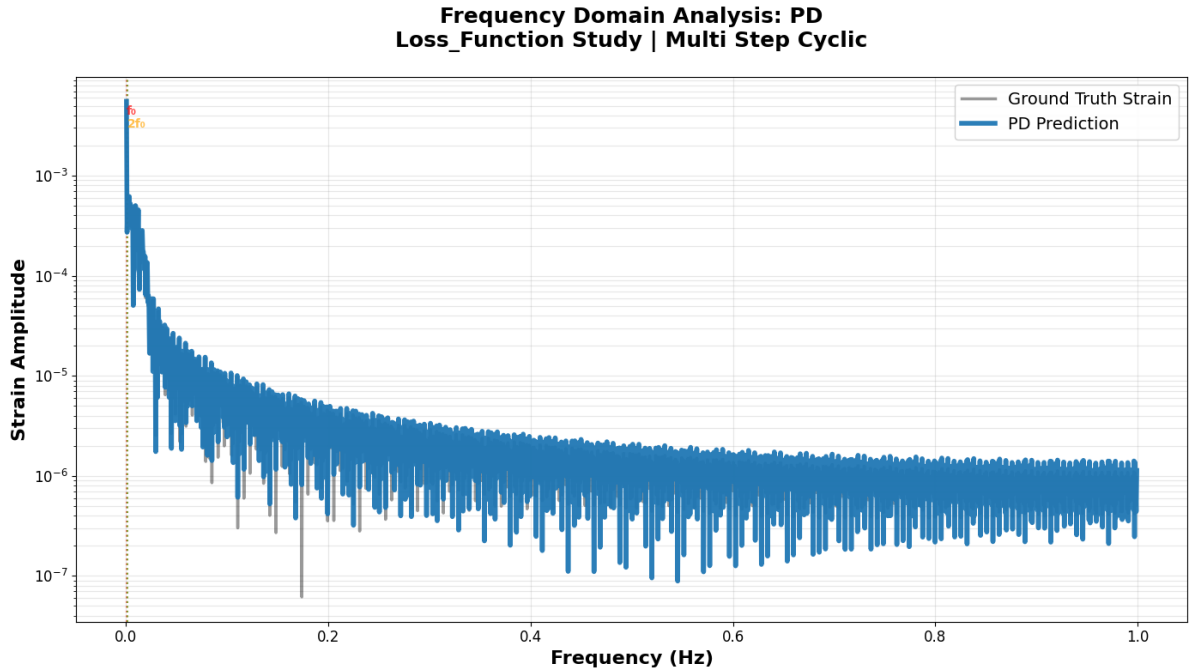

Figure A.22: Frequency domain analysis using Percentage Difference loss function.

A.3. Relaxation Spectrum Sensitivity Analysis

These figures present model prediction behaviour across different relaxation spectrum configurations, demonstrating how physics representation quality influences neural network integration effectiveness for material characterisation applications.

A.3.1. Time Domain Analysis

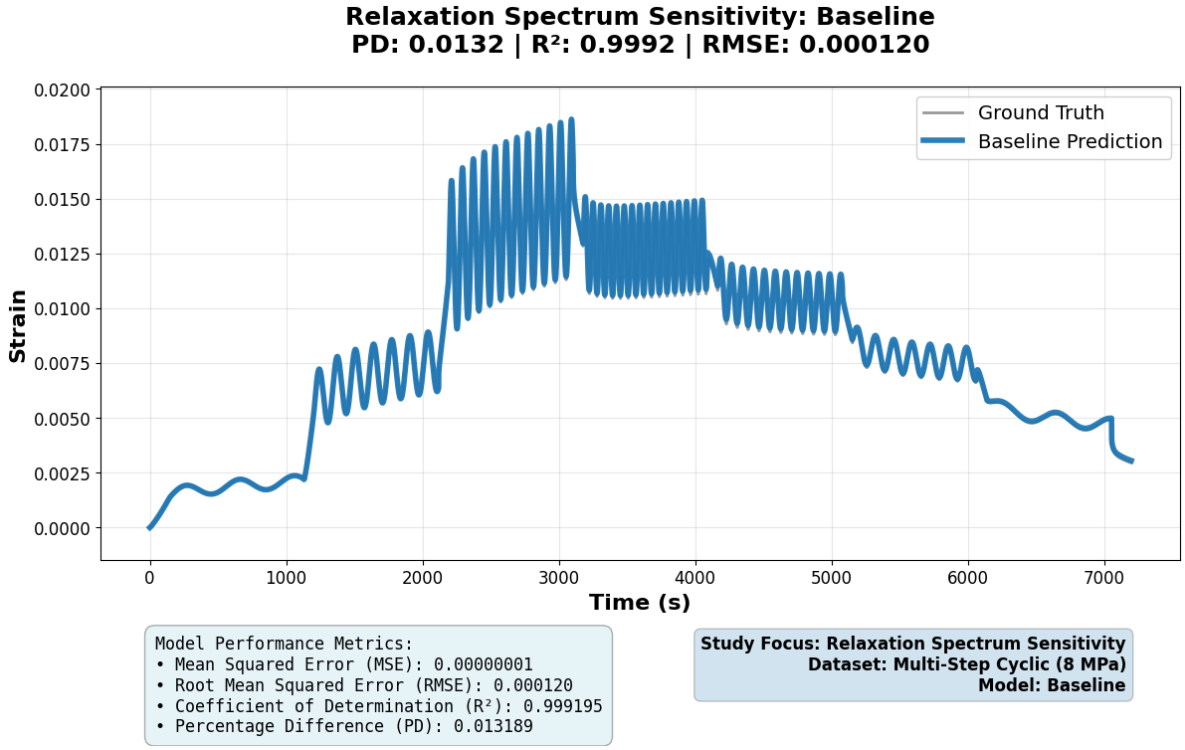

Figure A.23: Model prediction accuracy using Baseline relaxation spectrum configuration.

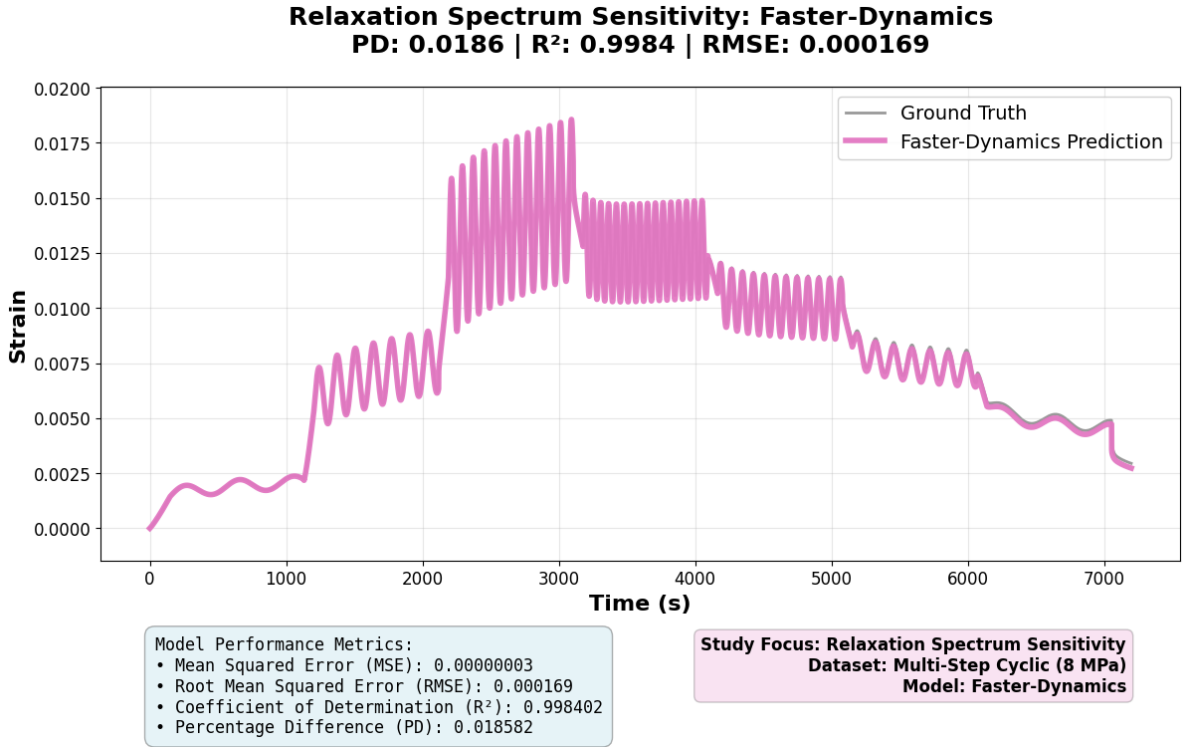

Figure A.24: Model prediction accuracy using Faster-Dynamics spectrum configuration.

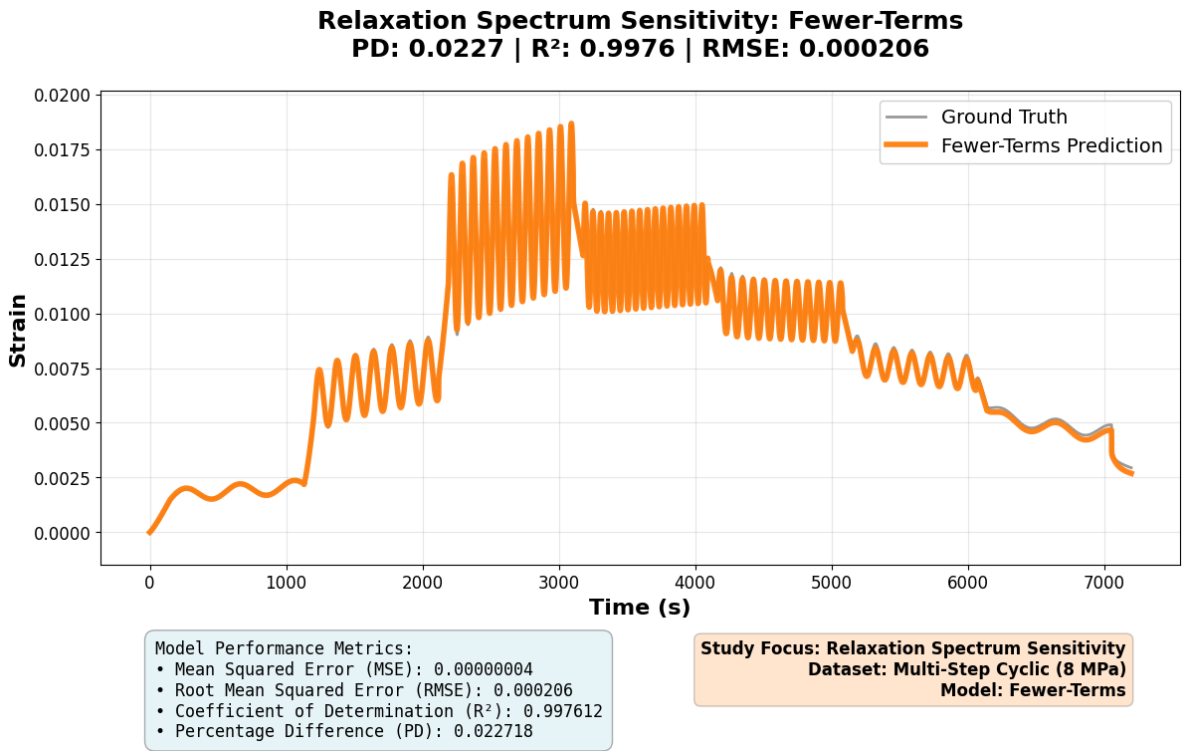

Figure A.25: Model prediction accuracy using Fewer-Terms spectrum configuration.

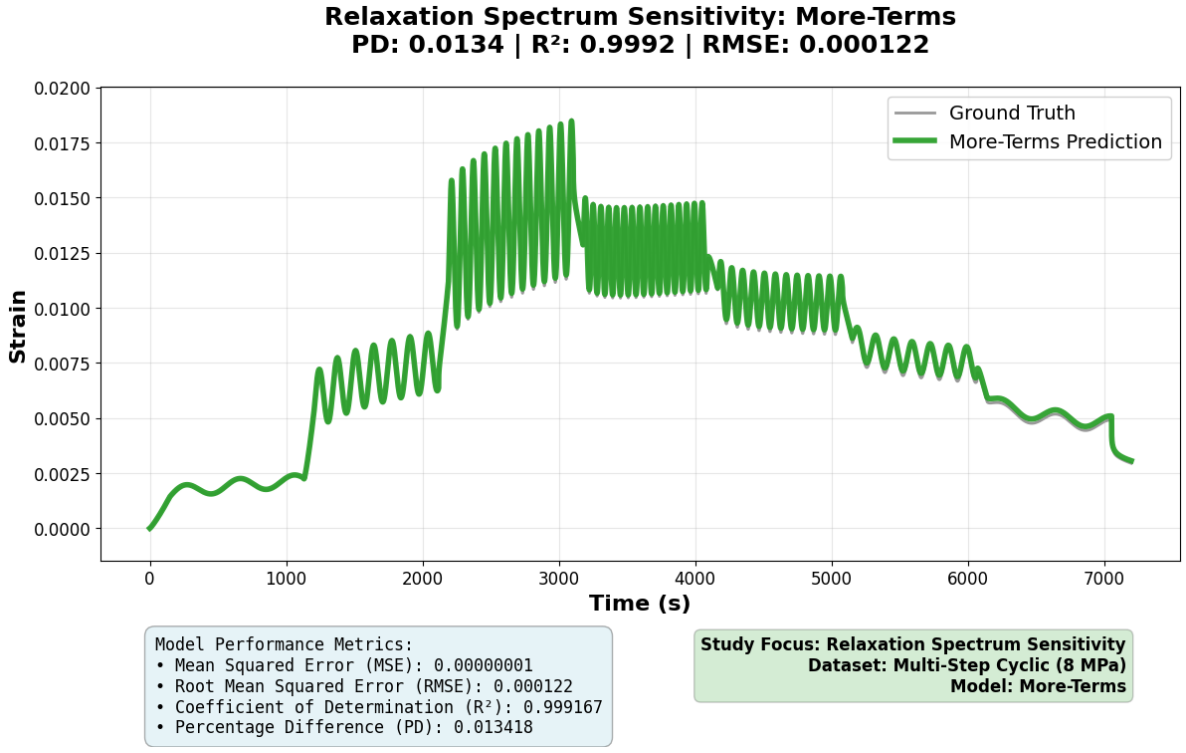

Figure A.26: Model prediction accuracy using More-Terms spectrum configuration.

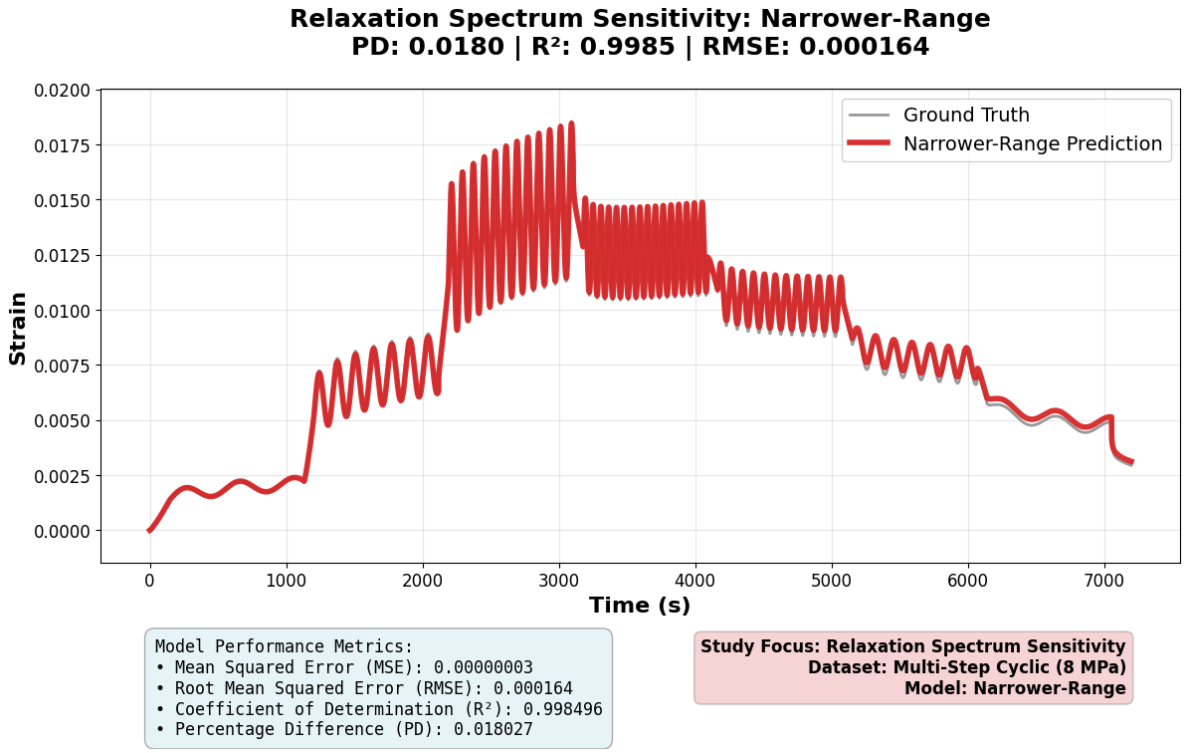

Figure A.27: Model prediction accuracy using Narrower-Range spectrum configuration.

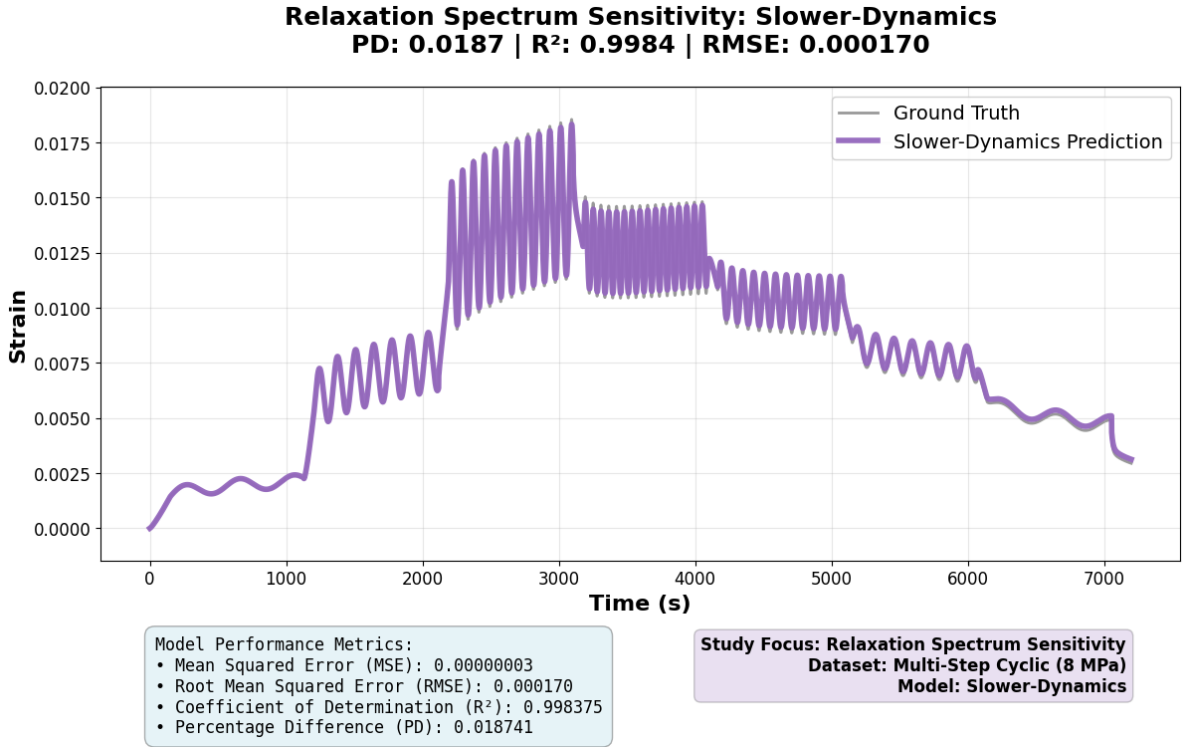

Figure A.28: Model prediction accuracy using Slower-Dynamics spectrum configuration.

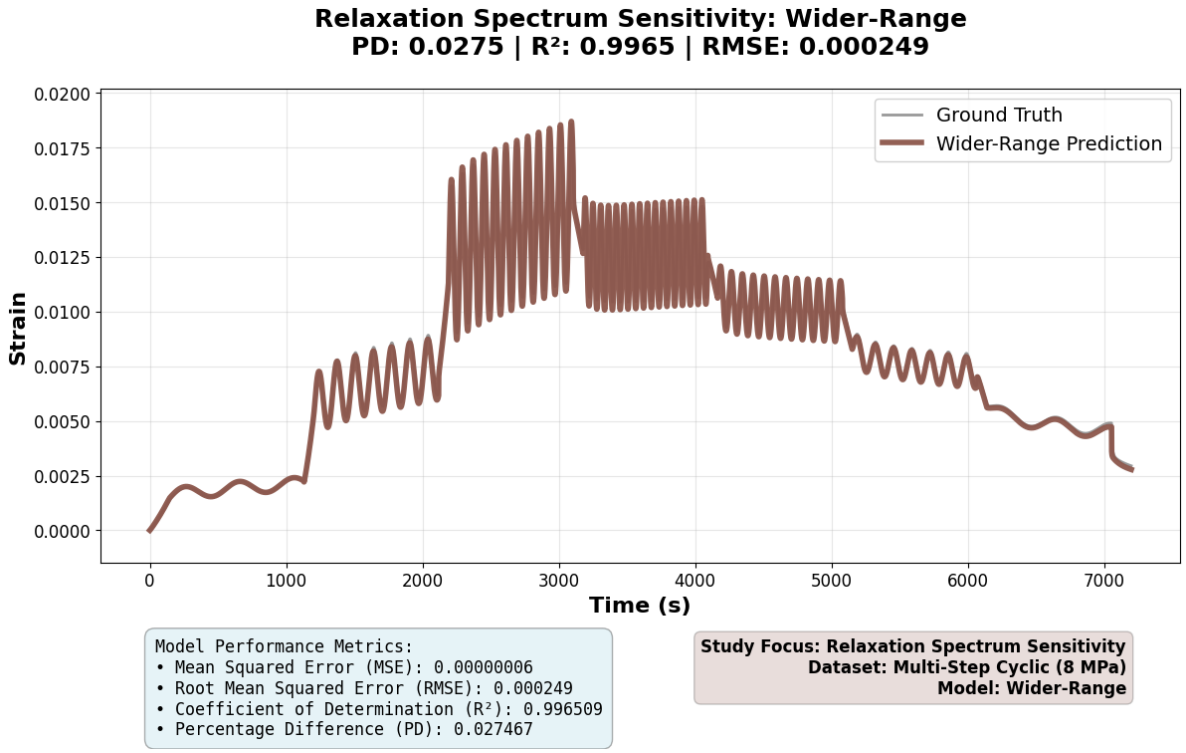

Figure A.29: Model prediction accuracy using Wider-Range spectrum configuration.

A.3.2. Frequency Domain Analysis

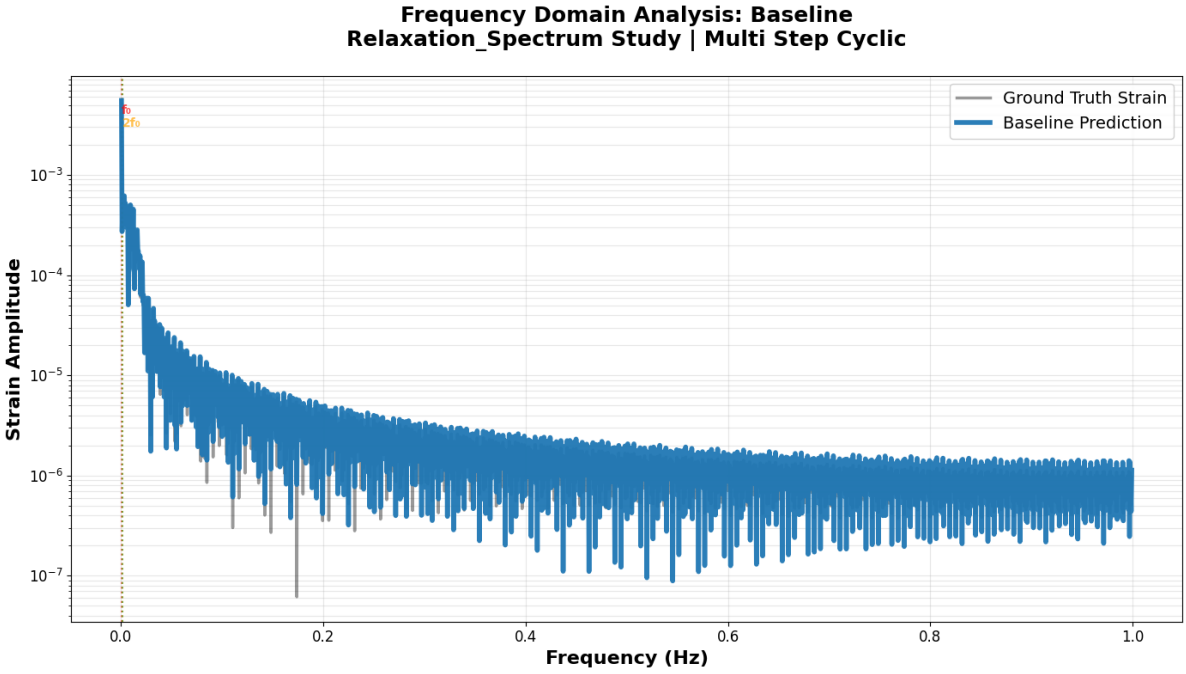

Figure A.30: Frequency domain analysis using Baseline relaxation spectrum configuration.

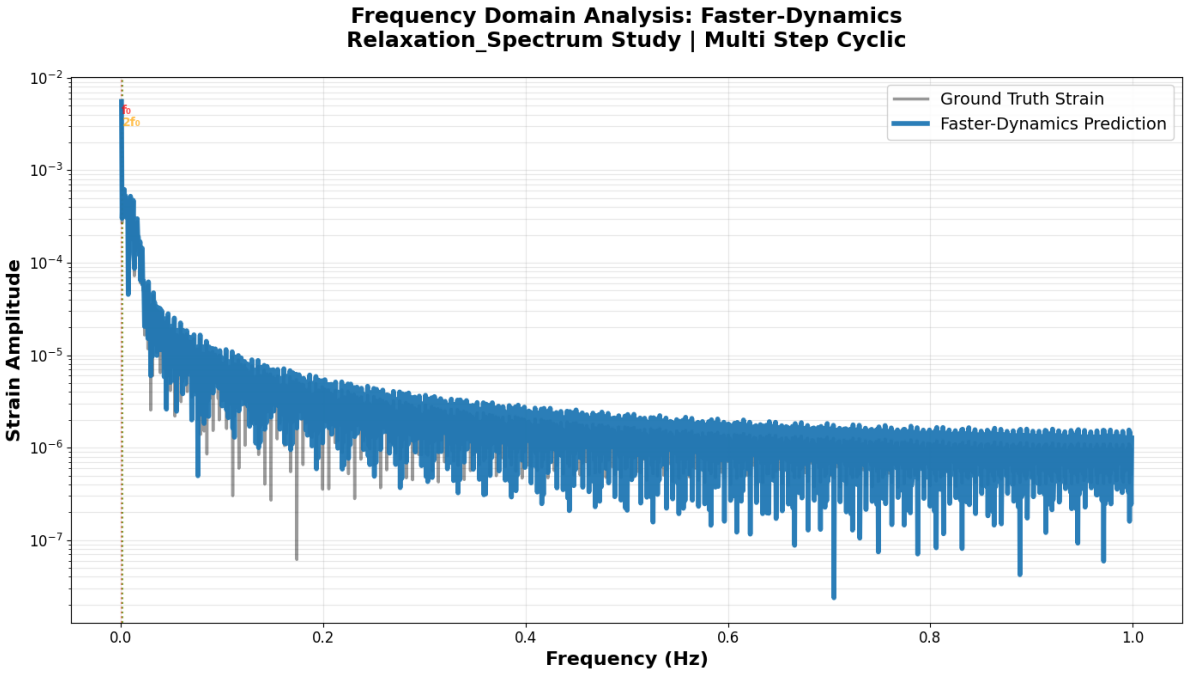

Figure A.31: Frequency domain analysis using Faster-Dynamics spectrum configuration.

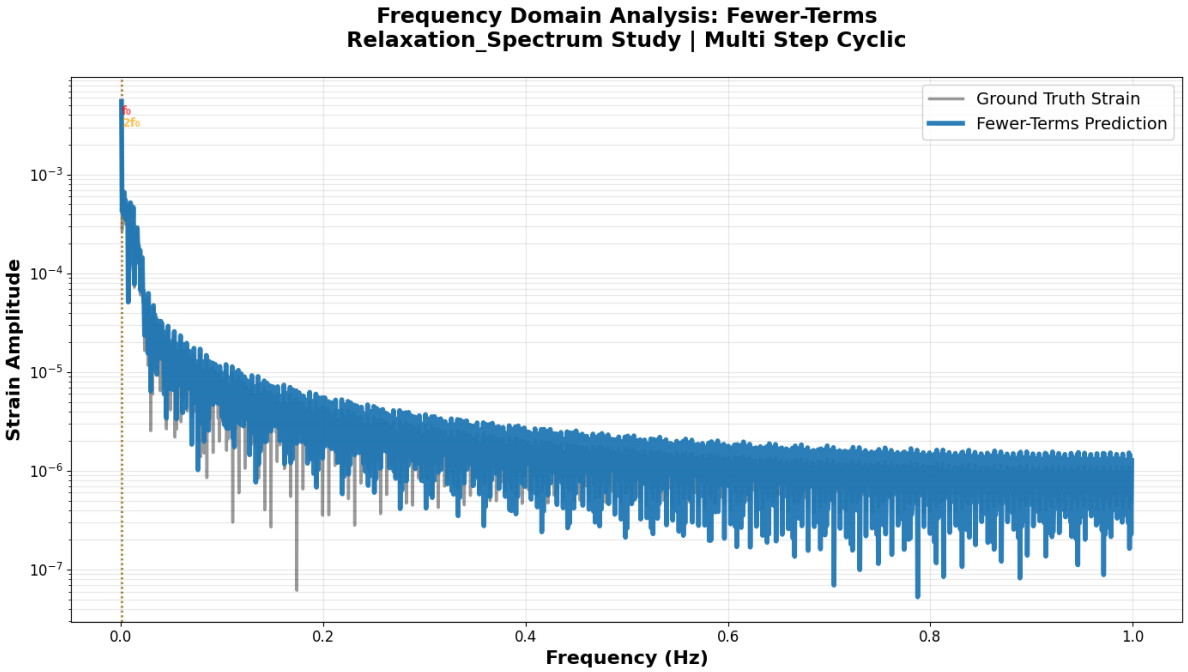

Figure A.32: Frequency domain analysis using Fewer-Terms spectrum configuration.

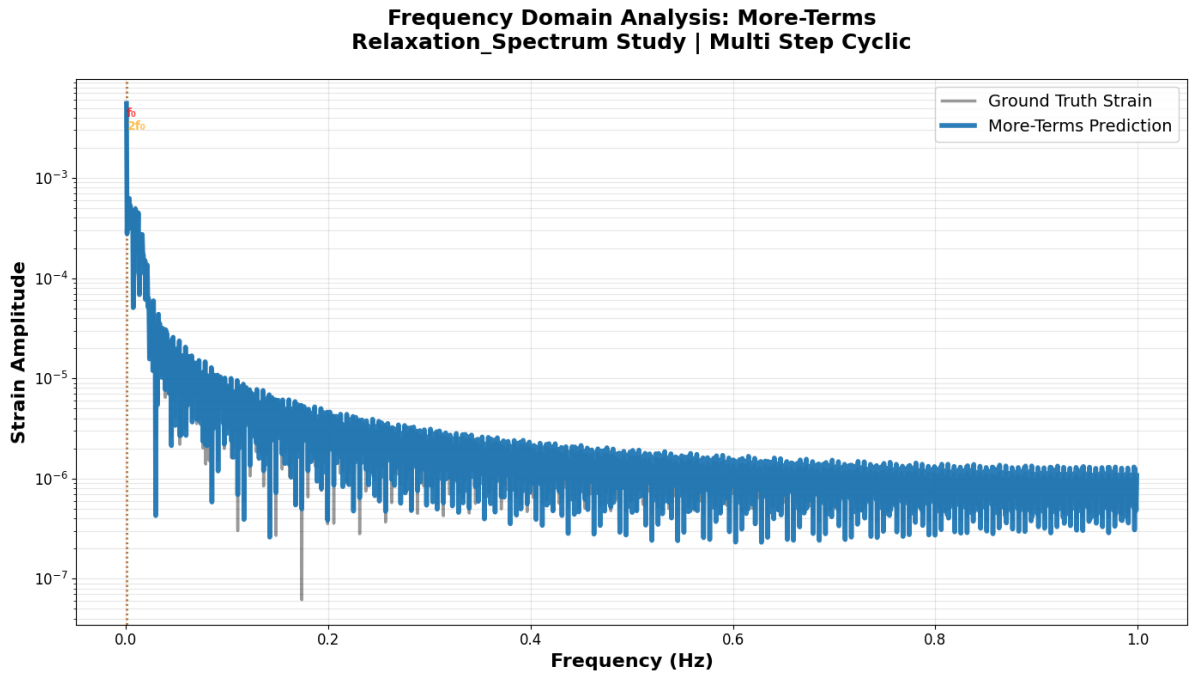

Figure A.33: Frequency domain analysis using More-Terms spectrum configuration.

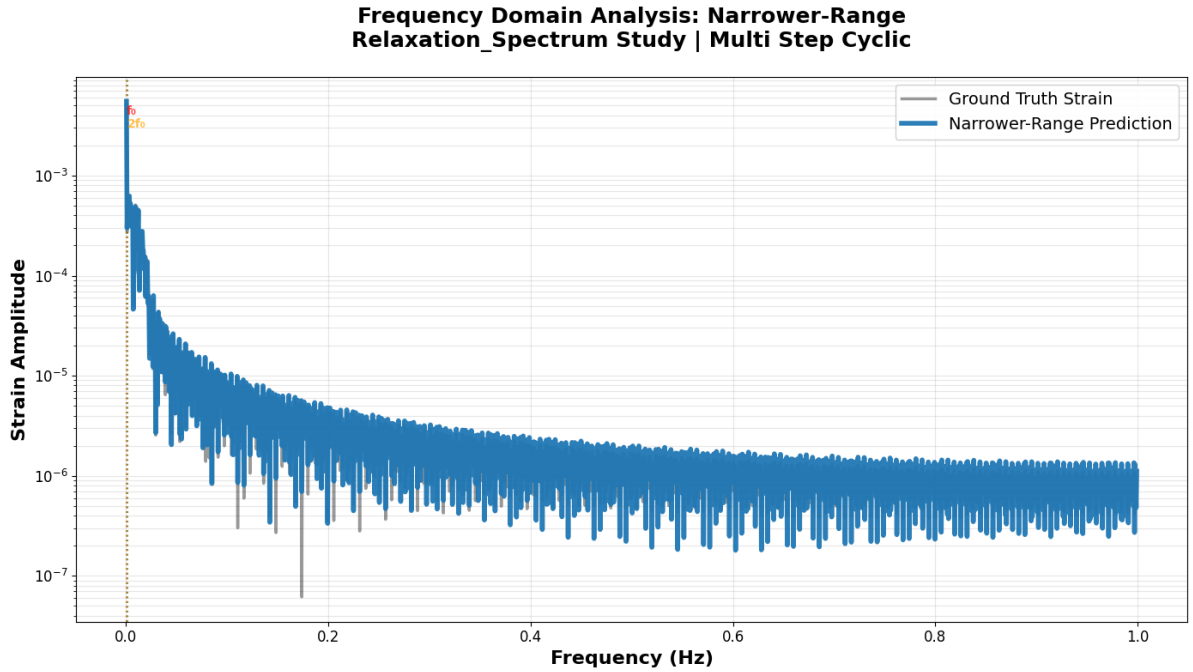

Figure A.34: Frequency domain analysis using Narrower-Range spectrum configuration.

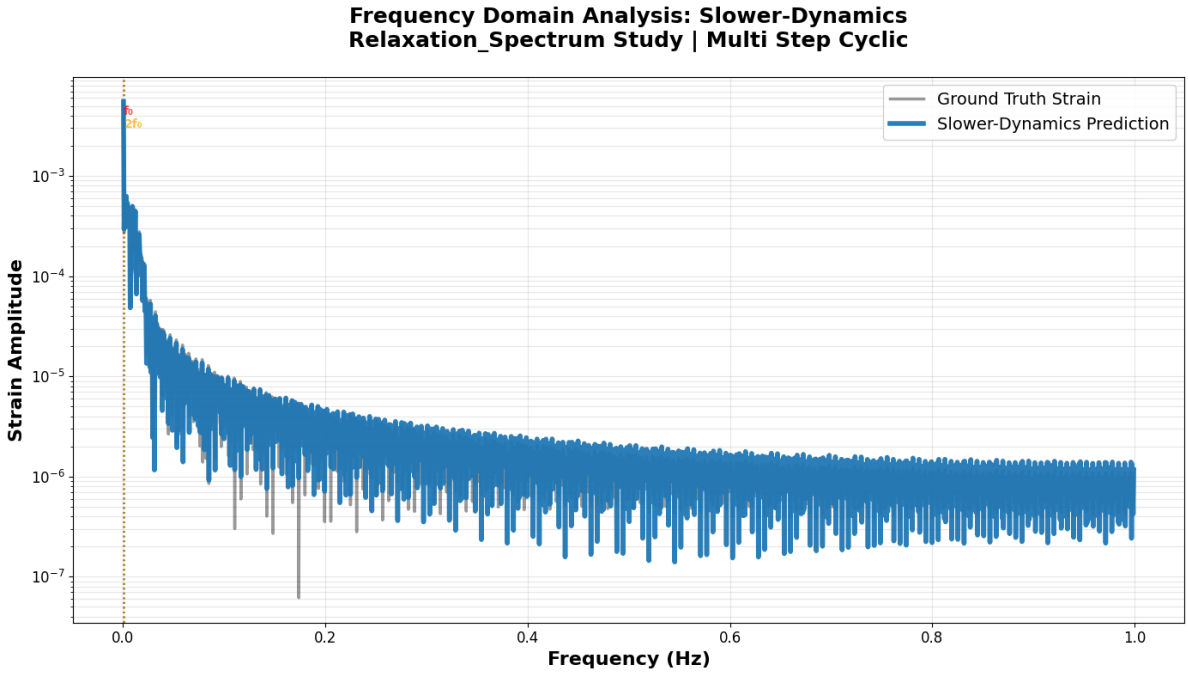

Figure A.35: Frequency domain analysis using Slower-Dynamics spectrum configuration.

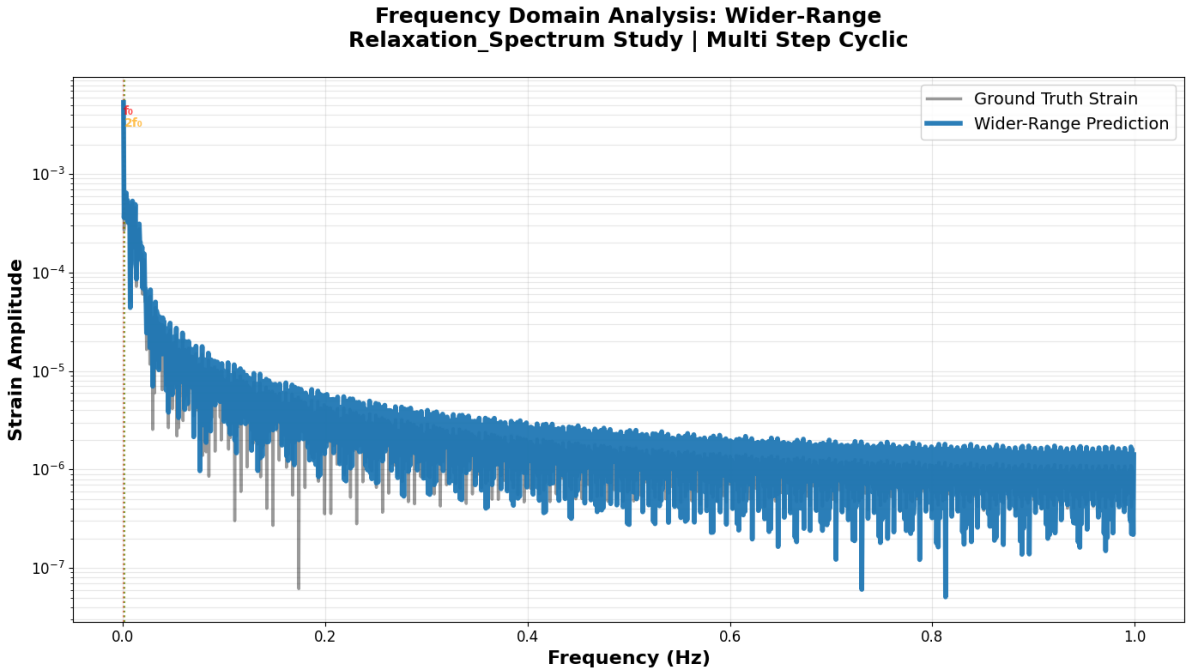

Figure A.36: Frequency domain analysis using Wider-Range spectrum configuration.